



Università degli Studi di Ferrara

DOTTORATO DI RICERCA IN  
SCIENZE CHIMICHE

CICLO XXVI°

COORDINATORE Prof. CARLO ALBERTO BIGNOZZI

**Adsorption properties of particles for environmental applications**

Settore Scientifico Disciplinare CHIM/01

**Dottoranda**

Dott. Sarti Elena

**Tutore**

Prof. Pasti Luisa

Anni 2011/2013

# INDEX

<b>INTRODUCTION .....</b>	<b>pag 1</b>
<b>LIST OF SYMBOLS .....</b>	<b>pag 4</b>
<b>CHAPTER 1 Water pollutants .....</b>	<b>pag 5</b>
1.1 Emerging pollutants .....	pag 5
1.1.1 Pharmaceuticals .....	pag 6
1.1.2 Perfluorinatedalkyl compounds .....	pag 8
1.2 Organic Pollutants .....	pag 10
1.2.1 BTEX ..	pag 10
1.2.2 Fuel oxygenate compounds .....	pag 10
1.3 Selected compounds .....	pag 11
1.3.1 PPCPs ..	pag 11
1.3.2 PFCs .....	pag 15
1.3.3 Organic pollutants .....	pag 16
1.4 Natural organic matter .....	pag 18
1.4.1 Lignin-derived phenolic monomers .....	pag 19
<b>CHAPTER 2 Porous silica materials .....</b>	<b>pag 23</b>
2.1 Zeolites .....	pag 23
2.1.1 Properties .....	pag 25
2.1.2 Applications .....	pag 29
2.1.3 Characterization .....	pag 30
2.2 Mesoporous materials .....	pag 31
2.3 Selected materials .....	pag 32
<b>CHAPTER 3 The adsorption process .....</b>	<b>pag 39</b>
3.1 Adsorption processes .....	pag 39
3.2 Theory of adsorption .....	pag 40
3.3 Adsorption isotherms .....	pag 46
3.3.1 Ideal adsorption on homogeneous surfaces .....	pag 46
3.3.2 Ideal adsorption on heterogeneous surfaces .....	pag 47
3.3.3 Non-ideal adsorption on homogeneous surfaces .....	pag 49
3.4 Adsorption kinetic .....	pag 50

<b>CHAPTER 4 Results .....</b>	<b>pag 55</b>
4.1 Drugs adsorption on zeolites .....	pag 55
4.1.1 Drugs adsorption on Beta .....	pag 56
4.1.1.1 Materials characterization .....	pag 57
4.1.1.2 Adsorption .....	pag 61
4.1.1.2.1 Effect of SAR .....	pag 62
4.1.1.2.2 Effect of pH and ionic strength .....	pag 69
4.1.1.2.3 Effect of solute's hydrophobicity .....	pag 74
4.1.2 Drugs adsorption on Y .....	pag 75
4.1.2.1 Adsorption .....	pag 76
4.1.2.1.1 Effect of pH .....	pag 82
4.1.2.1.2 Effect of solute's hydrophobicity .....	pag 84
4.1.2.2 Release tests .....	pag 85
4.2 PFOA adsorption on mesoporous materials .....	pag 87
4.2.1 Materials characterization .....	pag 88
4.2.2 Adsorption .....	pag 90
4.2.2.1 Effect of pH .....	pag 96
4.3 MTBE adsorption on Ferrierite .....	pag 98
4.3.1 Materials characterization .....	pag 99
4.3.2 Adsorption .....	pag 105
4.4 Toluene adsorption on ZSM-5 and competition with phenolic monomers .....	pag 110
4.4.1 Adsorption of toluene .....	pag 111
4.4.2 Adsorption of caffeic acid .....	pag 118
4.4.3 Adsorption of para-hydroxybenzaldehyde .....	pag 122
4.4.4 Competition toluene/caffeic acid .....	pag 124
4.4.5 Competition toluene/para-hydroxybenzaldehyde .....	pag 128
4.4.6 Effect of solute's hydrophobicity .....	pag 130
 <b>CONCLUSIONS .....</b>	 <b>pag 132</b>
<b>REFERENCES .....</b>	<b>pag 134</b>
<b>ACKNOWLEDGEMENTS .....</b>	<b>pag 149</b>

## INTRODUCTION

Research is documenting with increasing frequency that many chemical and microbial constituents that have not historically been considered as contaminants are present in the environment on a global scale: these are often generally referred to as “contaminants of emerging concern” (CECs) because the risk to human health and the environment associated with their presence, frequency of occurrence, or source may not be known. Some molecules ascribed as CECs are pharmaceuticals (human and veterinary drugs), personal care products, plasticizers, industrial and household products (such as insecticides, detergents, fire retardants, fuels).

Since CECs are contained in many products of common use, they are continuously released into the environment where they can accumulate over time. Many CECs have chemical properties which make them resistant to natural environmental degradation processes. Hence, some CECs can accumulate and persist in the environment, potentially causing adverse effects on biota. Even the compounds that undergo transformation or degradation can form other chemicals (i.e. metabolites) that are also potentially harmful. Effects of CECs on human and ecosystem health are largely unknown, and relatively little is known about the ways they travel through the environment or how they may be transformed or degraded. Some studies have shown that even very low exposure to certain CECs can have impacts on biological systems.

Conventional wastewater and recycled water treatments are only partially effective in their removal or degradation, so they are generally discharged into the environment with treated wastewater effluent, recycled water and plant sludge.

Other environmental exposure pathways of CECs are manufacturing and hospital effluents, land applications (e.g., biosolids and water reuse), concentrated animal feeding operations and direct disposal/introduction to environment.

Another category of water pollutants raising great attention is organic compounds such as BTEX (benzene, toluene, ethylbenzene, xylene), derived from oil refinement, and fuel oxygenate compounds (alcohols and ethers), added to gasoline to enhance octane number and to reduce emissions in exhaust gases. The presence of these pollutants in natural waters is mainly due to leaks from underground storage tanks, overfills of storage tanks, spills and landfills. Once released to the environment, BTEX can volatilize, dissolve, attach to soil particles or degrade biologically. If BTEX dissolve into water, then they can easily move while if they are sorbed onto soil particles, they move slower than the groundwater. If oxygen is present in sufficient quantities, BTEX

can also degrade biologically, albeit slowly. Fuel oxygenate compounds, especially methyl-tert-butyl ether, are characterised by high water-solubility which allow them to migrate into natural waters; moreover, their natural attenuation is slow due to the recalcitrance to biodegradation.

A great effort should be done to improve the removal of contaminants from water and to develop analytical methods able to detect these molecules at very low concentrations.

Advanced wastewaters treatments technologies have been identified to be successfully in treating contaminated waters, such as nanofiltration, reverse osmosis, ozonation and chemical oxidation. The latter processes, however, can lead to the formation of oxidation intermediates which are, to date, mostly unknown. In adsorption technology, inorganic adsorbents are often employed since they offer advantages due to their stability towards the chemical and thermal treatments which are necessary to induce the complete degradation of adsorbates and, therefore, the regeneration of exhausted adsorbents. Among inorganic adsorbents, it has been proven that zeolites are efficient in removing small organic compounds from the environmental matrix. Likewise, mesoporous silica materials and their surface modifications were also studied as adsorbent/supports in contaminant removal processes. To date, studies and applications on organic pollutant adsorption in microporous zeolitic materials from aqueous media have been relatively scarce. These siliceous materials could be also employed as adsorbent phase in pre-concentration methods.

This work of thesis focused on the adsorption onto microporous (zeolites) and mesoporous silica materials of some water pollutants: more specifically, four pharmaceuticals and a perfluorinated alkyl compound have been chosen to represent the CECs category, while toluene and methyl-tert-butyl ether belong to organic pollutants, BTEX and fuel oxygenate compounds respectively.

In particular, thermogravimetric, chromatographic and diffractometric techniques were employed to study the adsorption process in order to: 1) investigate the adsorptive properties of siliceous materials; 2) characterise their structures after the adsorption of the selected contaminants; 3) localise the organic species in the zeolites channel systems; 4) probe the interactions between organic molecules and framework oxygen atoms; 5) characterize the kinetic of the adsorption process.

The thermodynamics and kinetics of the adsorption process of contaminants on hydrophobic zeolites were studied by using complementary techniques: chromatography and thermogravimetry. Chromatography was mainly used to measure the adsorption isotherms of compounds of interest. The adsorption isotherm is useful for

representing the capacity of a zeolite for adsorbing organics from water, and in providing description of the functional dependence of capacity on the concentration of pollutants. Experimental determination of the isotherm allows for evaluating the feasibility of adsorption for treatment, in selecting a zeolite, and in estimating adsorbent dosage requirements. Moreover, from isotherm parameters it is possible to evaluate the adsorption energy distribution of the process. These techniques were also employed to investigate the kinetics of the adsorption. Kinetics deals with changes in chemical properties in time and is concerned especially with rates of changes: hence it plays a fundamental role in determine the proper contact time for the removal of pollutant components from wastewater. To investigate the adsorption mechanism, diffraction techniques were employed to localize the organic adsorbed into the zeolite structure. The information gathered by this last investigation - in cooperation with the Earth Science Department UNIFE - allow to define the interactions between organic molecules and zeolite framework. The influence on the adsorption of both adsorbents features (i.e. framework type, pore width, hydrophobicity, thermal treatments) and physico-chemical parameters of the solute (i.e. molecular dimensions, hydrophobicity, acid/base behaviour) was studied. For this purpose, the adsorption was tested by varying some important parameters of the aqueous solutions, such as pH, ionic strength, temperature.

To evaluate the possible competition of natural organic matter towards contaminants adsorption, the effect of two lignin-derived phenolic monomers (caffeic acid and para-hydroxybenzaldehyde) with molecular dimensions comparable to those of the pores of the adsorbent material on the adsorption properties of zeolites was considered. This last part of the work of thesis is a fraction of a wider project whose purpose is to study the interaction and mobility of groundwater pollutants adsorbed in zeolite pores in order to improve the efficiency of permeable reactive barriers. This project involves Ferrara, Bologna and Piemonte Orientale Universities with the financial and scientific support of ENI Research Center of San Donato Milanese.

The experimental data revealed a favourable adsorption kinetics along with the effective and selective adsorption of contaminants into zeolites and mesoporous siliceous materials. These findings make these cheap and environmentally-friendly materials a tool with interesting applications for the removal or enrichment of CECs from wastewaters.

## LIST OF SYMBOLS

CECs	Contaminants of emerging concern
PPCPs	Pharmaceuticals and personal care products
WWTPs	Wastewater treatments plants
PFCs	Perfluorinated alkyl compounds
PFOA	Perfluorooctanoic acid
PFOs	Perfluorooctanesulfonate
VOCs	Volatile organic compounds
BTEX	Benzene, Toluene, Ethylbenzene, Xylene
MTBE	Methyl <i>tert</i> -butyl ether
KTP	Ketoprofen
HCT	Hydrochlorothiazide
ATN	Atenolol
ERY	Erythromycin
TOL	Toluene
NOM	Natural organic matter
HS	Humic substances
CA	Caffeic acid
HBA	Para-Hydroxybenzaldehyde
SAR	SiO <sub>2</sub> /Al <sub>2</sub> O <sub>3</sub> ratio
TGA	Thermogravimetric analysis
DTA	Differential thermal analysis
XRD	X-ray diffraction
PFO	Pseudo-first order
PSO	Pseudo-second order

# CHAPTER 1

## Water Pollutants

### 1.1 Emerging pollutants

Recently, it has been considered a new class of contaminants present in water in concentrations ranging from a few ng/L to a few µg/L [Hartig et al., 1999; Kasprzyk-Hordern et al., 2007]. These pollutants have been called emerging contaminants or contaminants of emerging concern (CECs). The United States Geological Survey (USGS) provides the following definition of CECs [Arroyo 2013]: “any synthetic or naturally occurring chemical or any microorganism that is not commonly monitored in the environment but has the potential to enter the environment and cause known or suspected adverse ecological and/or human health effects. In some cases, release of emerging chemical or microbial contaminants to the environment has likely occurred for a long time, but may not have been recognized until new detection methods were developed. In other cases, synthesis of new chemicals or changes in use and disposal of existing chemicals can create new sources of emerging contaminants.”

CECs may be new substances, or they may have been around for a long time but only recently have been found in the environment. Emerging contaminants include agricultural runoff (pesticides, pathogens and fertilizers), fuel-based-compounds, chlorinated solvents, flame retardants (perfluorinatedalkyl compounds), plasticizers, explosives, dyes, pharmaceuticals, personal care products, endocrine disruptors, hormones [Lindsey et al., 2001; Petrovic et al., 2006; Richardson et al., 2011]. This wide range of compounds is characterized by different chemical-physical properties: for instance in Figure 1.1, these compounds are divided up on the basis of polarity and volatility.



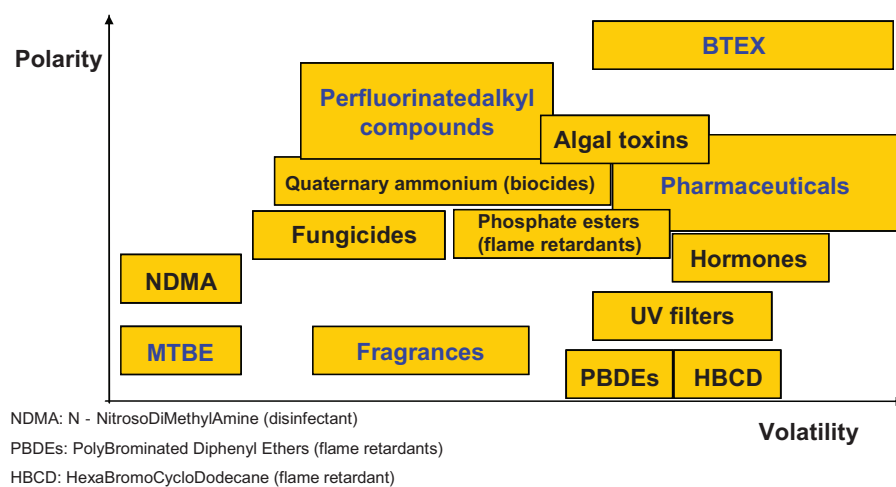


**Figure 1.1** Polarity and volatility of several classes of CECs

### **1.1.1. Pharmaceuticals**

Pharmaceuticals and personal care products (PPCPs) presence in water and wastewater has been frequently reported after the early findings [Richardson 2006; Trenholm et al., 2006]. Usually, they have been detected in the environment at very low concentrations, but these amounts are sometimes sufficient to affect significantly the quality of water [Kolpin et al., 2002]. In the aquatic environment many different compounds have been found such as analgesics and anti-inflammatory, antibiotics/bacteriostatics, anti-epileptics,  $\beta$ -blockers, oral contraceptives, antiseptics, blood lipid regulators, contrast media, etc.. [Daughton et al., 1999; Heberer, 2002].

The most often detected drugs in surface waters are usually the ones employed in largest quantities, but with many exceptions. In fact, there are drugs used in large quantities that are not found in the environment because they are rapidly degraded (for example, amoxicillin); on the other hand, there are others which are employed in smaller quantities but that are detected in high concentrations because they are extremely persistent [Zuccato et al., 2007]. Several PPCPs were found to be both ubiquitous and persistent (e.g. codeine, carbamazepine, gabapentin), hence they could bioaccumulate in aquatic organisms [Regueiro et al., 2009] and easily move along the food chain.

These compounds are a source of concern because they are used and released in large quantities and their physical and chemical properties contribute to their widespread distribution into the environment. Moreover, they are usually molecules with pharmacological activity, that can therefore affect the biota. The presence of low concentrations of PPCPs has been associated to chronic toxicity, endocrine disruption and development of pathogen resistance in the biota. The consequences of

environmental contamination by PPCPs are particularly worrying in aquatic organisms as they are subjected to multigenerational exposure. In fact, PPCPs, as already mentioned, are not present at very high concentrations, but their frequent occurrence and their possible synergic action is of concern. In fact, it has to be considered that PPCPs in the environment are present as a complex mixture and that the relative toxicity of the mixture could be different than that of the individual compounds. For instance, [Cleuvers, 2008] showed that the toxicity of a mixture of non-steroidal anti-inflammatory drugs against *Daphnia* is considerably higher when compared with that evaluated for each single compound having the same concentration of the mixture.

There is mounting evidence that these low level emerging contaminants present in natural waters and sediments may affect wildlife, sometimes causing non-lethal but adverse ecological health effects. However, the primary concern is their potential estrogenic effects at relatively low concentrations: in recent years, researchers have uncovered new environmental effects, such as feminization by hormones or structurally related compounds (xenoestrogens) that exhibited effects on fishes at concentrations lower than 1 ng/L [Mitra 2006; Leardi 2009]. Studies were launched to investigate the effects of individual PPCPs on biota [Dejaegher et al., 2009; Poiger et al., 2008]; however, because of incomplete assessment data, researchers still lack a complete understanding of the environmental effects of most PPCPs.

Another relevant impact on human health from PPCPs is their possibility to be found in drinking water; in addition there is quite limited information on their transformation during drinking water disinfection treatment.

For some of these compounds, limits on concentrations have been proposed [COM (2006) 397], but many are still not regulated [Barceló 2003; Bertanza et al., 2009; Bolong et al., 2009]. In addition, in order to limit the negative effects of these substances, the FDA (Food and Drug Administration) requires ecotoxicological tests when the environmental concentration exceeds 1 µg/L [Bolong et al., 2009]. For most of the occurring emerging pollutants, risk assessment and ecotoxicological data are still not available and therefore it is difficult to predict the effects they may have on humans health, terrestrial, aquatic organisms and ecosystems.

Conventional wastewater treatments plants (WWTPs) effluents are the major sources of environmentally relevant emerging contaminants, since pharmaceuticals are normally excreted by humans as a combination of intact and metabolized molecules and products for the care and personal hygiene are present in domestic sewage as a result of normal

domestic activities. Also the improper disposal of unused or expired pharmaceuticals must be taken into account.

Many of these substances escape to conventional depuration allowing them to reach surface water streams and distribute in the environment. Conventional water treatment processes appear to be insufficient in removing raw water residuals and require additional advanced treatments such as oxidation, adsorption or membrane filtration to achieve quantitative removal [Xiangli et al., 2006]. Without such additional treatment, PPCP residuals will be pseudo-persistent and liable to re-enter the urban water cycle.

An important contribution to the pharmaceutical compounds concentrations in wastewaters is due to the hospital discharges and to run-off from livestock and fish farms. The efficiency of the treatment units of sewage treatment plants, therefore, becomes crucial in the removal of these compounds in order to limit the introduction into the environment. The possible pathways of exposure of emerging contaminants, and in particular of PPCPs, are shown in Figure 1.2.

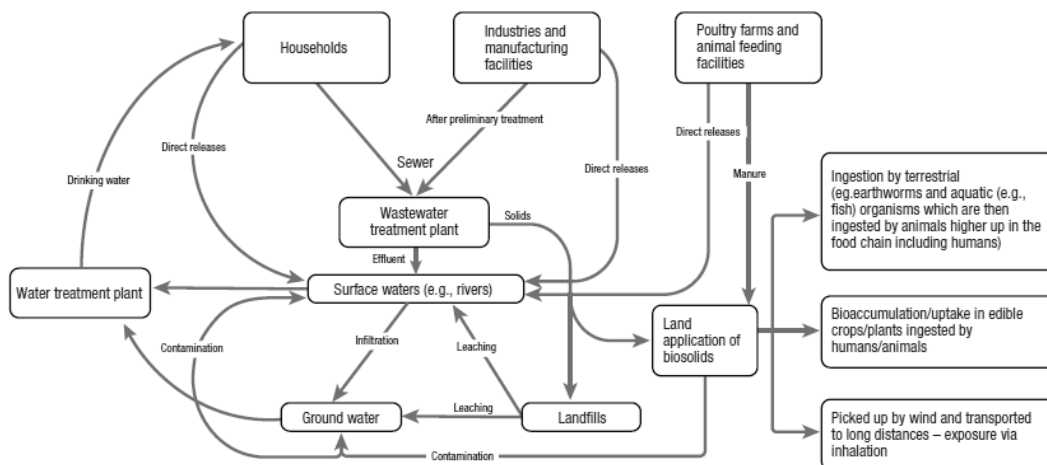


**Figure 1.2** Pathways of exposure for PPCPs from [Arroyo 2010]

PPCPs high transformation/removal rates is compensated by their continuous introduction into the environment. Following the discharge of treated sewage into the receiving water, residual PPCPs will be diluted and mixed with residuals derived from both direct surface water discharges and indirect groundwater seepage.

### **1.1.2 Perfluorinatedalkyl compounds**

As already mentioned, perfluorinatedalkyl compounds (PFCs) belong to emerging contaminants category: these molecules have received increasing attention in recent years as environmental contaminants due to their consistent detection in various

environmental matrices [Giesy et al., 2002] and their adverse effects in animal toxicity studies [Kennedy et al., 2004; Lau et al., 2007]. The two groups given the most scrutiny to date have been the perfluoroalkylsulfonates (PFASs) and the perfluorocarboxylic acids (PFCAs) and in particular the eight carbon members of these groups: perfluorooctanesulfonate (PFOS) and perfluorooctanoic acid (PFOA). These compounds have been produced commercially since the 1950s and used in a variety of consumer and industrial applications, including oil and water repellent surface coatings for packaging and textiles, surfactants and aqueous fire-fighting foams [Prevedouros et al., 2006; Paul et al., 2009]. In 2009 PFOS was added to the Stockholm Convention for Persistent Organic Pollutants [Stockholm Convention, 2010].

Production of PFOS and similar perfluorooctyl products was phased out in the USA and Europe in 2000–2002 [OECD, 2002], however ongoing production continues elsewhere [Wang et al., 2009].

PFOA and its salts continue to be used as processing agents in the manufacture of fluoropolymers but efforts have been made to reduce emissions from fluoropolymer manufacturing facilities.

PFOS and PFOA have been detected in surface water, seawater, groundwater and even tap water throughout the world [Fujii et al., 2007; Ahrens et al., 2010]: industrial and municipal wastewater treatment plants are the main point sources for PFOS and PFOA entering into natural waters [Prevedouros et al., 2006] because these compounds are inefficiently removed by primary and secondary wastewater treatment [Sinclair et al., 2006]. Various concentrations of PFOS and PFOA at the level of ng/L and µg/L were observed in the influents and effluents of wastewater treatment plants [Boulanger et al., 2005; Loganathan et al., 2007; Yu, Hu et al., 2009].

Long-chain PFCs ( $\geq 7$  perfluorinated carbons) are persistent organic pollutants that cannot be hydrolyzed, directly photolyzed, or biodegraded under environmental conditions [Nakayama et al., 2010]. PFCs have been found in fish, birds and mammals from mid-latitudes to the poles [Giesy et al., 2001, Martin et al., 2003]. PFCs in blood serum can disrupt human hormone activity, and their developmental toxicity to mammals has been reported [Jensen et al., 2008]. PFCs have relatively high solubility in water (i.e., 9.5 g/L for PFOA and 0.26 g/L for perfluorododecanoic acid PFDA) and low volatility and sorption potentials [Jensen et al., 2008; Bhatarai et al., 2012].

## **1.2 Organic pollutants**

The class of organic micropollutants includes a huge number of substances with chemical and physical characteristics very different from each other.

According to EC Directive 1999/13/EC (Solvent Emissions Directive), Volatile Organic Compounds (VOCs) are functionally defined as organic compounds having at 293.15 K a vapour pressure of 0.01 kPa or more, or having a corresponding volatility under particular conditions of use. Within this category two major classes of pollutants of interest for water can be distinguished, aromatic and aliphatic compounds. Both classes also include halogenated compounds or compounds where hydrogen atoms have been substituted with heteroatoms. These compounds are of great importance in the chemistry of the water because they are toxicants to the environment and living beings. Benzene belongs to the class referred as BTEX, together with its alkylated compounds (Toluene, Ethylbenzene, Xylene) which are often used in place of benzene, with which they share numerous chemical and toxicological properties.

Another category of organic micropollutants are fuel oxygenate compounds which, similarly to BTEX, find large applications in oil refinement and in many industrial processes, like paints, polymers, etc. production. Hence, principal sources of water contamination are due to accidental or deliberate oil spills, watercraft and urban runoff.

### **1.2.1 BTEX**

BTEX are found in petroleum products such as diesel fuel, home heating oil and gasoline. BTEX in groundwater can originate from many sources such as leaks from underground storage tanks, overfills of storage tanks, spills and landfills. When released, BTEX have the ability to dissolve into water, allowing them to move in the groundwater. Since BTEX can also be adsorbed by soil particles, these chemicals may move slower than the groundwater. If underground conditions are right, BTEX can be degraded biologically. The technologies of purifying water polluted by BTEX include biological processes, air stripping, membrane processes [Banat et al., 1996] and adsorption on a solid matrix [Bansode et al., 2003]. In more recent times oxidative processes with UV/H<sub>2</sub>O<sub>2</sub> have been proposed [Daifullah et al., 2004].

### **1.2.2 Fuel oxygenate compounds**

The 1990 Clean Air Act Amendments required fuel oxygenates to be added to gasoline to reduce atmospheric concentrations of carbon monoxide or ozone.

Oxygenated compounds that can be added to gasoline are either alcohols, namely methanol, ethanol and *tert*butyl alcohol (TBA), or ethers such as methyl *tert*-butyl ether (MTBE), ethyl *tert*-butyl ether (ETBE) and *tert*amyl methyl ether (TAME). Ethers have been generally preferred to alcohols which can be corrosive to some materials used in engines and can also lead to problems of phase separation when mixed with hydrocarbons [Fayolle et al., 2001]. From a physico-chemical point of view and as octane enhancers, MTBE, TAME and ETBE exhibit similar properties, but mainly owing to its production cost, MTBE is the dominant fuel oxygenate.

Gasoline must contain no less than 2.7% oxygen by weight, which is equal to 15% MTBE by volume, to meet this oxygen requirement [Squillace et al., 1996].

The most frequent sources of groundwater contamination are releases from gasoline storage and distribution systems [Squillace et al. 1996]. To a lesser extent, surface waters can also be polluted by direct release of unburned MTBE-containing fuel by recreational watercraft [Fayolle et al., 2001].

### **1.3 Selected compounds**

In this work, the interaction between different contaminants belonging to the above mentioned classes and different mesoporous and microporous materials was systematically investigated by considering the effect of surrounding pH, ionic strength, and thus chemical state of compounds, in order to evaluate the role of hydrophobic and electrostatic forces in the interaction between the selected molecule and the adsorbent. In the following some characteristics of the studied compounds are reported.

#### **1.3.1 PPCPs**

The selected pharmaceutical compounds were ketoprofen (KTP), hydrochlorothiazide (HCT), atenolol (ATN) and erythromycin (ERY) which belong to different therapeutic classes and have been detected in natural waters of several countries [Y. Valcárcel et al., 2011; S. Castiglioni et al., 2006 ; M. Gros et al., 2010; D. Bendz et al., 2005] because the removal efficiency of conventional wastewaters treatments plants towards them have been demonstrated to be scarce (Figure 1.3). Moreover they are characterized by different physico-chemical properties as molecular dimensions, acid/base behaviour, hydrophobicity, ecc.

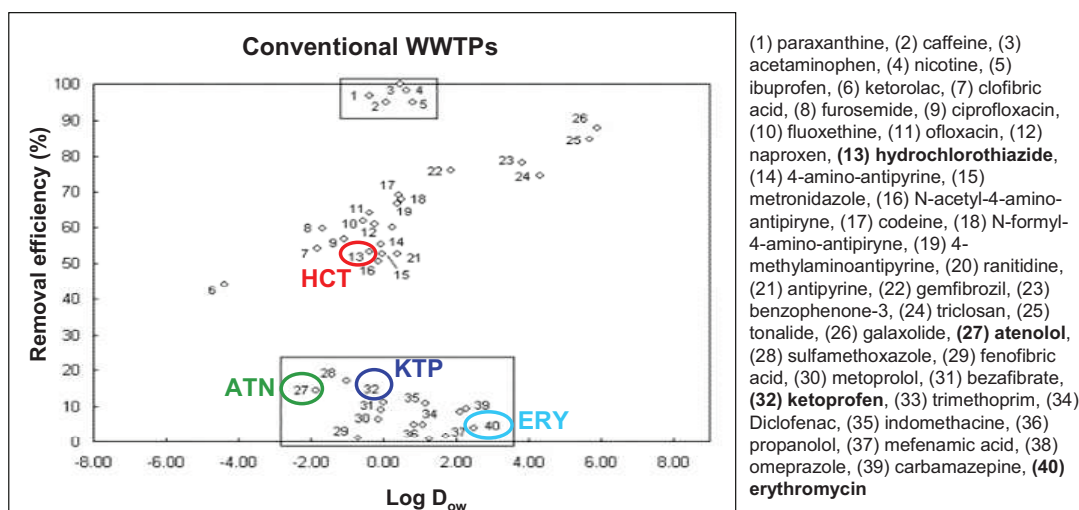


**Figure 1.3** Removal efficiency of conventional wastewaters treatment plants vs. pharmaceuticals hydrophobicity [Rosal et al., 2010]. The selected drugs have been highlighted.

### KETOPROFEN

**Table 1.1** Some chemical properties of ketoprofen

Formula	Molecular Weight	Structure	Water solubility	pK <sub>a</sub>	Log K <sub>ow</sub>
C <sub>16</sub> H <sub>14</sub> O <sub>3</sub>	254.28		0.5 g/L [Gantiva et al., 2010]	4.02 [Meloun et al., 2007]	3.12 [Radjenović et al., 2008]

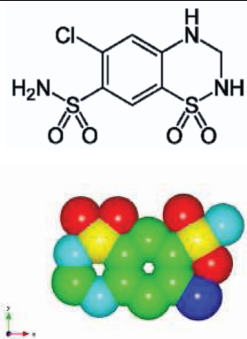
Ketoprofen, (RS)2-(3-benzoylphenyl)-propionic acid, is one of the propionic acid class of Non-Steroidal Anti-Inflammatory Drugs (NSAID) with analgesic and antipyretic effects. It acts by inhibiting the body's production of prostaglandin. The main mechanism of action of the drug is due to the inhibition of cyclo-oxygenase leading to block the synthesis of prostaglandins responsible for inflammation and tissue damage. The drug is light sensitive, so it is necessary to avoid exposure to direct sunlight: in some cases, in fact, there has been the emergence of photo-allergic and photo-toxicity. Ketoprofen is also employed as antipyretic and analgesic in veterinary field. Recent studies have found ketoprofen, like diclofenac, causing lethal effects in red-headed

vultures: vultures feeding on the carcasses of recently treated livestock suffer acute kidney failure within days of exposure.

There is a chiral center in the carbon  $\alpha$  to the carbonyl. Furthermore, it presents a site donor and acceptor sites of three hydrogen bonds.

### HYDROCHLOROTHIAZIDE

**Table 1.2** Some chemical properties of hydrochlorothiazide

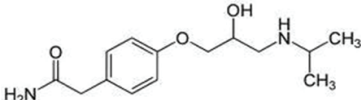
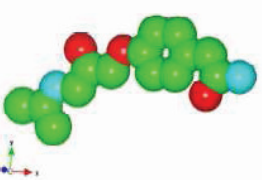
Formula	Molecular Weight	Structure	Water solubility	pK <sub>a</sub>	Log K <sub>ow</sub>
C <sub>7</sub> H <sub>8</sub> ClN <sub>3</sub> O <sub>4</sub> S <sub>2</sub>	297.74		0.6-1 g/L [Deppeler, 1981]	pK <sub>a1</sub> =7.9 pK <sub>a2</sub> =9.2 [Radjenović et al., 2008]	-0.07 [Radjenović et al., 2008]

Hydrochlorothiazide is a diuretic drug of the thiazide class that acts by inhibiting the kidneys' ability to retain water. This reduces the volume of the blood, decreasing blood return to the heart and thus cardiac output and, by other mechanisms, is believed to lower peripheral vascular resistance. Hydrochlorothiazide is frequently used for the treatment of hypertension, congestive heart failure, symptomatic edema, diabetes insipidus, renal tubular acidosis and the prevention of kidney stones. Thiazides are also used in the treatment of osteoporosis. Thiazides decrease mineral bone loss by promoting calcium retention in the kidney, and by directly stimulating osteoblast differentiation and bone mineral formation. Five centers acceptors of hydrogen bonds and three centers donors of hydrogen bonds are present.



ATENOLOL

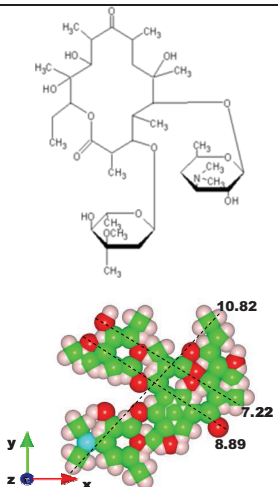
**Table 1.3** Some chemical properties of atenolol

Formula	Molecular Weight	Structure	Water solubility	pK <sub>a</sub>	Log K <sub>ow</sub>
C <sub>14</sub> H <sub>22</sub> N <sub>2</sub> O <sub>3</sub>	266.34	 	13.3 g/L [Küster et al., 2009]	9.6 [Küster et al., 2009]	0.16-0.50 [Küster et al., 2009]

Atenolol is a selective  $\beta_1$  receptor antagonist, a drug belonging to the group of beta blockers ( $\beta$ -blockers), a class of drugs used primarily in cardiovascular diseases. Introduced in 1976, atenolol was developed as a replacement for propranolol in the treatment of hypertension. Unlike propranolol, atenolol does not pass through the blood–brain barrier thus avoiding various central nervous system side effects. Atenolol is used for a number of conditions including: hypertension, angina, acute myocardial infarction, supraventricular tachycardia, ventricular tachycardia, and the symptoms of alcohol withdrawal. Its structure shows three donor sites of hydrogen bonds and four hydrogen bond acceptor sites.

## ERYTHROMYCIN

**Table 1.4** Some chemical properties of erythromycin

Formula	Molecular Weight	Structure	Water solubility	pK <sub>a</sub>	Log K <sub>ow</sub>
C <sub>37</sub> H <sub>67</sub> NO <sub>13</sub>	733.9		2 g/L [Scheytt et al., 2005]	8.90 [Persson 1968]	3.06 [Sugawara et al., 1998]

Erythromycin is a macrolide antibiotic that has an antimicrobial spectrum similar to or slightly wider than that of penicillin, hence it is often prescribed for people who have an allergy to penicillin. For respiratory tract infections, it has better coverage of atypical organisms, including Mycoplasma and legionellosis. Erythromycin is produced from a strain of the actinomycete *Saccharopolyspora erythraea*.


In structure, this macrocyclic compound contains a 14-membered lactone ring with ten asymmetric centres and two sugars (L-cladinose and D-desosamine), making it a compound very difficult to produce via synthetic methods. The ketonic function is very important for its reactivity: it acts by inhibiting bacterial protein synthesis, thus acting as bacteriostatic. Erythromycin is well absorbed orally, spreading easily in tissues, however, is not able to cross the blood-brain barrier.

### **1.3.2 PFCs**

The selected perfluorinated alkyl compound is perfluorooctanoic acid because, different from other PFCs, it is highly water-soluble and thus it is easy to transport in an aquatic environment. At the same time, the hydrophobic chain and hydrophilic functional groups may provide opportunities for PFOA to adsorb onto the surfaces of a variety of environmental solid matrices.

## PERFLUOROOCCTANOIC ACID

**Table 1.5** Some chemical properties of perfluorooctanoic acid

Formula	Molecular Weight	Structure	Water solubility	pK <sub>a</sub>	Log K <sub>ow</sub>
C <sub>8</sub> HF <sub>15</sub> O <sub>2</sub>	414.07		9.5 g/L [Thompson et al., 2011]	2 - 3 [Prevedouros et al., 2006]	Not measurable [Prevedouros et al., 2006]

Perfluorooctanoic acid (PFOA) is a synthetic chemical that does not occur naturally in the environment. In 1951, the American chemical company *DuPont* started using PFOA in the manufacturing of fluoropolymers, substances which impart fire resistance and oil, stain, grease and water repellency. They provide non-stick surfaces on cookware and waterproof, breathable membranes for clothing, and are used in many industry segments, such as aerospace, automotive, building/construction, chemical processing, electronics, semiconductors and textile industries.

In 1999 the United States Environmental Protection Agency (US-EPA) began investigating perfluorinated chemicals, founding that PFOA is very persistent in the environment and causes adverse effects in laboratory animals [US-EPA PFOA]: for these reasons, in 2000 PFOA, PFOS and related products production was phased-out. PFOA can also be produced by the breakdown of some fluorinated telomers, which are used in surface treatment products to impart soil, stain, grease and water resistance. Some telomers are also employed as high performance surfactants in products that must flow evenly, such as paints, coatings, and cleaning products, fire-fighting foams for use on liquid fuel fires, or the engineering coatings used in semiconductor manufacture.

### 1.3.3 Organic Pollutants

The selected organic pollutants were toluene and methyl-tert-butyl ether: they were chosen as representative of two classes of organic pollutants, BTEX and oxygenate compounds respectively. Because of its high water solubility and hence high bioavailability, MTBE could be ascribed also as emerging contaminant.

METHYL TERT-BUTYL ETHER (MTBE)

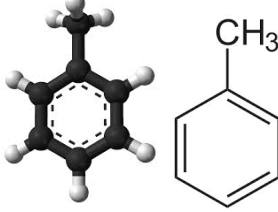
**Table 1.6** Some chemical properties of methyl tert-butyl ether

Formula	Molecular Weight	Structure	Water solubility	Log K <sub>ow</sub>
C <sub>5</sub> H <sub>12</sub> O	88.15	$\begin{array}{c} \text{CH}_3 \\   \\ \text{H}_3\text{C}-\text{C}-\text{O}-\text{CH}_3 \\   \\ \text{CH}_3 \end{array}$	43.0 - 54.3 g/L [Mackay et al., 2006]	1.18

Methyl-*tert*-butyl-ether (MTBE) is the most commonly used fuel oxygenate because of its low cost, ease of production, favourable transfer and blending characteristics [Squillace et al., 1996]. It can be produced at the refinery, it blends easily without phase separation in gasoline, and the gasoline blend can be transferred through existing pipelines. Feedstock for MTBE includes isobutylene and methanol. It is a widely used octane enhancing fuel additive which constitutes an important environmental pollutant due to its high aqueous solubility (43 000 – 54 300 mg L<sup>-1</sup>), low Henry’s law constant (0.023 – 0.12 dimensionless), low vapour pressure ( $\approx$  43 mg L<sup>-1</sup> and 249 mmHg at 25 °C), small molecular size and high resistance to biodegradation [Mackay et al., 2006; Squillace et al., 2009]. MTBE sources include gasoline leaking from underground fuel-storage tanks, watercraft and urban runoff. In contrast with other gasoline components like BTEX compounds, MTBE is less adsorbable in soils while is highly soluble in mobile water in ground water [Achten et al., 2002; Moulijn et al., 2001]. This pollutant has recently been reported in surface waters, in groundwater and in urban storm water [Johnson et al., 2000]. Such widespread occurrences, combined with possible human carcinogenic effects [Amberg et al., 2001; OEHHA Office of Environmental Health Hazard Assessment, 1999], have led the US Environmental Protection Agency (EPA) to estimate that MTBE levels in drinking water should not exceed 20 µg L<sup>-1</sup> in terms of odour and 40 µg L<sup>-1</sup> in terms of taste [US EPA, 1997].

## TOLUENE

**Table 1.7** Some chemical properties of toluene

Formula	Molecular Weight	Structure	Water solubility	Log $K_{ow}$
$C_7H_8$	92.15	 The structure column contains two representations of toluene. On the left is a ball-and-stick model showing a benzene ring with a methyl group attached. On the right is a skeletal structure of a benzene ring with a methyl group (CH <sub>3</sub> ) attached to the top carbon.	0.47 g/L	2.69

Toluene occurs as a colorless, flammable, refractive liquid, that is slightly soluble in water. The major use of toluene is as a mixture added to gasoline to improve octane ratings. It is employed to produce benzene and as a solvent in paints, coatings, synthetic fragrances, adhesives, inks and cleaning agents. Toluene is also used in the production of polymers used to make nylon, plastic soda bottles. Automobile emissions are the principal source of toluene to the ambient air but it may also be released to the ambient air during the production, use and disposal of industrial and consumer products that contain this compound. For what concerns health effects, EPA found toluene to potentially cause both short-term and long-term adverse effects [US-EPA Toluene]. Available studies in workers have reported limited or no evidence of the carcinogenic potential of toluene.

Toluene released to soil will be lost by evaporation from near-surface soil and by leaching to the groundwater. Its breakdown by soil microbes is slow. Toluene evaporates within a few hours when released to water, and it has little tendency to accumulate in aquatic life. In addition, toluene could be removed by biological organisms, through adsorption and bioaccumulation: this removal is certainly slower, especially at high concentrations of hydrocarbon, and can lead to organisms death caused by intoxication.

### **1.4 Natural organic matter**

Efficient technologies turned towards the improvement in water pollutants removal should take into account of compounds which are currently present in natural waters, for example NOM (Natural Organic Matter), and that could influence the removal process.

Our study was undertaken to characterize the adsorption of selected aromatic compounds allelochemicals by microporous materials as part of a broader study on the influence of natural organic matter on adsorption of organic contaminants onto microporous adsorbents. Allelochemicals are low molecular weight compounds secreted into soil by plant tissues and/or decay of plant residues that influence the interaction of plants with other individuals of the same species, other plant species, microbes, viruses, or insects. Allelochemicals play an important role in agricultural and ecological dynamics. An important class of allelochemicals is the single-ring “phenolic monomers”, which are described in the followings.

#### **1.4.1 Lignin-derived phenolic monomers**

Lignin-derived phenolic monomers commonly isolated from plant cell walls include derivatives of cinnamic and benzoic acids, benzaldehyde and acetophenone.

Monomeric phenolic compounds are ubiquitous in the environment accounting for up to 10% of the dissolved organic carbon in soil. Phenolic compounds of natural origins are derived from microbial degradation of biomass (especially plant residues), microbial synthesis and plant root exudation. Phenolic monomers accumulate in all the organs of the plant and such accumulation occurs specifically in the various tissues according to types of plant. With the exception of lignin, phenolic compounds accumulate preferentially in the aerial organs of the plant (stems, leaves, flowers and fruits) rather than in roots. This preferential localization is related with the effect of sunlight on the phenolic metabolism and with the protective role carried out by phenolic compounds against ultraviolet radiation.

Their presence in the environment is further enhanced by anthropic activities because wastewater irrigation and solid-compost application of industrial waste also introduce phenolic compounds (including chlorinated and nitrified phenols) into the environment, as phenolic compounds are widely used as intermediates in production processes [Li et al., 2012]. Domestic wastewaters can be a further source of phenolic compounds because of their use in several classes of pharmaceuticals.

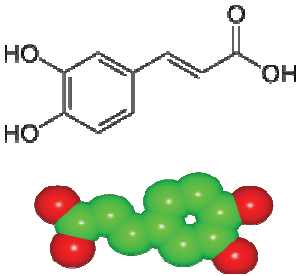
The phenol derivatives in the environment go under the processes of humification and the monomers are precursors of humic substances. Humic substances (HS) are major components of NOM in soil and water as well as in geological organic deposits such as lake sediments, peats, brown coals and shales. They make up much of the characteristic brown colour of decaying plant debris and contribute to the brown or black color in surface soils. They are major components of NOM in surface waters and at higher

concentrations can impart a dark colour, especially in brown fresh water ponds, lakes and streams. Humic substances are very important components of soil that affect physical and chemical properties and improve soil fertility. In aqueous systems, like rivers, about 50% of the dissolved organic materials are HS that affect pH and alkalinity. In terrestrial and aquatic systems HS influence the chemistry, cycling and bioavailability of chemical elements, as well as transport and degradation of xenobiotic and natural organic chemicals. They affect biological productivity in aquatic ecosystems, as well as the formation of disinfection by-products during water treatment. Humic substances are complex and heterogeneous mixtures of polydispersed materials formed by biochemical and chemical reactions during the decay and transformation of plant and microbial remains (a process called humification). Plant lignin and its transformation products, as well as polysaccharides, melanin, cutin, proteins, lipids, nucleic acids, fine char particles, etc., are important components taking part in this process. Humic substances in soils and sediments can be divided into three main fractions: humic acids (HA), fulvic acids (FA) and humin. The HA and FA are extracted from soil and other solid phase sources using a strong base. Humic acids are insoluble at low pH and they are precipitated by adding strong acid. Humin cannot be extracted with either a strong base or a strong acid. Most of the data on HA, FA and humin refer to average properties and structure of a large ensemble of components of diverse structure and molecular weight. The precise properties and structure of a given HS sample depends on the water or soil source and the specific conditions of extraction.

The selected phenolic monomers are caffeic acid and p-hydroxybenzaldehyde. They can be found in natural waters not only because they derive from lignin but also because they are employed in pharmaceutical and cosmetic formulations: hence they could also be classified as emerging contaminants even if no adverse health effects have been observed for these compounds.

## CAFFEIC ACID

**Table 1.8** Some chemical properties of caffeic acid

Formula	Molecular Weight	Structure	Water solubility	pK <sub>a</sub>	Log K <sub>ow</sub>
C <sub>9</sub> H <sub>8</sub> O <sub>4</sub>	180.16		Soluble in hot water	pK <sub>a1</sub> = 4.36 pK <sub>a2</sub> = 8.48 pK <sub>a3</sub> = 11.38	1.15

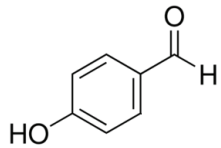
The caffeic acid (3,4-dihydroxycinnamic acid) is an organic acid derived by 4-hydroxycinnamic acid and its fundamental structure is the catecholic ring (1,2-dihydroxybenzene). The caffeic acid was so named because it was originally found in coffee extracts. The molecule, as is or as derivatives is present in a wide variety of foods and beverages [Wang et al., 2008]. Hydroxycinnamic acid derivatives are widely distributed in the plants and may have an important role in the overall mechanism of defense against infections. The possible employ of hydroxycinnamic acid derivatives as natural antioxidants has attracted attention because of their ubiquitous presence in nature. The caffeic acid is the most abundant phenolic acid in the seeds of many plant species and largely influences the solubility of proteins in plants.

The caffeic acid belongs to a class of natural substances which has been proven to have significant value in medical and pharmaceutical industries. In fact, many studies are focused on its antioxidant [Yoon et al., 2012; Xu et al., 2005; Raneva et al., 2001;], antibacterial [Tsou et al., 2000; Lo et al., 1999], anti-inflammatory [Giovannini et al., 2002], antiviral [Bailly et al., 2005], antimetastatic and antitumor [Perez-Alvarez et al., 2001; Chung et al., 2004] properties. It has been also demonstrated that caffeic acid is useful in skin protection from the harmful effects of UV radiation and in particular of those most dangerous (UV-B and UV-C).



PARA-HYDROXYBENZALDEHYDE

**Table 1.9** Some chemical properties of para-hydroxybenzaldehyde

Formula	Molecular Weight	Structure	Water solubility	pK <sub>a</sub>	Log K <sub>ow</sub>
C <sub>7</sub> H <sub>6</sub> O <sub>2</sub>	122.12		1.3 g/L	7.72	1.38

Para-hydroxybenzaldehyde is one of the three isomers of hydroxybenzaldehyde. It can be found in some orchids and in vanilla. Benzaldehyde, the simplest representative of the aromatic aldehydes, is a key intermediate for the processing of perfume and flavouring compounds and in the preparation of certain aniline dyes. Benzaldehyde can have carcinostatic or antitumor properties [Andersen 2006; Liu et al., 2008]. Hydroxybenzaldehydes are used primarily as chemical intermediates for a variety of products. Out of the three isomers, ortho-hydroxybenzaldehyde (or salicylaldehyde) is used in the manufacture of coumarin [Mishra et al., 2013], which is used in soaps, flavors and fragrances, electroplating.

Para-hydroxybenzaldehyde seemed to be the main responsible for ammonium oxidation inhibition and its oxidation the limiting step in p-cresol mineralization by the nitrifying consortium. It should be minded that in nitrogen removal from wastewaters, nitrification is commonly the rate-limiting step of the overall nitrogen removal [Silva et al., 2009]. High sensitivity of nitrifying bacteria to the toxic or inhibitory effects of organic compounds is well-known. Inhibitory effects of phenolic compounds on the nitrification process have been previously reported [Texier and Gomez, 2002; Amor et al., 2005]. Finally, para-hydroxybenzaldehyde could be found in olive mill wastewater generated by the olive-oil extracted industry [Lafont et al., 1999; Aktas et al., 2001]. These wastewaters are considered as pollutants because of their high organic load and also phytotoxic and antibacterial phenolic substances which resist biological degradation.

## CHAPTER 2

### Porous silica materials

#### 2.1 Zeolites

The history of zeolites began in 1756 when the Swedish mineralogist Cronstedt discovered the first zeolite mineral, stilbite. He recognized zeolites as a new class of minerals consisting of hydrated aluminosilicates of the alkali and alkaline earths. Since the crystals exhibited intumescence when heated in a blowpipe flame, Cronstedt called the mineral “zeolite” because the term derived from two Greek words, “zeo” and “lithos” meaning “to boil” and “stone” respectively. Natural zeolites occur in many regions of the world and over 170 types of synthetic zeolites are known.

Zeolites are microporous inorganic crystalline materials with uniform pore dimensions. The zeolite framework consists of  $TO_4$  tetrahedra units, where T is predominantly either a Si(IV) or Al(III) atom located at the centre of the tetrahedron. Other T-atoms, such as Fe, Ti, Ge, Ga and Se, can be incorporated usually in small amounts, as impurities and for special purposes. Tetrahedral units are joined together in various regular arrangements through shared oxygen atoms, to form an open crystal lattice containing pores of molecular dimensions into which guest molecules can penetrate (see Figure 2.1).

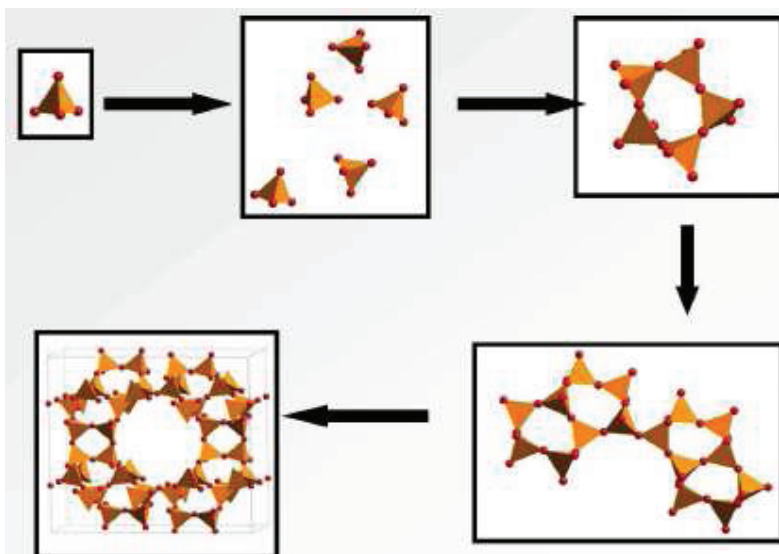


**Figure 2.1** From  $TO_4$  tetrahedra to a 12-ring channel

A description of zeolite structure almost always begins with a description of the framework type in terms of the size of the pore opening and the dimensionality of the channel system. A three-letter code is assigned to confirmed framework types by the Structure Commission on Zeolite Association according to rules set up by an IUPAC Commission on Zeolite Nomenclature. The codes are normally derived from the name of the zeolite or “type material”, e.g. FAU from the mineral faujasite.

Pore-opening are characterized by the size of the ring which defines the pore, designed as n-ring where n is the number of T-atoms in the ring. The pore size regularity makes zeolites different from other molecular sieves such as the microporous charcoal and amorphous carbon. Zeolite pore openings range from 3 to  $> 7 \text{ \AA}$  depending on the framework structure [Szostak 1998].

The crystalline zeolite framework carries a negative charge and its magnitude depends on the amount of isomorphically substituted Al(III). This charge is balanced by cations localized in non-framework positions (incavities or channels) to obtain a neutral net charge of the structure.

Typical cations include the alkaline ( $\text{Li}^+$ ,  $\text{Na}^+$ ,  $\text{K}^+$ ,  $\text{Rb}^+$ ,  $\text{Cs}^+$ ) and the alkaline earth ( $\text{Mg}^{2+}$ ,  $\text{Ca}^{2+}$ ,  $\text{Ba}^{2+}$ ) cations, as well as  $\text{NH}_4^+$ ,  $\text{H}_3\text{O}^+$ ,  $\text{TMA}^+$  (tetramethylammonium) and other nitrogen-containing organic cations [Szostak 1998]. The framework charge and cations are important as they determine the ion exchange properties of the material. Zeolites with low Al content or constituted exclusively of Si in the tetrahedral sites have low negative or neutral framework charge and therefore exhibit a high degree of hydrophobicity and poor ion exchange capacity [Szostak 1998]. The zeolite’s degree of hydrophobicity increases with  $\text{SiO}_2/\text{Al}_2\text{O}_3$  ratio (named silica alumina ratio - SAR) and their pore size and geometry relative to the size of the organic in consideration play a role in determining the suitability of zeolites for the removal of organic contaminants from aqueous solutions [Giaya et al., 2000; Erdem-Senatalar et al., 2004; Kawai et al., 1994; Li et al., 2003].

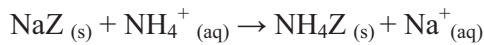
By appropriate choice of framework structure,  $\text{SiO}_2/\text{Al}_2\text{O}_3$  ratio and cationic form, adsorbents with widely different adsorptive properties can be prepared. It is therefore possible, in certain cases, to tailor the adsorptive properties of zeolite materials to achieve the adsorption selectivity required for a particular application.

### **2.1.1 Properties**

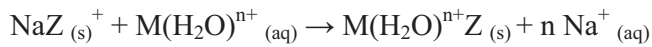
#### **CATALYTIC ACTIVITY**

Zeolites as solid acids and bases are characterized by the type (Brønsted or Lewis acid sites), the concentration (number of sites: extensive factor) and the strength of the acid sites (intensive factor). Type and concentration of the acid sites are mainly governed by the location of Al at the framework (tetrahedral positions) and non-framework position. The strength of Brønsted acid site increases with the Al content and it is higher for isolated Al-O tetrahedra. It has been demonstrated that the acidity increases for Al amount lower of 15 mol %; at higher Al concentration, when Al tetrahedra begin to have next nearest neighbours, the acidity decreases [Čejka et al., 2007]. The Lewis acidity is mainly associated to the presence of three-coordinated Al, which can accept an electrons pair and acts as a Lewis acid. In industrial processes based on the use of zeolites as catalysts, it is often necessary to produce Brønsted acid sites and hence hydroxyl groups inside the structure. These can be formed by exchange with ammonium or polyvalent cations followed by calcination, as represented as follows:

a) Ammonium exchange



b) Polivalent cations exchange



The simplified mechanism of formation of Lewis and Brønsted acid sites is shown in Figure 2.2.

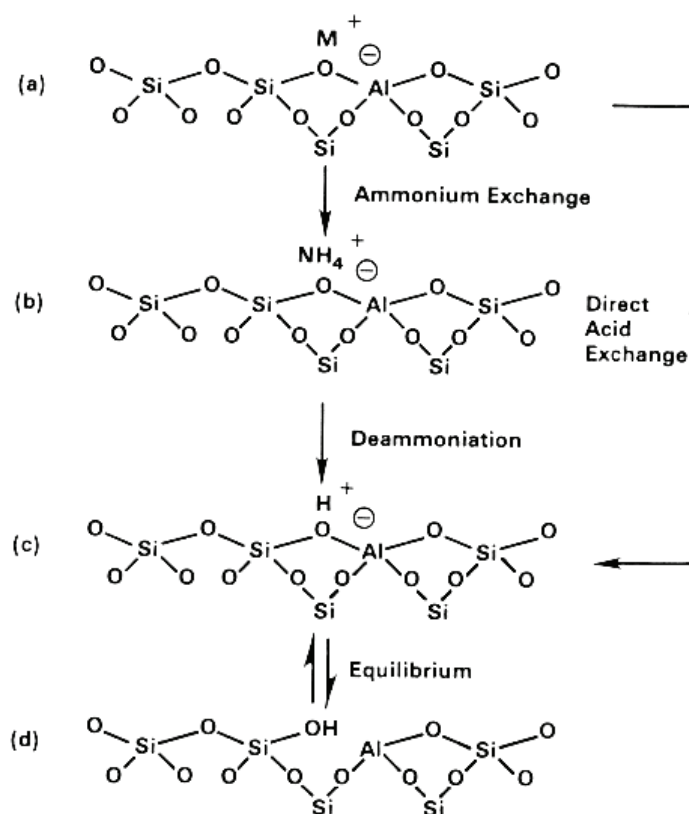


**Figure 2.2** Formation of Brønsted and Lewis acid sites in a zeolite: (a) as synthesized zeolite, where  $M^+$  represents a generic cation; (b) ionic exchange with  $NH_4^+$ ; (c) thermal treatment to produce the acid form of zeolite, which is in equilibrium with the form shown in (d)

Usually, metal cations (in natural and synthetic zeolites) or organic cations (only in synthetic ones) balance the charges in the framework (Step a of Figure 2.2). By exchanging these cations, partially or totally, commonly through an acidic solution of ammonium (Step b of Figure 2.2) or by polyvalent cations, the precursors of the H-zeolites, the  $NH_4$ -zeolites, are formed. Through a subsequent thermal treatment, said calcination,  $NH_3$  is eliminated (Step c of Figure 2.2) and H-zeolites are obtained. After the calcination, the positive charges extraframework are due to protons which constitute OH groups. Ideally, in these protonated forms, hydroxyls bind to framework oxygens in a bond Si-O-Al, thus generating Brønsted sites. At temperatures higher than  $200^\circ C$ , protons have great mobility and, as pointed out by thermal analysis, at approximately  $550^\circ C$  they leave the structure as water molecules giving rise to Lewis acid sites (Step d of Figure 2.2): in this case, the zeolite interacts with the adsorbed molecule as acceptor of an electrons pair.

The presence of hydroxyl groups, which balance the negative charges inside the tetrahedral framework and which are responsible of Bronsted acidity, are mainly due to Al content and hence to the SAR ratio.

### CATIONIC EXCHANGE

Zeolites having an high Al content show high ionic exchange capacity of their extra-framework cations: as represented in Figure 2.3, extra-framework cations can be reversibly substituted with other cations.

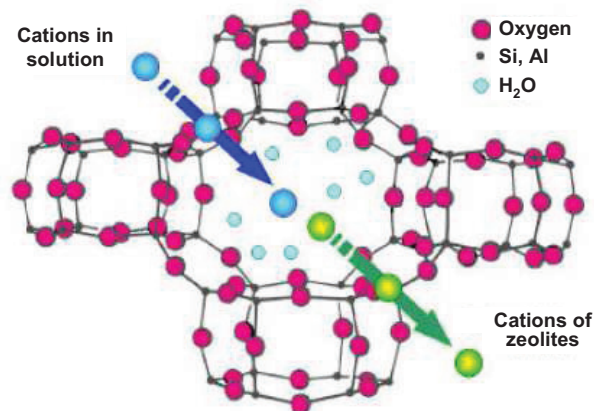


**Figure 2.3** Representation of cationic exchange

Cationic exchange leads to extraction from solutions of ions which better fit to zeolitic structure, based on their charge, ionic radius and dimension: this feature represents the high selectivity of zeolites towards host ions or molecules.

### SHAPE SELECTIVITY

One of the most important features of zeolites is their highly selective adsorption towards host molecules, strongly affected by the internal pore structure, especially shape and dimension of channels and cages. Adsorption phenomena are found in many domains including catalysis, pollution control, gas separation and storage. Recent environmentally driven applications have arisen using the hydrophobic molecular sieves as adsorbent for the removal and recovery of VOCs which offers the promise of significant market growth. A new scientific direction has emerged over the last few years for exploring molecular sieves as advanced solid state materials: this research includes zeolite electrodes, batteries and chemical sensors [Čejka et al., 2007; Van Bekkum et al., 2001].

### STABILITY

The most widely used methods to characterize the thermal behaviour and the dehydration processes in zeolites are thermogravimetric analysis (TG and DTG) and differential thermal analysis (DTA). With dehydration, the extra-framework cations tend to change their coordination sites and, in general, weakly polarizing cations migrate towards oxygen atoms of the framework, after the loss of water molecules. The deformation of the framework after migration of the cations tends to increase with the decrease of the cationic radius of the exchangeable ions. In general, the thermal stability of zeolites is controlled by factors such as:

- a) SAR. The thermal stability increases with increasing silicon content: the energy required for the break of an Al-O bond is minor than that necessary for the breaking of a Si-O bond.
- b) Extra-framework cations. Zeolites abundant in alkali cations, in particular  $K^+$ , are more thermally stable than the ones abundant in  $Ca^{2+}$ .
- c) Framework topology. The critical parameter for the thermal stability of the framework is given by the angular values T-O-T: isometric rings are more stable than stretched or distorted rings, which are characterized by small angles T-O-T.

Zeolites are expected to remain active for long periods of time, despite that their replacement or regeneration is easily achieved. After adsorption, the exhausted zeolites are normally subjected to a regeneration process by operating at temperatures ranging from 250° to 350°C, for a time ranging from 30 minutes to 1.5 hours, and in the presence of an air flow. Under these particularly mild conditions zeolite materials maintain their structural integrity, so that they can be regenerated several times without substantially modifying their adsorbing properties.

### AVAILABILITY AND COST

Considerable quantities of both natural or synthetic zeolites can be purchased at low prices.

### ENVIRONMENTAL COMPATIBILITY

It is important that the reactive media does not form any by products when reacting with contaminants and that it is not a source of contamination itself by solubilisation or other mobilization mechanisms. Respect activated carbon, several zeolites are environmentally friendly materials because of their chemical composition.

### 2.1.2 Applications

Applications of zeolites and molecular sieves in the 80's and 90's showed a growth in petroleum refining applications with an emphasis on resid cracking (Figure 2.4) and octane enhancement: this is mainly due to the zeolites surface acidity. Zeolites confine molecules in small spaces, which causes changes in their structure and reactivity. The hydrogen form of zeolites are powerful solid-state acids and can facilitate a host of acid-catalyzed reactions, such as isomerisation, alkylation and cracking.

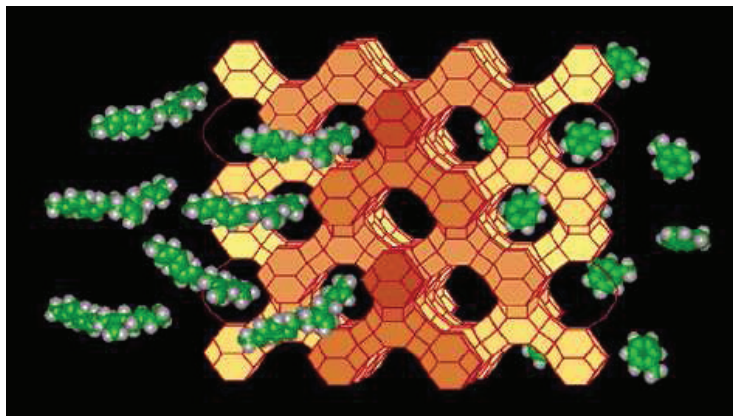


**Figure 2.4** Representation of hydrocarbons cracking by Y zeolite

ZSM-5 was commercialized as an octane enhancement additive in fluid catalytic cracking (FCC) where Si-enriched Y zeolites serve as the major catalytic component in high-octane FCC catalysts.

The use of zeolite catalysts in the production of organic (fine) chemicals appeared as a major new direction, because if zeolite has high silica content in the framework, it resists at the high temperatures that occur during catalytic and regeneration cycles.

Some zeolites characterized by high ion exchange capacity are used to purify waters and to remove toxic metal cations; this property also allowed Sr, Cs and other radioisotopes to be scavenged from nuclear waste [Vignola et al., 2009; Vignola et al., 2005; Čejka et al., 2007]. Zeolites are also used in the management of leaks of radioactive materials.

Zeolites with maximum cationic exchange capacity are of interest as detergents in removing from water calcium and magnesium which hinder washing efficiency. In past years, this function has been performed mainly by phosphates which are now discouraged by environmental pressures because they favour eutrophication in natural waters.

Thanks to their environmental friendly composition, some natural zeolites can be also employed in agriculture as source of slowly released potassium or nitrogen.



### **2.1.3 Characterization**

#### **THERMAL ANALYSIS**

A common technique to characterize zeolites is thermal analysis, where the properties of materials are studied as they change with temperature. There are several methods belonging to thermal analysis family and each one is distinguished from one another by the property which is measured.

Thermogravimetric analysis (TGA) is a method of thermal analysis in which changes in weight of the sample are measured as a function of increasing temperature (with constant heating rate), or as a function of time (with constant temperature and/or constant mass loss). TGA can provide information about physical phenomena, such as second-order phase transitions, including vaporization, sublimation, absorption, adsorption and desorption. Likewise, TGA can provide information about chemical phenomena including chemisorptions, desolvation (especially dehydration), decomposition and solid-gas reactions (e.g., oxidation or reduction).

TGA is commonly used to determine selected characteristics of materials that exhibit either mass loss or gain due to decomposition, oxidation or loss of volatiles (such as moisture). Common applications of TGA are materials characterization through analysis of characteristic decomposition patterns, studies of degradation mechanisms and reaction kinetics, determination of organic or inorganic content in a sample, which may be useful for corroborating predicted material structures or simply used as a chemical analysis. When TG analysis is applied to the study of adsorption onto a solid material, it should be minded that weight losses at temperature below 100°C are ascribed to species adsorbed solely on the external surface, while weight losses at major temperatures could be due to species adsorbed at a structural level. In this last case, it is not possible to discriminate between structural water and the solute under investigation.

Differential thermal analysis (or DTA) is a thermoanalytic technique, where the material under study and an inert reference are made to undergo identical thermal cycles, while recording any temperature difference between sample and reference. This differential temperature is then plotted against time, or against temperature. Changes in the sample, either exothermic or endothermic, can be detected relative to the inert reference. Thus, a DTA curve provides data on the transformations that have occurred, such as glass transitions, crystallization, melting and sublimation. The area under a DTA peak is the enthalpy change and is not affected by the heat capacity of the sample. A DTA curve can be used only as a *finger print* for identification purposes but usually the applications

of this method are the determination of phase diagrams, heat change measurements and decomposition in various atmospheres.

### X-RAY DIFFRACTION

Powder diffraction techniques are used on a routine basis by many zeolite scientists. Probably the most common application is the use as “fingerprint” in the identification of synthetic products [Čejka et al., 2007].

A powder diffraction pattern has several features that can be of interest to a zeolite scientist: the peak positions, their relative intensities, their widths and the background.

The peak position in a powder diffraction (usually measured in  $2\theta$ ) are determined only by geometry of the unit cell, which describes the 3-dimensional repeat unit of a crystal structure.

The relative intensities are determined by the type and position of the various atoms within the unit cell. The width of the peaks in the pattern give an indication of the crystalline quality of the sample. Finally the background in a powder diffraction indicates whether or not an amorphous material is present in the sample.

Changes in the relative intensities of the peaks indicate that a structural modification has occurred, changes in the positions of the lines indicate that the unit cell has deformed in some way, broader (or narrower) lines indicate that the crystallinity has deteriorated (or improved). In general, non-framework species have a pronounced effect on the low-angle region of the pattern. For example, a calcined material will tend to have higher relative intensities in this region than the corresponding as-synthesized or loaded sample. The high-angle region is less sensitive to the presence or absence of electron density in the channels and cages and more sensitive to distortions in the framework. More detail can be extracted from the powder pattern if a full Rietveld (whole-profile) structure refinement is performed.

## **2.2 Mesoporous materials**

Mesoporous silicas are inorganic materials synthesized in the presence of surfactants as templates for the polycondensation of silic species, originating from different sources of silica (sodium silicate, alkoxydes like tetraethylortosilicate TEOS and tetramethylortosilicate TMOS). Synthesis conditions such as source of silica, type of surfactant, ionic strength, pH and composition of the reaction mixture, temperature and duration of synthesis affect the surfactant micellar conformation, the silica–surfactant interactions and the degree of silica polycondensation. These conditions determine the

characteristics of the porous structure (type of mesostructure, diameter and volume of the pores, wall thickness) and the macroscopic morphology [Giraldo et al.,1997].

The pore size can be modulated during the synthesis by controlling reaction time and temperature, by using swelling organic molecules like aromatic hydrocarbons and trialkylamines, by adjusting the surfactant and co-cation concentration or by postsynthesis treatment like water-amine treatment or changing the calcinations conditions [Giraldo et al.,1997].

The control of the morphology by the synthesis conditions has been explained by the influence of defects during the nucleation and growth process or by the formation mechanism.

Different types of silanol groups (single, hydrogen-bonded and geminal) are present on the surface of a mesoporous silica. Their content depends on the way by which the surfactants were removed and can be modulated by postsynthesis treatments.

Due to their highly organized porosity, high surface area, high pore volume, tailorable pore size, wall thickness, chemical nature and morphology the mesoporous silica are attractive materials for several applications in catalysis, adsorption, separation, sensing, drug delivering devices and nanotechnology.

## **2.3 Selected materials**

### **ZSM-5 (MFI)**

The most important member of the MFI family is the ZSM-5 zeolite because it possesses unusual catalytic properties and have high thermal stability [Kokotailo et al., 1978]. The pure silica form of ZSM-5 zeolite is known as silicalite. The MFI framework is presented in Figure 2.5. Zeolite ZSM-5 is constructed from pentasil units that are linked together in pentasil chains. Mirror images of these chains are connected by oxygen bridges to form corrugated sheets with ten-ring channel openings.. Oxygen bridges link each sheet to the next to form a three-dimensional structure with straight ten-ring channels parallel to the corrugations along y intersected by sinusoidal ten-ring channels perpendicular to the sheets along z [McCusker et al., 2001]. The minor and major axis dimensions are 5.1 x 5.5 Å for the sinusoidal channels and 5.3 x 5.6 Å for the straight channels (Figure 2.6) [IZA] .

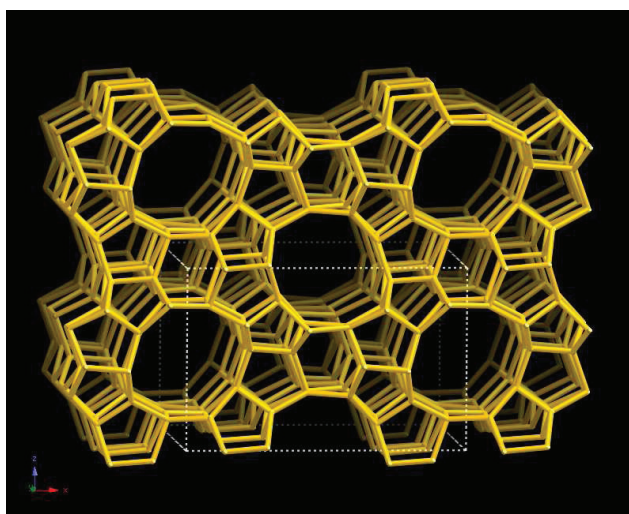
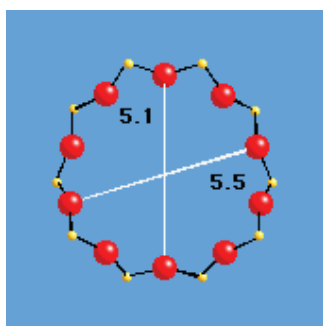
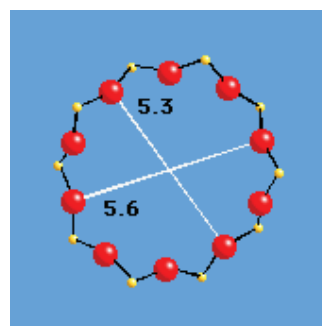


**Figure 2.5** ZSM-5 framework viewed along (010) [IZA]



10-ring viewed along [100]

5.1 x 5.5 Å



10-ring viewed along [010]

5.3 x 5.6 Å

**Figure 2.6** ZSM-5 channels

### BETA (BEA)

Beta zeolite (BEA) is a microporous material with large pores which was synthesized for the first time from Wandlinger et al. for the Mobile Oil Corporation in 1967, by employing tetraethylammonium (TEA) as templating agent [Wandlinger et al., 1967].

The crystalline structure of Beta was first resolved in 1988 by Newsam, who defined this zeolite as a hybrid grown of two distinct but strictly connected structures, that is two different polytypes [Newsman et al., 1988]. The two principal polytypes, named polytype A and polytype B which are shown in Figure 2.7, are tetragonal and monoclinic, respectively; [Newsman et al., 1988] reported that the synthetic Beta zeolite is composed by monoclinic polytype B for its 56%.

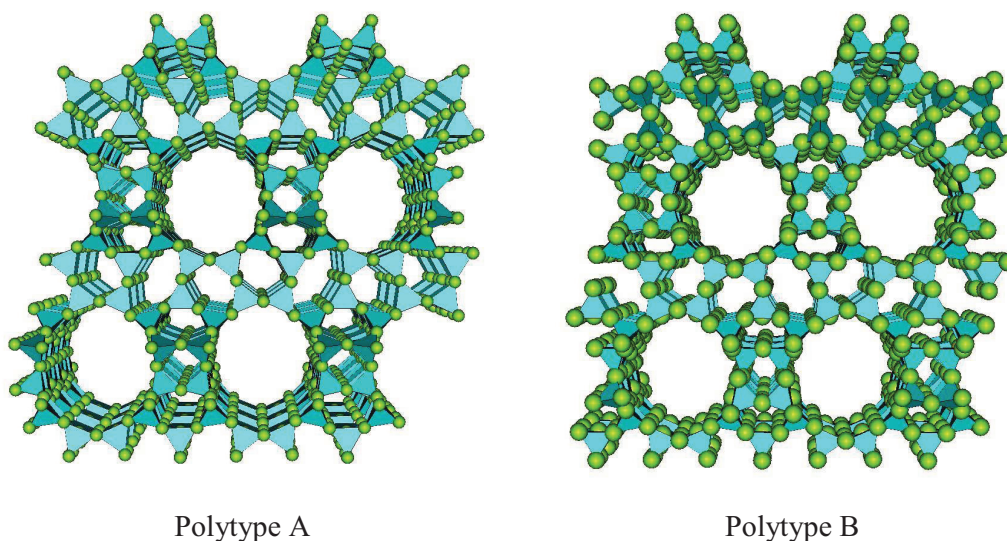


**Figure 2.7** Two polytypes of Beta zeolite

Beta zeolites have well-defined layers comprised of four 5-ring subunits joined by 4-ring subunits that are stacked in a disordered way along the z direction: the whole structure is represented in Figure 2.8. Despite this disorder, a three-dimensional 12-ring channel system is formed [McCusker et al., 2001]. The tetragonal polytype A presents two 12-ring channels highly elliptical, parallel to [100] and [010] directions, with pore dimensions of about  $7.3 \times 5.8\text{-}6.6 \text{ \AA}$ , and a more contorted 12-ring channel parallel to [001] direction, with pore dimensions of about  $5.6\text{-}5.8 \times 5.6\text{-}5.8 \text{ \AA}$  (Figure 2.9) [IZA].

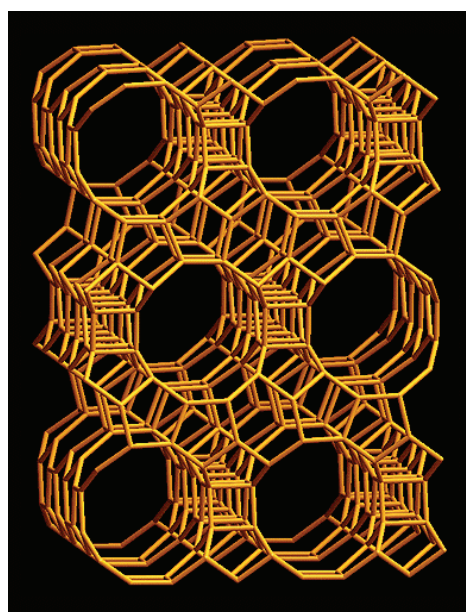


**Figure 2.8** Beta framework viewed along (100) [IZA]

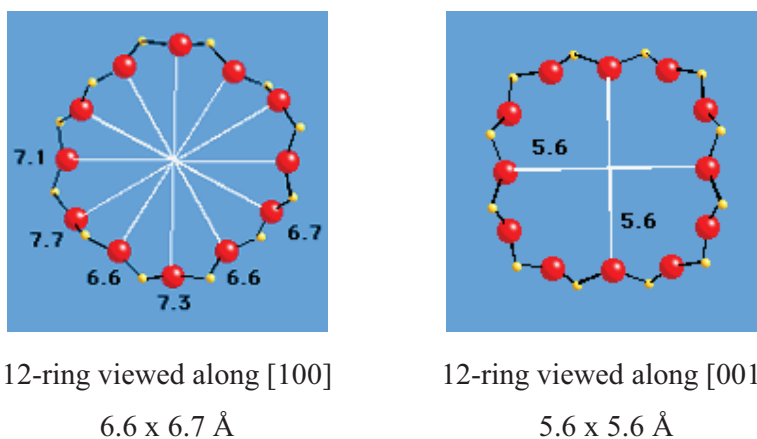


**Figure 2.9** Beta channels in Polytype A

The porous structure and the strong acidity, both as Brønsted and as Lewis sites, make Beta zeolites highly selective towards host molecules and catalytically active, so that it is employed in a huge number of industrial processes.

### Y (FAU)

Breck [Breck, 1964] first discovered the molecular sieve zeolite type Y, with a Si/Al ratio of from 1.5 to 3.0, and a framework topology like that of zeolite X and the rare zeolite mineral faujasite.

The framework of the faujasite structure can be described as a linkage of  $\text{TO}_4$  tetrahedra in a condensed octahedron. The condensed octahedron is referred to as the sodalite unit or sodalite cage. In the faujasite structure (Figure 2.10), the sodalite units are linked together at the 6-ring ends in a manner that is analogous to the arrangement of C-atoms in diamonds. The Y-zeolite (faujasite structure) has circular 12-ring windows with a diameter of 7.4 Å (or 7.4 x 7.4 Å) (Figure 2.11) and supercages with a diameter of about 13 Å [IZA].

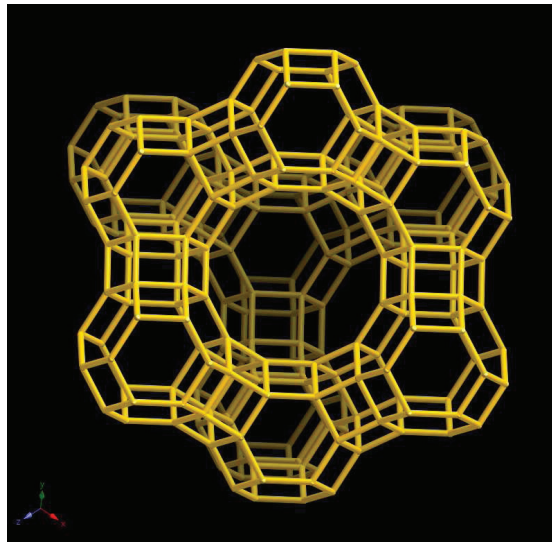
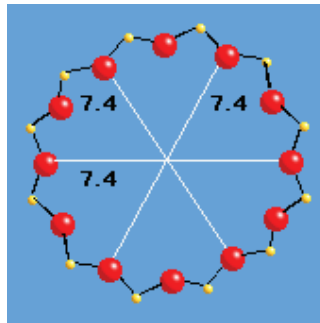


**Figure 2.10** FAU framework viewed along (111) [IZA]



12-ring viewed along [111]

7.4 x 7.4 Å

**Figure 2.11** Y channels

*FERRIERITE (FER)*

Ferrierite [Baerlocher *et al.*, 2001] is a medium pore material whose structure, showed in Figure 2.12, contains cavities known as FER cages, formed by the intersection of the 8-ring channels and the 6-ring channels (parallel to the *c*-axis), usually indicated as  $[5^8 6^6 8^2]$  cages [Baerlocher *et al.*, 2001]. The framework is characterized by 10-ring channels running parallel to the crystallographic [001] direction and by 8-ring channels running parallel to the [010] direction (Figure 2.13).

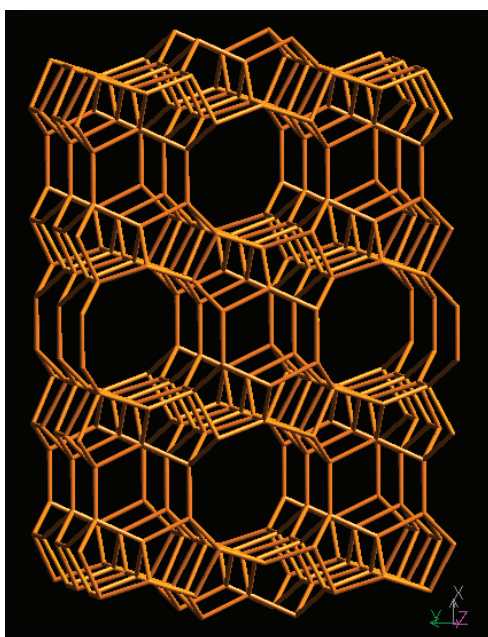
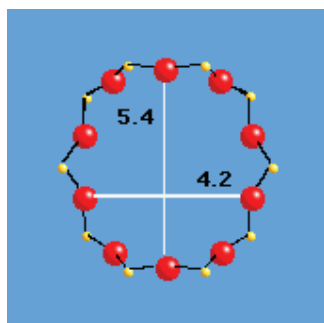
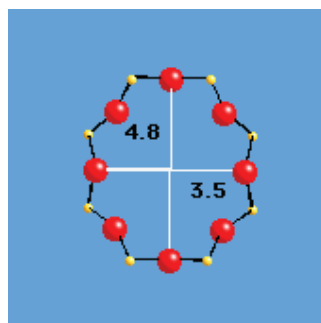


**Figure 2.12** Ferrierite framework viewed along (001) [IZA]



10-ring viewed along [001]  
4.2 x 5.4 Å



8-ring viewed along [010]  
3.5 x 4.8 Å

**Figure 2.13** Ferrierite channels

### MCM-41

A major advance in molecular sieve materials was reported in 1992 by researchers at Mobil. Kresge et al. and Beck et al. describe a new family of mesoporous silicate and aluminosilicate materials (Micelle-Templated Silicas, MTS), designated M41S. One member of this family, MCM-41 (MCM: Mobile Crystalline Material), shows a regular hexagonal array of uniform pores with diameters in the range of 20–100 Å. These materials are synthesized using micellar arrays of templating agents and aluminium can be introduced into their frameworks in tetrahedral coordination (Figure 2.14).



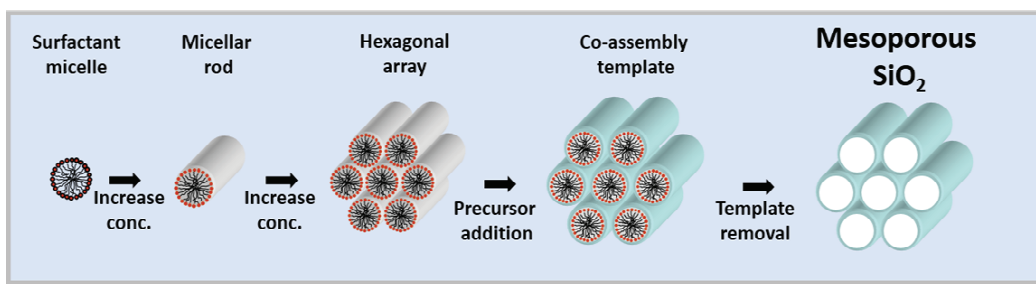


**Figure 2.14** MCM-41 self-assembly

MCM-41 is an acid catalyst and its Si/Al ratio can be varied in a wide range. It cannot only be used for the cracking of heavy oil feedstocks, but also for the processing of fine chemicals in liquid phase reactions because fast diffusion of molecules in the mesopores enables good conversions [Hitz et al.,1997]. Before MCM-41 can be used as a catalyst, large amounts of organic surfactant template must be removed from the pores to make them accessible. Usually the template is burnt during calcination at 540 °C but part of it can be extracted from the silicate framework [Hitz et al., 1997].

### HMS

Another material belong to the MCM-41 class of molecular sieves is HMS (Hexagonal Mesoporous Silica). Its synthesis was described for the first time by Tanev and Pinnavaia [Tanev et al., 1995; Tanev et al., 1996]. The formation of HMS materials is mostly based on hydrogen bonding and self-assembly between neutral primary amine surfactants and neutral inorganic silica precursors (TEOS, tetraethoxysilane). This initial neutral templating route leads, during the formation of the material, to a mixture of neutral and protonated amines inside the silica mesopores due to hydrogen-bonding with silanols and electrostatic interactions of protonated amines (proton transfer from the silica surface to the amine) with  $\text{SiO}^-$ , respectively [Tanev et al., 1996]. The surfactant can be readily removed from HMS mesostructures by solvent extraction or by calcination [Meier et al., 1961; Csicsery et al., 1976].

## CHAPTER 3

### The adsorption process

#### 3.1 Adsorption processes

Adsorption universally means the enrichment of one or more of the components in the region between two bulk phases. One of these phases is a solid (adsorbent or sorbent) and the other is a fluid, i. e. a gas or a liquid. With certain systems, the adsorption process is accompanied by absorption, that is the penetration of the fluid into the solid phase.

The terms adsorption and desorption are often used to indicate the direction from which the equilibrium states have been approached. Adsorption hysteresis arises when the amount adsorbed is not brought to the same level by the adsorption and desorption approach to a given equilibrium pressure or bulk concentration.

In the adsorption process, two kinds of forces are involved, which give rise to either physical adsorption (physisorption) or chemical adsorption (chemisorption), which are characterized by the features summarized in Table 3.1.

**Table 3.1** Principal features of physisorption and chemisorption

PHYSISORPTION	CHEMISORPTION
Low degree of specificity	Dependent on the reactivity of the adsorbent and adsorptive
At high relative pressure, it general occurs as a multilayer	It is usually limited to a monolayer
A physisorbed molecule keeps its identity and on desorption returns to the fluid phase in its original form	If a chemisorbed molecule undergoes reaction or dissociation, it loses its identity and cannot be recovered by desorption
It is always exothermic and the energy involved is not much larger than the energy of condensation of the adsorptive	The energy is the same order of magnitude as the energy change in a comparable chemical reaction

Physisorption systems generally attain equilibrium fairly rapidly, but equilibration may be slow if the transport process is rate-determining	An activation energy is often involved and at low temperature the system may not have sufficient thermal energy to attain thermodynamic equilibrium
-----------------------------------------------------------------------------------------------------------------------------------------------	-----------------------------------------------------------------------------------------------------------------------------------------------------

Adsorption is typically operated as an equilibrium-limited process; the adsorbent must be in equilibrium with the surrounding fluid phase to obtain the maximum adsorption. It is also important to consider the various transport processes involved and the rate at which adsorption occurs.

As a molecule approaches the solid surface, a balance is established between the intermolecular attractive and repulsive forces. The forces responsible for physisorption always include the dispersion attractive interactions and the short-range repulsions. These interactions don't depend on the polar nature of the adsorbent or adsorptive and are regarded as non-specific.

### **3.2 Theory of adsorption**

The earliest studies were focused on gas adsorption on solid phase, due to the greater simplicity than a liquid-solid system. In the case of gas-solid adsorption, the adsorbable specie is a pure compound and no interactions with other components must be considered. The first theoretical elaborations were applied on gas-solid adsorption and only at a later stage they were extended on the much complex liquid-solid systems.

The amount of gas adsorbed by the mass of solid is dependent on the equilibrium pressure, the temperature and the nature of the gas-solid system. Functions describing the relationship between the amount adsorbed by unit mass of solid and the equilibrium pressure (or relative pressure) at a specific and constant temperature (isothermal conditions) are called adsorption isotherms. Several different adsorption isotherm models are available for describing single component as well as n-component systems at constant temperature. The majority of these isotherms which result from physical adsorption may be grouped into six classes in the IUPAC classification, as shown in Figure 3.1.

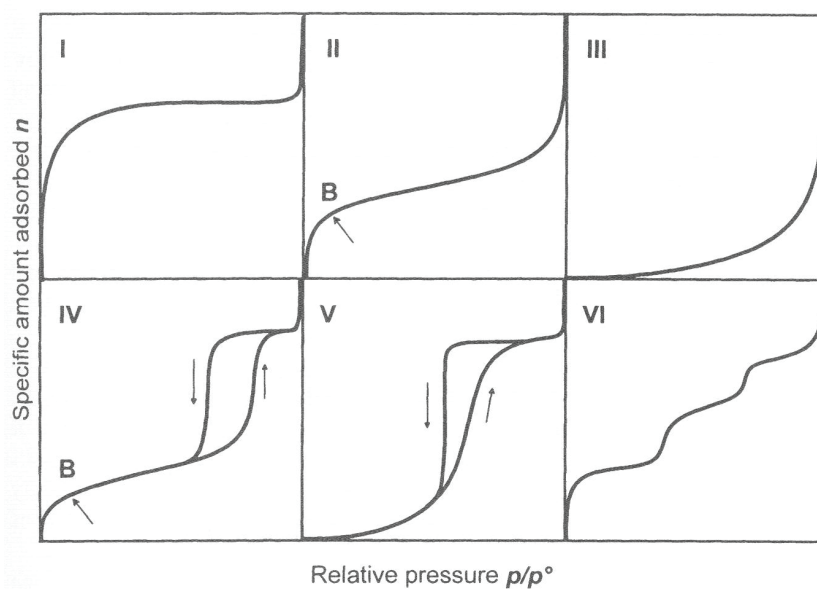


**Figure 3.1** The six main types of gas physisorption isotherms according to IUPAC 1985 classification [Rouquerol et al.]

In Type I isotherm, the amount adsorbed by the unit mass of solid approaches a limiting value as the relative pressure approaches to 1. This isotherm is suitable when adsorbent-adsorbate interactions occur in micropores of molecular dimensions. A decrease in the micropores width results in both an increase in the adsorption energy and a decrease in the relative pressure at which the filling occurs.

The Type II isotherm indicates the formation of an adsorbed layer whose thickness increases progressively with increasing relative pressure. The uptake at point B is usually considered to represent the completion of the monolayer and the beginning of the formation of the multilayer. The ordinate of point B represents the amount of adsorbate required to cover the unit mass of solid surface (monolayer capacity). This isotherm is obtained with non-porous or macroporous adsorbents.

The Type III isotherm is not common and indicates weak adsorbent-adsorbate interactions.

The Type IV isotherm exhibits a hysteresis loop, which is usually associated with the filling and emptying of mesopores.

The Type V isotherm, similarly to Type III isotherm, is rare and is associated with weak adsorbent-adsorbate interactions. This isotherm exhibits a hysteresis loop.

Finally, the Type VI isotherm, which is relatively rare, is associated with layer-by-layer adsorption on a highly uniform surface.

This classification is only applicable to the adsorption of a single-component gas within its condensable range of temperature.

In the text below, an introduction about the thermodynamic quantities for the processing and interpretation of adsorption isotherm is reported.

It can be supposed that the local concentration  $c = dn/dV$  of the adsorbable component decreases progressively with the increased distance  $z$  from the adsorbent surface; at distance  $z = t$  ( $t$  is the thickness of the adsorbed layer), this concentration reaches the constant value of the gas phase  $c^g$ . The volume  $V^a$  of the adsorbed layer can be expressed as

$$V^a = At \quad (3.1)$$

where  $A$  is the interfacial area. The amount adsorbed  $n^a$  in the adsorbed layer is defined as

$$n^a = \int_0^{V^a} c dV = A \int_0^t c dz \quad (3.2)$$

The total amount  $n$  of the adsorbable substance in the whole system can be divided into two contributes, the amount adsorbed and the amount remaining in the gas phase:

$$n = A \int_0^t c dz + c^g V^g \quad (3.3)$$

where  $V^g$  is the volume occupied by the gas at the concentration  $c^g$ . Therefore

$$n^a = n - c^g V^g \quad (3.4)$$

The evaluation of  $n^a$  requires the knowledge of either the exact value of  $V^g$  or of the variation of the local concentration  $c$  with respect to  $z$ , but it isn't easy to attain either of these requirements.

To resolve this problem Gibbs introduced the concept of "surface excess" to quantify the amount adsorbed. A reference system is divided into two zones by an imaginary surface, named Gibbs dividing surface (GDS), which is placed parallel to the adsorbent surface. Surface excess is the difference between the amount of a component actually present in the system and that which would be present in a reference system if the bulk concentration in the adjoining phases were maintained up to a chosen GDS, i.e. as though the interface had no effect. Schematically

$$[n_i]_{\text{surface}} = [n_i]_{\text{real}} - [n_i]_{\text{reference}} \quad (3.5)$$

where  $[n_i]_{\text{surface}} = n_i^\sigma$  is the surface excess amount of component  $i$ ,  $[n_i]_{\text{real}} = n_i$  is the total amount of that component in the real system and  $[n_i]_{\text{reference}}$  is the amount which would

be present in the volume  $V^{g,0}$  of the reference system if the final equilibrium concentration  $c^g$  was constant up to the GDS. Thus

$$n^\sigma = n - c^g V^{g,0} \quad (3.6)$$

It is convenient to locate GDS exactly on the surface which is accessible, so that  $V^{g,0} = V^a + V^g$ . Under these conditions:

$$n^\sigma = n - c^g V^g - c^g V^a \quad (3.7)$$

Combining equation 3.7 with 3.4, it can obtain:

$$n^a = n^\sigma + c^g V^a \quad (3.8)$$

Usually in the experimental conditions the final concentration  $c^g$  of the gas is small and the volume  $V^a$  of the adsorbed layer is negligible compared with the gas volume  $V^g$ , so

$$n^a \approx n^\sigma \quad (3.9)$$

In the case of adsorption from solution, the competition between the solvent and the solute must be taken into account. The adsorption of the solute at the liquid-solid interface is usually evaluated as the decrease in its concentration when kept in contact with the adsorbent. The surface excess amount  $n_i^\sigma$  is defined as

$$n_i^\sigma = n_i - c_i^l V^{l,0} \quad (3.10)$$

where  $n_i$  is the total amount of the component  $i$  in the system,  $c_i^l$  is its concentration in the liquid after adsorption and  $V^{l,0}$  is the volume of the liquid. The surface excess amount depends on the position of GDS because any displacement of the GDS normal to the surface produces a change in the volume  $V^{l,0}$ . In order to replace  $n_i^\sigma$  by a quantity invariant with respect to the position of GDS, equation 3.10 can be written for each component (1 and 2):

$$n_2^\sigma - n_1^\sigma \frac{c_2^l}{c_1^l} = n_2 - n_1 \frac{c_2^l}{c_1^l} \quad (3.11)$$

The variables both on the right and on the left side are independent of the position of GDS; variables on the right are experimental quantities while the ones on the left represent the **relative surface excess** of component 2 respect to component 1 ( $n_2^{\sigma(1)}$ ), defined as

$$n_2^{\sigma(1)} = n_2^\sigma - n_1^\sigma \frac{c_2^l}{c_1^l} \quad (3.12)$$

$$n_2^{\sigma(1)} = n_2 - n_1 \frac{c_2^l}{c_1^l} \quad (3.13)$$

The corresponding equations for the relative surface excess of the component 1 with respect the component 2 are:

$$n_1^{\sigma(2)} = n_1^\sigma - n_2^\sigma \frac{c_1^l}{c_2^l} = n_1 - n_2 \frac{c_1^l}{c_2^l} \quad (3.14)$$

The ratio of concentrations expressed as amounts per unit volume can be replaced by the ratio of molar fractions  $x_2^l/x_1^l$ ; taking into account that  $x_1^l=1-x_2^l$ , equations 3.11 and 3.12 can be transformed as:

$$n_2^{\sigma(1)} = n_2 - n_1 \frac{x_2^l}{x_1^l} = n^\circ \frac{\Delta x_2^l}{x_1^l} \quad (3.15)$$

where  $n^\circ = n_1+n_2$ ,  $n_2 = n^\circ x_2^{l,\circ}$  and  $\Delta x_2^l = x_2^{l,\circ} - x_2^l$  is the change due to adsorption.

Another function independent with respect the position of GDS is the **reduced surface excess** amount and it is derived from equation 3.10 as

$$n_2^\sigma = n_2 - V^{l,\circ} c_2^l \quad (3.16)$$

$$n^\sigma = n_2^\sigma - V^{l,\circ} c^l \quad (3.17)$$

where  $n^\sigma = n_1^\sigma + n_2^\sigma$ ,  $n^\circ = n_1 + n_2$  and  $c^l = c_1^l + c_2^l$ . Replacing  $c_2^l/c^l$  with  $x_2^l$ , the following equation is obtained:

$$n_2^\sigma - n^\sigma x_2^l = n_2 - n^\circ x_2^l = n^\circ \Delta x_2^l \quad (3.18)$$

The right side depends only on experimentally measurable quantities and not on the position of GDS: this function is defined as the reduced surface excess amount of component 2:

$$n_2^{\sigma(n)} = n_2^\sigma - n^\sigma x_2^l \quad (3.19)$$

By combining equations 3.15, 3.18 and 3.19, the relationship between the relative and the reduced surface quantities is obtained

$$n_2^{\sigma(1)} = n_2^{\sigma(n)} / x_1^l \quad (3.20)$$

The reduced surface excess amounts offer the most convenient way of reporting experimental results [Rouquerol et al.]. The quantity plotted to represent adsorption of component 2 is often in the form  $n^\circ \Delta x_2^l$ , according to equation 3.18. The isotherm obtained is generally named “composite isotherm” or “isotherm of apparent adsorption”: the term “composite” refers to the fact that the single isotherm contains information about the adsorption of both components 1 and 2. Figure 3.2 gives the two most important shapes of reduced surface excess isotherms (S-shape and U-shape) for completely miscible liquids.

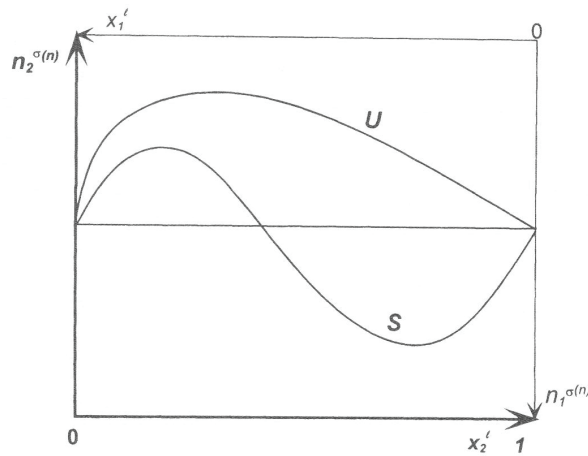


**Figure 3.2** The two basic shapes of reduced surface excess isotherms: S-shaped (S) and inverted U-shaped (U) [Rouquerol et al.]

When the adsorption from dilute solutions is studied, the solvent is considered as component 1 and hence  $x_1^l = 1 - x_2^l \approx 1$ : from equations 3.15, 3.18 and 3.20

$$n_2^{\sigma(1)} \approx n_2^{\sigma(n)} \approx n_2^{\sigma} \quad (3.21)$$

Any of these quantities can be plotted to represent the adsorption data in the isotherm. Although many shapes have been distinguished, three main shapes are particularly interesting and they are represented in Figure 3.3: a L-shaped (analogous to Type I of IUPAC classification) as in the Langmuir or Tóth models, a S-shaped (analogous to Type V of IUPAC classification) as in the Moreau model, or a less common stepwise (analogous to Type VI of IUPAC classification).

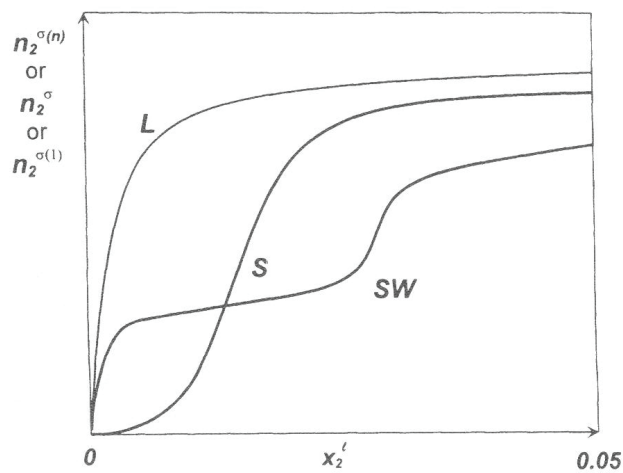


**Figure 3.3** Typical shapes of surface excess isotherms from dilute solutions: L-shaped (L), S-shaped (S) and stepwise (SW) [Rouquerol et al.]



If higher concentrations can be attained, the reduced surface excess eventually reaches a maximum and then decreases as shown in Figure 3.2. However, if the solute solubility is low, the saturation at high concentrations cannot be determined.

### **3.3 Adsorption isotherms**

#### **3.3.1 Ideal adsorption on homogeneous surfaces**

##### *THE LINEAR ISOTHERM*

When a very dilute solution is considered, the adsorption isotherm is usually linear, i. e. the relationship between the adsorbed amount ( $q$ ) and the concentration in solution ( $C$ ) is linear:

$$q = aC \quad (3.22)$$

The proportionality constant ( $a$ ) is referred as the Henry's constant of adsorption. This model is valid when molecules behave independently each others as the free surface available for adsorption is much larger compared to molecular dimensions. At higher concentrations, the molecules compete for the adsorption on an adsorbent surface with finite capacity and other models must be employed.

##### *THE LANGMUIR ISOTHERM*

Langmuir [Langmuir, 1916] proposed a model for adsorption in a gas-solid system. The model extended to liquid-solid systems assumed that an ideal adsorption occurs on homogeneous surface, that the solute is adsorbed in a monolayer and that minimal competition from the solvent takes place. The Langmuir equation for liquid-solid adsorption is

$$q = \frac{q_s b C_e}{1 + b C_e} \quad (3.23)$$

where  $q$  is the amount of solute on one unit of adsorbent,  $C_e$  is the solute concentration at equilibrium,  $b$  is an empirical constant related to the energy of adsorption and  $q_s$  is the saturation capacity (it is the monolayer capacity of the adsorbent,  $\text{mg g}^{-1}$ ). The ratio  $\Theta = q/q_s$  is called the fractional surface coverage. The slope of the isotherm at infinite dilution defines the Henry's constant of the adsorption ( $a = b q_s$ ). Langmuir equation is an excellent approximation for single-component adsorption equilibrium in liquid-solid chromatography.

### **3.3.2 Ideal adsorption on heterogeneous surfaces**

#### **THE BI-LANGMUIR ISOTHERM**

The bi-Langmuir isotherm was first suggested by Graham [Graham 1953] to account for adsorption behaviour on certain inhomogeneous surfaces, in particular on a mixed surface covered with two different kinds of chemical groups [Guiochon et al., 1994]. With such a surface covered with two different kinds of sites which behave independently, the equilibrium isotherm results from the addition of the two independent contributions of the two sites [Stanley et al., 1995]. Such an isotherm is called a bi-Langmuir isotherm. Since in most cases the Langmuir isotherm is appropriate to account for single-component adsorption on a homogeneous surface, the following isotherm is obtained:

$$q = \frac{q_{S1}b_1C_e}{1+b_1C_e} + \frac{q_{S2}b_2C_e}{1+b_2C_e} \quad (3.24)$$

where 1 and 2 refers to the type of adsorption sites.

#### **THE TÓTH ISOTHERM**

The Tóth isotherm [Tóth 1971] was originally derived for the study of gas-solid equilibria, however, like the Langmuir isotherm model, it can be extended to the description of liquid-solid system. The Tóth isotherm accounts for adsorption on a heterogeneous surface, with no adsorbate-adsorbate interactions. The equation of the Tóth isotherm is:

$$q = \frac{q_s b C_e}{[1 + (b C_e)^n]^{1/n}} \quad (3.25)$$

This isotherm is similar to the Langmuir model, to which it becomes identical for  $n = 1$ : this parameter accounts for the heterogeneity of the distribution of adsorption energies.

#### **THE FOWLER-GUGGENHEIM ISOTHERM**

The Fowler isotherm was designed by Fowler and Guggenheim [Guiochon et al., 1994] to correct for the first-order deviation from the Langmuir isotherm. It assumes ideal adsorption on localized sites with weak interaction between molecules adsorbed on neighbouring sites. It also assumes that the interaction energy between two solute molecules is small enough that the random character of the solute molecule distribution on the adsorbent surface is not significantly altered. Under these assumptions, the following equation is obtained:

$$\Theta = \frac{KC_e \exp(\alpha\Theta)}{1 + KC_e \exp(\alpha\Theta)} \quad (3.26)$$

where  $\Theta = q/q_s$ , K is the adsorption constant and  $\alpha$  is the interaction coefficient: if  $\alpha > 0$  the interactions between adsorbed molecules are attractive, if  $\alpha < 0$  repulsive interactions take place.

### THE FREUNDLICH ISOTHERM

The Freundlich isotherm equation is an empirical equation and may be derived by assuming a heterogeneous surface with adsorption on each class of sites that have obeyed the Langmuir equation [Tóth 1971]. The Freundlich equation is commonly used as

$$q = KC_e^{1/n} \quad (3.27)$$

where q is the adsorption capacity, C is the adsorption equilibrium concentration and K and n are empirical constants, which depend on the nature of adsorbent and adsorbate and on the temperature.

The Freundlich isotherm accounts for the adsorption of strongly polar compounds on polar or strongly polar adsorbents (inhomogeneous surface) in low- or medium polarity solvents, but it isn't restricted to the formation of monolayers [Guiochon et al., 2006]. If  $n = 1$  the adsorption is linear: this means that the adsorption sites are homogeneous (as in the Langmuir model) in energy and no interaction take place between the adsorbed species. If  $1/n < 1$  then the sorption capacity increases and new adsorption sites occur, reflecting favourable adsorption. When  $1/n \gg 1$ , the adsorption bond becomes weak: unfavourable adsorption takes place, as a result of the decreasing adsorption capacities [Safa Özcan et al., 2004].

### THE LANGMUIR-FREUNDLICH ISOTHERM

The Langmuir-Freundlich isotherm is an empirical isotherm and it is a combination of two classical models, the Langmuir and the Freundlich models discussed earlier:

$$q = q_s \frac{(KC_e)^v}{1 + (KC_e)^v} \quad (3.28)$$

where v is the heterogeneity parameter. This model, at low concentration, reduces to the Freundlich isotherm, but it reduces to the Langmuir model for the case of a homogeneous surface. This model has been used in simple studies of the adsorption behaviour on heterogeneous surfaces.

### **3.3.3 Non-ideal adsorption on homogenous surfaces**

Depending on the extent of solute-solute interactions, the isotherm is convex or S-shaped. Common models are the quadratic, the extended BET and the Moreau isotherms. All of these tend toward the Langmuir model when the solute-solute interactions tend towards zero.

#### **THE QUADRATIC ISOTHERM**

This model is valid when adsorbate-adsorbate interactions are not negligible.

$$q = q_s \frac{C_e(b + 2cC_e)}{1 + bC_e + cC_e^2} \quad (3.29)$$

where  $q_s$  and  $b$  represent the saturation capacity and the adsorption constant, respectively, while the parameter  $c$  accounts for the cooperation between adsorbed molecule.

#### **THE BET ISOTHERM**

The Brunauer-Emmet-Teller (BET) isotherm developed by Brunauer et al. (1938) is one of the most successful models to express adsorption phenomena [Ebadi et al., 2009]. It assumes that the solute molecules can be adsorbed from the solution onto either the bare surface of the adsorbent or a layer of solute already adsorbed. The expression is:

$$q = q_s \frac{K_s C_e}{(1 - K_l C_e)(1 - K_l C_e + K_s C_e)} \quad (3.30)$$

where  $K_s$  and  $K_l$  are the equilibrium constants of adsorption of the compound on the bare surface and on a layer of adsorbate previously adsorbed, respectively. However, both constants are related to the strength of the solute-solute interactions. If  $K_l C_e \ll 1$ , the system can be described by a simple adsorbed monolayer, that is the Langmuir isotherm.

#### **THE MOREAU ISOTHERM**

The Moreau isotherm is the simplest model for a homogeneous adsorbent surface with lateral interactions (i.e. adsorbate-adsorbate). The equation is:

$$q = q_s \frac{K_r C_e + I(K_r C_e)^2}{1 + 2K_r C_e + I(K_r C_e)^2} \quad (3.31)$$

where  $q_s$ ,  $K_r$  and  $I$  are the monolayer saturation capacity, the equilibrium constant at infinite dilution and the adsorbate-adsorbate interaction parameters, respectively. The adsorbate-adsorbate parameter  $I$  can be written as:

$$I = \exp\left(\frac{\varepsilon_{AA}}{RT}\right) \quad (3.32)$$

where  $\varepsilon_{AA}$  is the interaction energy (by convention  $\varepsilon_{AA} \geq 0$ ) between two neighbour molecules of adsorbate A [Ebadi et al., 2009; Guiochon et al., 2006; Safa Özcan et al., 2004].

### **3.4 Adsorption kinetic**

The description of adsorption kinetics is a much more complicated problem than the theoretical description of adsorption equilibria. This is because the expressions describing the thermodynamic quantities at equilibrium are the only limiting forms of the expressions describing time evolution of these quantities under non-equilibrium conditions. Substantial progress has been made during the last few decades where gas/solid systems are concerned. The physical nature of solid/solution systems is much more complicated, which also makes the theoretical interpretation of the adsorption kinetics in these systems much more difficult.

The sorption mechanism can be divided into four consecutive steps represented in Figure 3.4:

- 1) transport of solute in the bulk solution;
- 2) diffusion of solute through the liquid film surrounding the adsorbent particles;
- 3) diffusion of solute in the pores of the sorbent (intraparticle diffusion);
- 4) chemical reaction as adsorption and desorption on the solid surface.

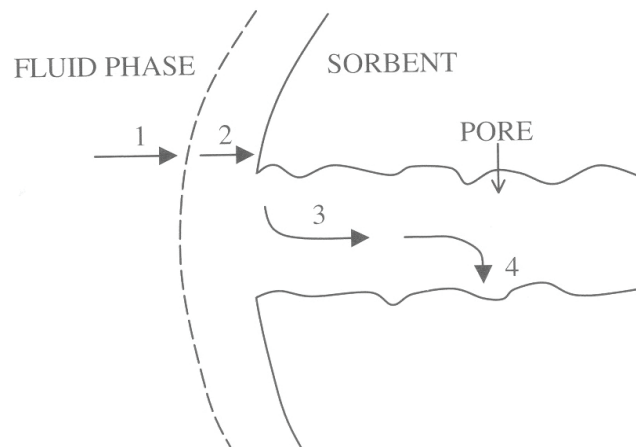


**Figure 3.4** Representation of adsorption mechanism [Noble-Terry]

The overall rate of the sorption process may be controlled by any of these steps or in some cases by combination of two steps. Various kinetic models have been used for solid/solution adsorption batch systems. For example, Langmuir, statistical rate theory (SRT), pseudo first-order (PFO), pseudo second-order (PSO), Elovich and intraparticle diffusion model (IDM) are the most well-known sorption kinetic models. Among the mentioned equations, the intraparticle diffusion model is applicable when the rate determining step is the mass transfer of adsorbate to the solid surface sites (step 3), whereas the other ones are used for description of adsorption kinetics when the overall sorption rate is controlled by the rate of surface reaction (step 4) [Haerifar et al., 2013]. Rudzinski et al. [Rudzinski et al., 2006] demonstrated that the common pseudo-first and the pseudo-second order kinetic equations are only simplified forms of a more general kinetic equation. One possible form of such general equation has been developed by applying the new approach to the rate of interfacial transport, called the Statistical Rate Theory.

The empirical kinetic equation proposed by Lagergren in 1898 [Lagergren, 1898] is still the most widely used rate equation for sorption of a solute from a liquid solution [Rudzinski et al., 2006]:

$$\frac{dN_t}{dt} = k_1(N^{(e)} - N_t) \quad (3.33)$$

where  $N_t$  is the amount of the solute adsorbed at a time  $t$ ,  $k_1$  and  $N^{(e)}$  are some constants. They can be easily found from the following linear regression of experimental data:

$$\ln(N^{(e)} - N_t) = \ln N^{(e)} - k_1 t \quad (3.34)$$

which represents the integral form of equation 3.33, corresponding to the boundary condition  $N_t(t=0) = 0$ . According to the commonly accepted interpretation,  $k_1$  is the pseudo-first order constant and  $N^{(e)}$  should be the amount adsorbed at equilibrium. This makes equation 3.33 a “pseudo-first order” equation, by comparison with the kinetic adsorption term of the “true” first-order equation in which  $N^{(e)}$  is the maximum amount that can be adsorbed.

By comparison with the adsorption term of the true first-order process, the form of equation 3.33 seemed to suggest a one-site-occupancy adsorption when the adsorbing molecule reacts with one adsorption site. Thus, it seemed natural to propose that in the case of two-site occupancy adsorption, i.e., when the solute molecule reacts with two adsorption sites, the rate of adsorption should be given by the following:

$$\frac{dN_t}{dt} = k_2(N^{(e)} - N_t)^2 \quad (3.35)$$

Equation 3.35 has commonly been called the “pseudo-second-order rate equation” [Blanchard et al., 1984 ; Azizian et al., 2004]. The integral form of this equation, obtained with the boundary condition  $N_t(t=0) = 0$ , can be written as:

$$\frac{t}{N_t} = \frac{1}{N^{(e)}} t + \frac{1}{k_2(N^{(e)})^2} \quad (3.36)$$

The equation is usually applied for kinetic data by plotting of  $t/N_t$  versus  $t$ : a linear relationship should be obtained where  $1/N^{(e)}$  and  $1/k_2(N^{(e)})^2$  are the slope and the intercept, respectively.

However, it should be emphasized that both equations 3.33 and 3.35 are essentially empirical equations; Rudzinski et al., [Rudzinski et al., 2006] assumed these equations are simplified forms of another rate equation, hence they searched for a more general rate equation having a well-established theoretical background, applying this to the Statistical Rate Theory of Interfacial Transport (SRT).

Assuming that the transport of molecules between two neighbouring phases through their phase boundary results primarily from single molecular events, the rate of molecular transport  $R_{12}$  between two phases 1 and 2 is expressed as

$$R_{12} = R_e \left[ \exp\left(\frac{\mu_1 - \mu_2}{kT}\right) - \exp\left(\frac{\mu_2 - \mu_1}{kT}\right) \right] \quad (3.37)$$

where  $\mu_1$  and  $\mu_2$  are the chemical potentials of the molecules in phases 1 and 2 at non-equilibrium conditions and  $R_e$  is the exchange rate at equilibrium to which the system would evolve after being closed and equilibrated. The new SRT approach may also explain the successful application of the empirical Lagergren equation for describing adsorption kinetics at the solid/solution interfaces. As the Lagergren kinetic equation has always been associated with the model of one-site-occupancy adsorption, Rudzinski et al. [Rudzinski et al., 2006] accepted the Langmuir adsorption model in their theoretical investigation. Thus, they assumed that the chemical potential of the solute molecules adsorbed on a solid surface  $\mu_s$  can be expressed as:

$$\mu_s = kT \ln \frac{\Theta}{1 - \Theta} - kT \ln q_s \quad (3.38)$$

where  $\Theta = N_t/N_m$  and  $q_s$  is the molecular partition function of the adsorbed solute molecule. In equation 3.38,  $N_m$  is the maximum amount that can be adsorbed, usually called the adsorption capacity. In terms of the Langmuir model, this is the total number of the adsorption sites on the surface, available for adsorption of solute molecules. For the chemical potential of the solute molecules in the bulk solution  $\mu_b$ , the following expression was assumed:

$$\mu_b = \mu_b^\circ + kT \ln c \quad (3.39)$$

where  $c$  is the bulk solution concentration. equations 3.38 and 3.39 lead to the Langmuir adsorption isotherm at equilibrium (see equation 3.23):

$$\Theta^{(e)} = \frac{K_L c^{(e)}}{1 + K_L c^{(e)}} \quad (3.40)$$

where

$$K_L = q_s \exp\left(\frac{\mu_b^\circ}{kT}\right) \quad (3.41)$$

and the superscript  $(e)$  will always denote equilibrium conditions. The corresponding SRT expression for the adsorption kinetics is

$$\frac{d\Theta}{dt} = K_{ls}' \left[ \exp\left(\frac{\mu_b - \mu_s}{kT}\right) - \exp\left(\frac{\mu_s - \mu_b}{kT}\right) \right] \quad (3.42)$$

in which  $K_{ls}'$  is the rate of adsorption at equilibrium. In the Langmuir model of adsorption,  $K_{ls}'$  is proportional to the frequency of the collisions of the solute molecules with the surface and to the number of the free molecules available for the adsorption sites  $(1 - \Theta^{(e)})$ . Thus,  $K_{ls}'$  can be written as:

$$K_{ls}' = K_{ls} c^{(e)} (1 - \Theta^{(e)}) \quad (3.43)$$

While assuming that the rate of desorption is proportional to  $\Theta^{(e)}$ , the Langmuir isotherm (equation 3.40) is again obtained. The classical kinetic equation of the fundamental TAAD approach (Theory of Activated Adsorption/Desorption), used throughout the last 20<sup>th</sup> century, is:

$$\frac{d\Theta}{dt} = K_a c (1 - \Theta)^s - K_d \Theta^s \quad (3.44)$$

where  $s$  is the number of sites occupied by one adsorbed molecule,  $K_a$  and  $K_d$  are temperature-dependent constants. From equation 3.44 one can arrive either at Lagergren ( $s = 1$ ), or at pseudo-second-order equation ( $s = 2$ ) by neglecting the desorption term in that fundamental TAAD equation, and yet defining  $\Theta$  as an “efficient” surface coverage equal to  $N_v/N^{(e)}$ .

The experiments show that the coefficients  $k_1$  and  $k_2$  in the empirical equations 3.34 and 3.36 depend, for instance, on the initial concentration but there is no theoretical explanation for that. The SRT equation explains it because  $c^{(e)}$  and the total adsorption coverage  $\Theta_t^{(e)}$  depend on the amount of solid adsorbent, the volume of the solute solution, and its initial concentration. There, we studied, for instance the case of “volume dominated” systems, when the amount of the bulk molecules dominates the amount of adsorbed molecules in experiment to such an extent that the bulk



concentration is essentially unchanged during the kinetic experiment. In our case, it means that the concentration  $c$  can be identified with the equilibrium concentration  $c^{(e)}$ . After several calculations reported in [Rudzinski et al., 2006], the following equation is obtained:

$$\frac{d\Theta_t}{dt} = K_{ls}c^{(e)}(1-\Theta_t^{(e)}c^{(e)}) \left[ \exp\left(\frac{(\Theta_t^{(e)}-\Theta_t)(\varepsilon_m-\varepsilon_l)}{kT}\right) - \exp\left(-\frac{(\Theta_t^{(e)}-\Theta_t)(\varepsilon_m-\varepsilon_l)}{kT}\right) \right] \quad (3.45)$$

where  $\varepsilon$  is the energy of adsorption.

The applicability of the Lagergren (equation 3.33) would suggest that  $d\Theta_t/dt$  is proportional to the difference  $(\Theta_t^{(e)}-\Theta_t)$ . So, it is possible to expand the exponents within the square bracket into Taylor series around  $\Theta_t = \Theta_t^{(e)}$ . With this assumption, the terms of order  $\geq 3$  are very small and, therefore, can be neglected. Now the pseudo-first order constant  $k_1$  is defined as:

$$k_1 = \frac{2K_{ls}c^{(e)}(1-\Theta_t^{(e)}c^{(e)})(\varepsilon_m-\varepsilon_l)}{kT} \quad (3.46)$$

The SRT approach shows that the empirical Lagergren kinetic equations should apply best in the case of “volume dominated” kinetic experiments. When noticeable changes of the bulk concentration will be observed during a kinetic experiment, then deviations from the pseudo-first-order Lagergren equation are to be expected.

In the cases where change of adsorbate concentration is noticeable, the terms of order  $\geq 3$  of Taylor expansions cannot be all neglected and other calculations leads to the pseudo-second order kinetic (equation 3.35): the pseudo-second order rate equation is just an intuitive generalization of the Lagergren equation.

Model investigations based on the general kinetic equations show that deviations of the observed kinetics from the behaviour predicted by the pseudo-first and the pseudo-second-order kinetic equations may be due to the approximate character of these equations.

## CHAPTER 4

### RESULTS

#### **4.1 Drugs adsorption on zeolites**

Many data which will be next reported are part of my work of thesis and have been recently published: [Pasti L., Sarti E., Cavazzini A., Marchetti N., Dondi F., Martucci A., J. Sep. Sci. 2013, 36, 1604–1611].

#### **INTRODUCTION**

In the European Union around 3000 different PhACs (Pharmaceutical Active Compounds) are used in human medicine belonging to different medicinal classes. Thus, their main route into the aquatic environment is ingestion following excretion and disposal via wastewater: after administration, pharmaceuticals can be excreted either as an unchanged parent compound or in the form of metabolites or as conjugates. Conventional wastewater treatments plants (WWTPs) effluents are the major sources of emerging contaminants, since many of these substances escape to conventional depuration [Petrovic et al., 2005] allowing them to reach surface water streams, where they are usually present at low concentrations; other environmental exposure pathways of PhACs are manufacturing and hospital effluents, land applications (e.g., biosolids and water reuse), concentrated animal feeding operations and direct disposal/introduction to environment [Daughton and Ternes, 1999]. Several studies reported on the limited degradability of pharmaceuticals under conventional treatments applied in the WWTPs [Radjenovic, et al., 2007; Carballa et al., 2005], suggesting that their upgrade and implementation of advanced treatment technologies are required to achieve high-quality treated effluents [Radjenovic et al., 2009]. Even if emerging pollutants are found in natural waters at low concentrations levels, many compounds revealed adverse health and environmental effects. Hence, it is important to develop analytical methods able to detect these molecules in accurate way and to enhance abatement technologies for water remediation.

Several methods have been reported for degrading emerging organic contaminants. In addition to nanofiltration and reverse osmosis, other techniques including ozonation and

chemical oxidation have been identified in successfully treating organic contaminants in water [Daughton et al., 2001; Huber et al., 2003; Ternes et al., 2002; Ternes et al., 2003]. The latter processes can lead to the formation of oxidation intermediates which are, to date, mostly unknown. In adsorption technology, inorganic adsorbents are often employed since they offer advantages due to their stability towards the radioactive and thermal treatments which are necessary to induce the complete degradation of adsorbates and, therefore, the regeneration of exhausted adsorbents. Among inorganic adsorbents, it has been proven that zeolites are efficient in removing small organic compounds from the environmental matrix [Zhao et al., 1998; Anderson 2000; Li et al., 2003; Hung et al., 2006].

In this work, the interaction between two organophilic zeolites (Beta and Y) with different  $\text{SiO}_2/\text{Al}_2\text{O}_3$  ratio (SAR) (Beta: SAR 25, 38 and 360; Y: SAR 200) and four drugs (ketoprofen, hydrochlorothiazide, atenolol and erythromycin), differing in chemical properties and molecular dimensions, was studied in order to evaluate the potential use of zeolites as adsorbents both in abatement systems of emerging contaminants in natural waters and in analytical systems of pre-concentration.

The interaction was systematically investigated by considering the effect of surrounding pH, ionic strength and chemical state of drugs, in order to evaluate the role of hydrophobic and electrostatic forces in the interaction between the pharmaceutical molecule and the adsorbent. Also the potential effect of thermal treatment of the adsorbents has taken into account. Based on adsorption data, release experiments have been carried in different conditions of pH and organic solvent, in order to reach the best conditions for a good recovery.

#### **4.1.1 Drugs adsorption on BETA**

##### **EXPERIMENTAL**

All the adsorbents (i.e. Beta25, Beta38, Beta360) were employed as received and after a calcination process. Calcination was carried out by raising the temperature from room temperature to 600°C in 1 h, then holding at 600°C for 4 hours. Finally, adsorbents were kept at room temperature for 3 h. Air circulation was maintained during heating. The calcined samples were kept in a desiccator and used within 2 days after thermal treatment.

In all adsorption experiments, binary solutions of drugs in water have been employed. Kinetic data show that equilibrium was reached after 2 hours (see Figure 4.4): in any case, for batch experiments, a contact time of 24 hours was employed, in order to

guarantee that the studied system reaches the equilibrium state. The concentrations of contaminant in the aqueous solutions were analyzed by HPLC/DAD and by HPLC/MS.

#### 4.1.1.1 MATERIALS CHARACTERIZATION

In Table 4.1, the main features of the selected BEAs are reported.

**Table 4.1** Zeolites characteristics.

	<b>Producer</b>	<b>SiO<sub>2</sub>/Al<sub>2</sub>O<sub>3</sub> ratio (SAR)</b>	<b>Nominal Cation Form</b>	<b>Surface Area (m<sup>2</sup>/g)</b>
<b>Beta25</b>	<b>Zeolyst (CP814E)</b>	25	Ammonium	680
<b>Beta38</b>	<b>Zeolyst (CP814C)</b>	38	Ammonium	710
<b>Beta360</b>	<b>Zeolyst (CP811C-300)</b>	360	Hydrogen	620

The studied zeolites have been characterized by Secondary Electron Microscopy (SEM) in order to verify particles shape and morphology, and by dynamic laser light scattering performed on Malver Z-Sizer to investigate their dimensions and polydispersity (Figure 4.1).

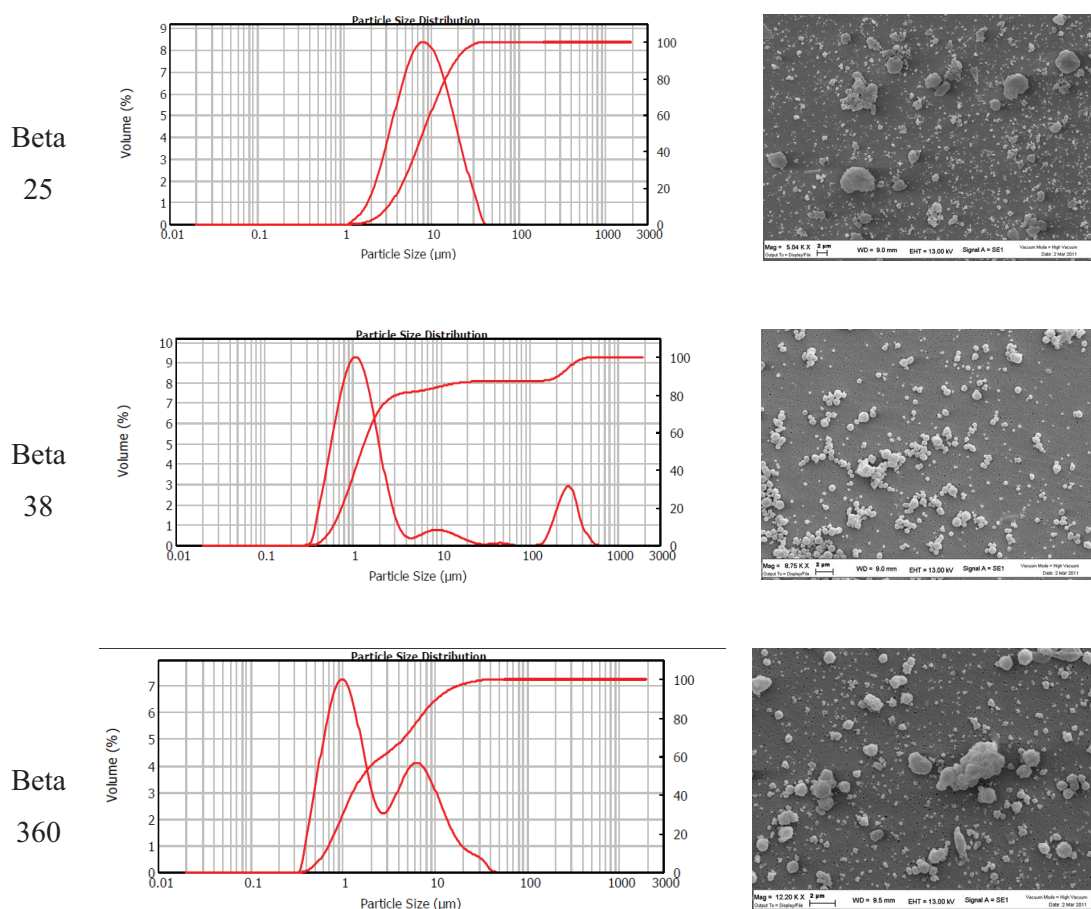


**Figure 4.1** Dimensional characterisation of the selected BEAs by dynamic laser light scattering and Secondary Electron Microscopy

From SEM images, Beta 38 particles seem to be the most homogeneous in dimension and shape (they are almost spherical), while Beta 25 and Beta 360 appear to be constituted by particles heterogeneous in shape and dimensions or by aggregates.

Dynamic laser light scattering analysis provides more detailed information about polydispersity: Beta 25 particles are the largest with a mean value of 8.148  $\mu\text{m}$  and standard deviation of 0.950  $\mu\text{m}$ , Beta 38 particles have a mean value of 1.259  $\mu\text{m}$  and standard deviation of 0.625  $\mu\text{m}$  with a little population larger than 100  $\mu\text{m}$ , finally Beta 360 is constituted by two particles populations, the most abundant with mean value of 1.660  $\mu\text{m}$  and standard deviation of 0.600  $\mu\text{m}$  and a larger one with mean value of 6.607  $\mu\text{m}$  and standard deviation of 0.750  $\mu\text{m}$ .

TG curves were recorded for both the as-received (i.e. Beta25, Beta38 and Beta360) and the calcined materials (i.e. Beta25c, Beta38c and Beta360c) and are reported in Figure 4.2.

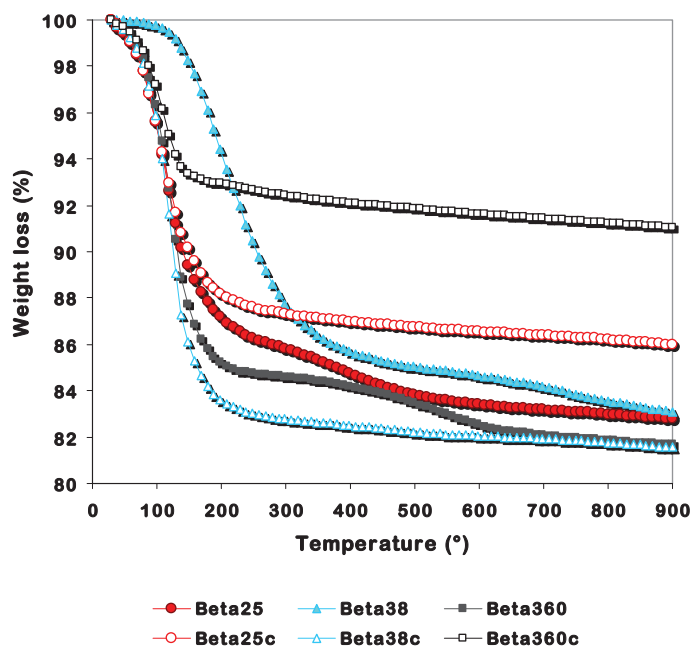


**Figure 4.2** Thermogravimetric curves of as-synthesized and calcined Beta25, Beta38 and Beta360

The TG curves of beta samples show a sudden slope change at low temperature (about 100°C), thus indicating the presence of water molecules which are weakly bonded to the surface. At the same time, weight losses at higher temperatures indicate the simultaneous presence of residual ammonium ions in Beta25 and Beta38 and structural water molecules in all the investigated samples. A 17–18% total weight loss was observed at 900°C for each sample.

On the basis of the TG data, it can be inferred that all three selected beta samples after calcination still contains water molecules weakly bonded to the surface (weight losses at 100°C: 5.7% for Beta25c, 6.0% for Beta38c and 3.8 % for Beta360c), as well as structural water trapped in the micro-porosities of zeolites samples (8.3% for Beta25c, 12.4% for Beta38c and 5.1% for Beta360c).

Diffraction analysis of the materials was carried out. The X-ray powder patterns of Beta25, Beta38 and Beta360 before and after calcination are reported in Figure 4.3 a) and b), respectively. The refined values of the unit cell parameters and volumes of both the tetragonal A and monoclinic B polytypes before and after thermal treatment for all the studied materials are given in Table 4.2.

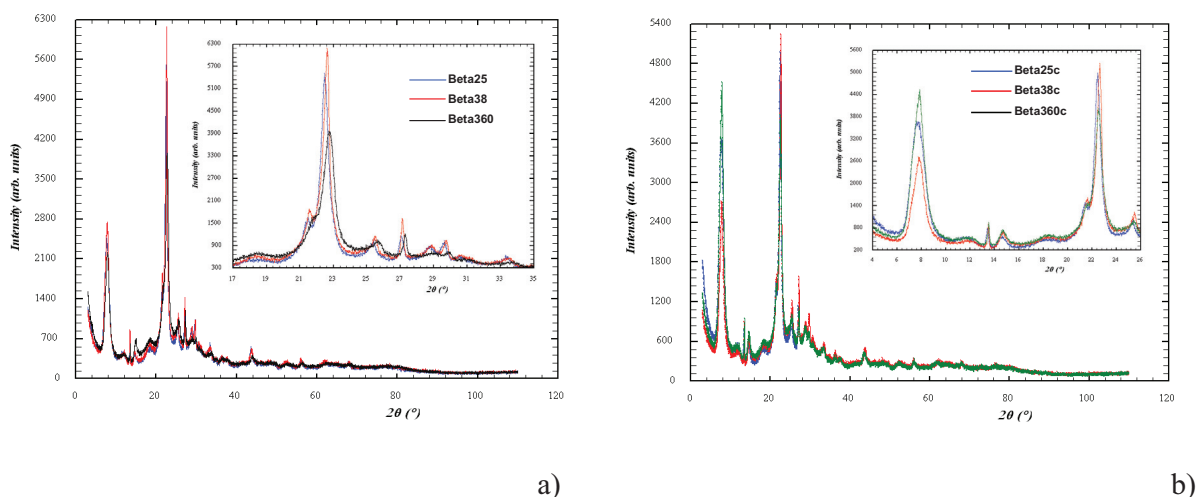


**Figure 4.3** X-ray powders diffraction of a) as-synthesized and b) calcined BEAs

**Table 4.2** Refined unit cell parameters of BEAs before and after thermal treatment.

<b>Polytype A, tetragonal, P4<sub>1</sub>22</b>						
	<b>Beta25</b>	<b>Beta25c</b>	<b>Beta38</b>	<b>Beta38c</b>	<b>Beta360</b>	<b>Beta360c</b>
<b>a (Å)</b>	12.470 (4)	12.457 (3)	12.471 (2)	12.458 (3)	12.478 (2)	12.496 (2)
<b>b (Å)</b>	12.470 (4)	12.457 (3)	12.471 (2)	12.458 (3)	12.478 (2)	12.496 (2)
<b>c (Å)</b>	26.549 (17)	26.606 (12)	26.571 (13)	26.585 (14)	26.644 (9)	26.699 (13)
<b>α</b>	90	90	90	90	90	90
<b>β</b>	90	90	90	90	90	90
<b>γ</b>	90	90	90	90	90	90
<b>V (Å<sup>3</sup>)</b>	4128.6 (31)	4128.6 (23)	4132.4 (24)	4125.9 (25)	4148.7 (17)	4169.2 (23)

<b>Polytype B, monoclinic, C/2c</b>						
	<b>Beta25</b>	<b>Beta25c</b>	<b>Beta38</b>	<b>Beta38c</b>	<b>Beta360</b>	<b>Beta360c</b>
<b>a (Å)</b>	17.986 (4)	17.645 (6)	17.988 (3)	17.958 (4)	17.972 (6)	17.966 (6)
<b>b (Å)</b>	17.870 (3)	17.751 (6)	17.864 (2)	17.902 (3)	17.875 (4)	17.875 (4)
<b>c (Å)</b>	14.617 (3)	14.581 (5)	14.610 (3)	14.570 (3)	14.610 (4)	14.605 (4)
<b>α</b>	90	90	90	90	90	90
<b>β</b>	114.85 (2)	114.55 (3)	114.89 (2)	115.19 (2)	114.97 (2)	114.99 (2)
<b>γ</b>	90	90	90	90	90	90
<b>V (Å<sup>3</sup>)</b>	4263.0 (15)	4154.5 (26)	4258.9 (14)	4238.1 (16)	4254.7 (21)	4251.1 (21)

After calcination in all samples the X-ray diffraction peak intensities increase, especially a low 2 $\theta$  values, with respect to those observed for the as-synthesised BEAs, thus explaining the contraction of unit cell volume. The higher weight loss of Beta38 observed in Figure 4.3 can explain the higher contraction of the unit cell volume of this material (see Table 4.2), before and after calcination, since lattice flexibility (expansion or contraction) has been observed following the incorporation of molecules in the porous structure (adsorption or desorption) [Pasti et al., 2012].

#### 4.1.1.2 ADSORPTION

Before studying the adsorption at equilibrium it is important to understand the necessary time so that the equilibrium is reached, hence kinetic tests have been carried out. As example, in Figure 4.4, the uptakes of KTP, HCT and ATN on Beta360 are shown, where it can be observed the high speed of the adsorption process.

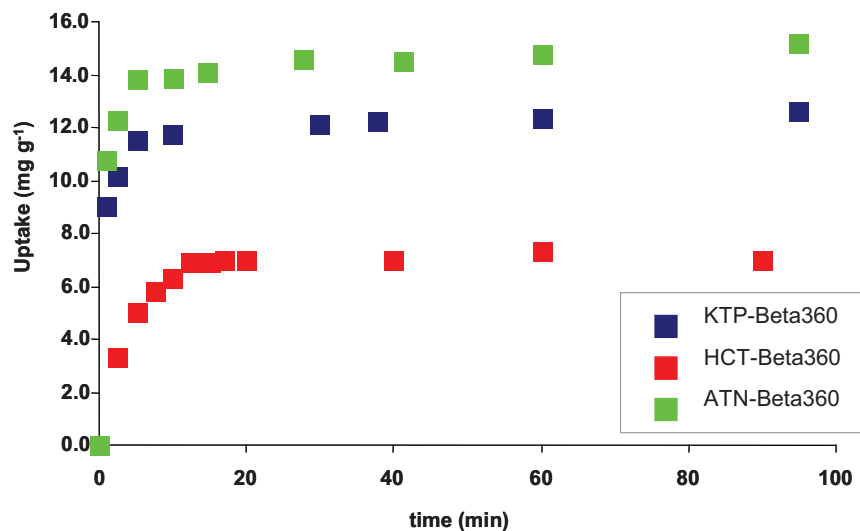


**Figure 4.4** Uptake of ATP, KTP and HCT on Beta360c vs. time.

Adsorption mechanisms of drugs on zeolites can involve both non-specific (ionic) and specific interactions due to the formation of well-defined local chemical bonds, either covalent or supramolecular (i.e. covalent or hydrogen bonding). For a given adsorbent material, the different interactions will depend on the acid-base properties, the number of H-donor groups, the hydrophobicity of drugs, etc. Recent studies evidenced the presence of stable H-bonded adducts for drug adsorbed from aqueous solution on zeolites [Martucci et al., 2012].



#### 4.1.1.2.1 Effect of SAR

Adsorption isotherms of KTP on the three as-synthesized BEAs are reported in Figure 4.5 and the related data, fitted with Langmuir model (see paragraph 3.3), are reported in Table 4.3.

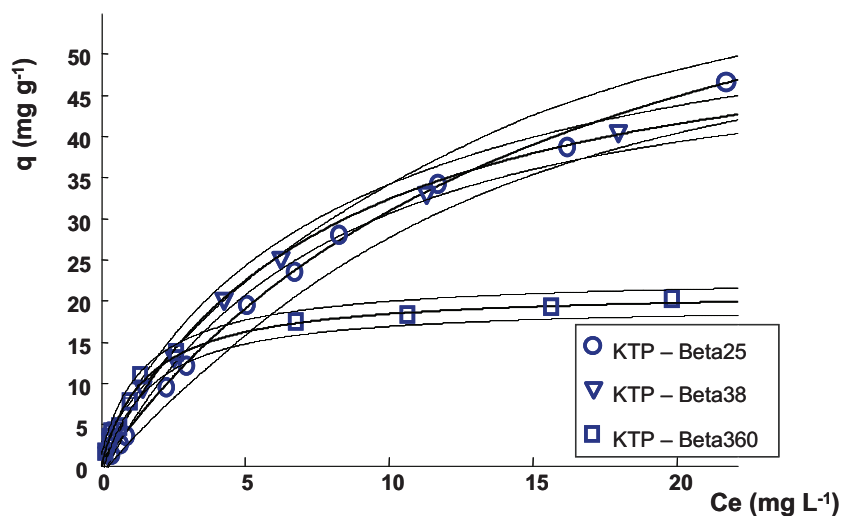


**Figure 4.5** Adsorption isotherms of KTP on as-synthesized BEAs

**Table 4.3** Parameters estimated by non linear fitting, according to Langmuir model, of KTP adsorption on as-synthesized BEAs. The confidence limits at 95% of probability of parameters are reported in brackets.

Drug-zeolite	b (L mg <sup>-1</sup> )	qs (mg g <sup>-1</sup> )	R <sup>2</sup>
KTP – Beta25	0.53 (0.41; 0.65)	58 (53; 62)	0.9856
KTP – Beta38	0.45 (0.34; 0.67)	48 (39; 57)	0.9787
KTP – Beta360	0.64 (0.51; 0.76)	21 (20; 23)	0.9876

An increase of KPT adsorption capacity with decreasing the SAR on the as-received materials was observed. A similar behaviour was also showed for both HCT and ATN (data are reported in Table 4.4)

**Table 4.4** Parameters estimated by non linear fitting, according to Langmuir model, of HCT and ATN adsorption on as-synthesized BEAs. The confidence limits at 95% of probability of parameters are reported in brackets.

<b>Drug_zeolite</b>	<b>b (L mg<sup>-1</sup>)</b>	<b>q<sub>s</sub> (mg g<sup>-1</sup>)</b>	<b>R<sup>2</sup></b>
<b>HCT – Beta25</b>	0.55 (0.36; 0.73)	70 (61; 79)	0.9812
<b>HCT – Beta38</b>	0.22 (0.15; 0.29)	62 (54; 70)	0.9866
<b>HCT – Beta360</b>	0.015 (0.013; 0.018)	21 (16; 28)	0.9911
<b>ATN – Beta25</b>	6.8 (4.9; 8.9)	166 (156; 176)	0.9892
<b>ATN – Beta38</b>	4.8 (3.3; 6.1)	140 (125; 155)	0.9804
<b>ATN – Beta360</b>	1.9 (0.5; 3.3)	95 (82; 108)	0.9793

From the fitting data of three drugs, it can be observed that the saturation capacity ( $q_s$ ) of Beta25 is not significantly different from that of Beta38. This is possibly a consequence of the similarity in the composition of these two materials. For this reason, solely Beta25 was selected for further investigation concerning the calcinations effect. On the contrary, the adsorption efficiency for Beta25 is significantly higher than for Beta360, in confirmation of the fact that zeolite hydrophobicity can influence the adsorption properties. However, other features of the two studied materials cannot be excluded as the origin of the observed differences: in particular Beta25 differs from Beta360 in surface area and counter cation type in zeolite lattice (see Table 4.1): essentially, Beta360 was provided in its acid form, whereas Beta25 was in ammonium form. To investigate the role played from the zeolite extra-framework cation type, the adsorption experiments were repeated on the calcined materials (i.e. Beta25c and Beta360c): it is well known, in fact, that thermal treatment removes water and ammonia from the zeolite.

Adsorption isotherms of KTP, HCT and ATN on the calcined BEAs are reported in Figure 4.6 a), b) and c) respectively, and the related data are reported in Table 4.5.

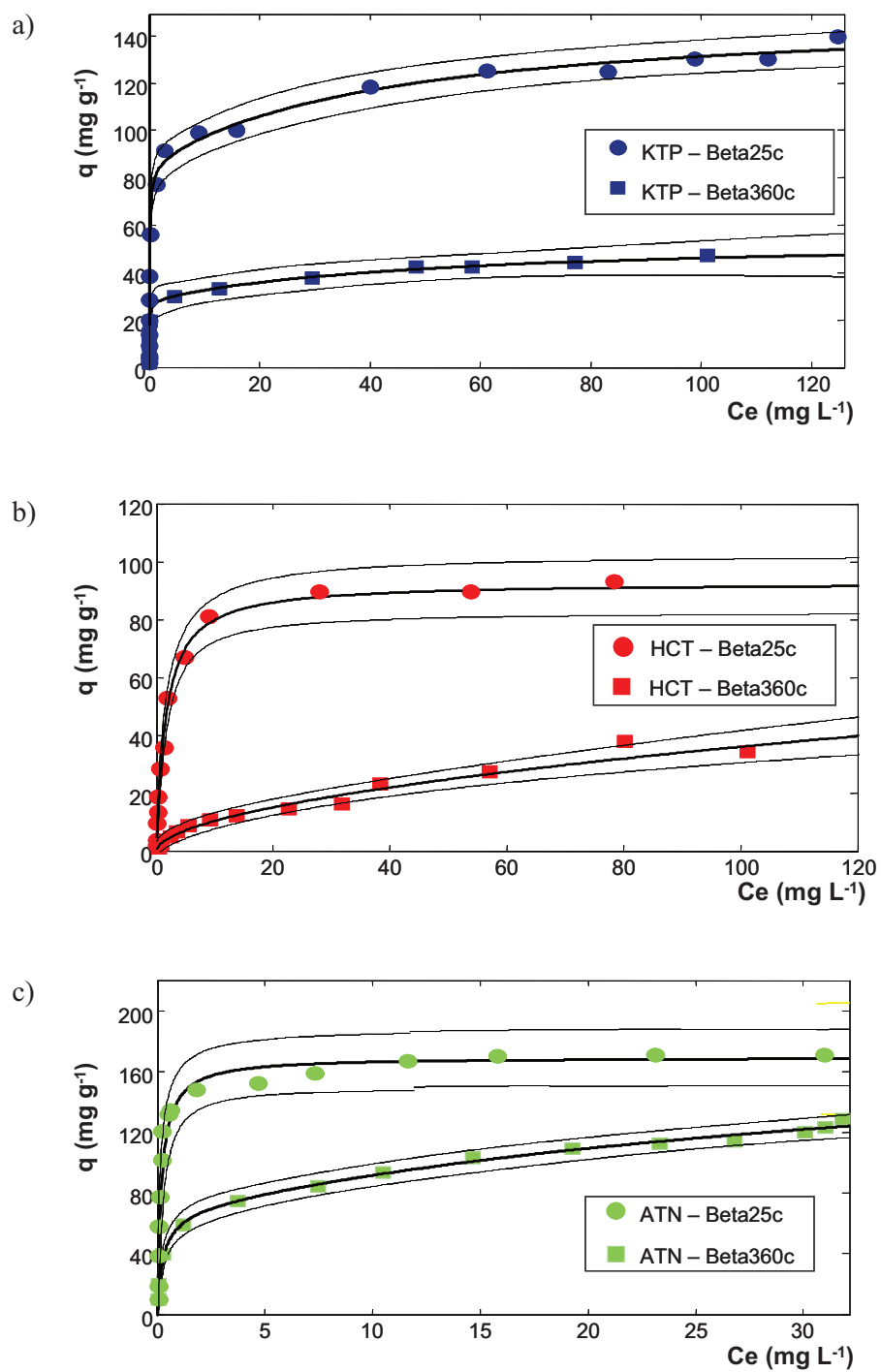


**Figure 4.6** Adsorption isotherms of a) KTP, b) HCT and c) ATN on calcined BEAs

**Table 4.5** Parameters estimated by non linear fitting, according to Langmuir model, of KTP, HCT and ATN adsorption on calcined BEAs. The confidence limits at 95% of probability of parameters are reported in brackets.

<b>Drug-zeolite</b>	<b>b (L mg<sup>-1</sup>)</b>	<b>q<sub>s</sub> (mg g<sup>-1</sup>)</b>	<b>R<sup>2</sup></b>
<b>KTP – Beta25c</b>	7.0 (5.1, 8.9)	145 (134, 156)	0.9758
<b>KTP – Beta360c</b>	6.4 (5.3, 7.2)	39 (32, 46)	0.9621
<b>HCT – Beta25c</b>	0.6 (0.47, 0.76)	93 (85, 101)	0.9826
<b>HCT – Beta360c</b>	0.061 (0.046, 0.076)	33 (24, 42)	0.9692
<b>ATN – Beta25c</b>	5.8 (3.0, 8.6)	160 (151, 170)	0.9832
<b>ATN – Beta360c</b>	1.9 (0.98, 2.9)	98 (89, 107)	0.9743

By comparing the data of adsorption onto as-synthesized (Tables 4.3 and 4.4) and calcined material (Table 4.5), it can be seen that the thermal treatment increases the adsorption efficiency of BEAs independently from their SAR values. For Beta25c, the saturation capacity increases due to the increase of acidity following the thermal release of ammonia. On the other hand, Beta360 was already in acid form: the improvement in adsorption, hence, can be due to the increase of acidity of hydrophobic Beta caused by surface and structural modifications induced by mild thermal treatments in humid air as described, for instance, in [Kunkeler et Al., 1998; Lohse et al., 1997]. Water loss seems to affect to a lesser degree the adsorption capability, since it was proved by TG analysis that the materials after thermal treatment were partially re-hydrated (see Figure 4.2). To clarify the role played by the porous structure of zeolites Beta, X-ray diffraction patterns were collected for the Beta25c before and after adsorption of ATN (Figure 4.7 and Table 4.6).

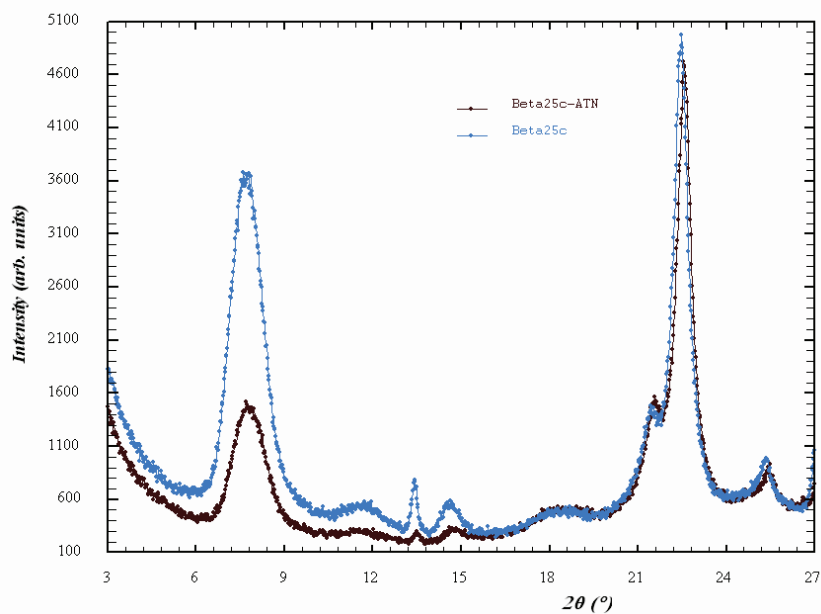


**Figure 4.7** X-ray powders diffraction of Beta25c before and after ATN adsorption

**Table 4.6** Refined unit cell parameters of Beta25c before and after ATN adsorption

<b>Polytype A, tetragonal, P4<sub>1</sub>22</b>		
	<b>Beta25c</b>	<b>Beta25c-ATN</b>
<b>a (Å)</b>	12.457 (3)	12.430 (3)
<b>b (Å)</b>	12.457 (3)	12.430 (3)
<b>c (Å)</b>	26.606 (12)	26.101 (2)
<b>α</b>	90	90
<b>β</b>	90	90
<b>γ</b>	90	90
<b>V (Å<sup>3</sup>)</b>	4128.6 (23)	4018.0 (32)

<b>Polytype B, monoclinic, C/2c</b>		
	<b>Beta25c</b>	<b>Beta25c-ATN</b>
<b>a (Å)</b>	17.645 (6)	17.746 (13)
<b>b (Å)</b>	17.751 (6)	17.746 (13)
<b>c (Å)</b>	14.581 (5)	14.708 (10)
<b>α</b>	90	90
<b>β</b>	114.55 (3)	115.77 (5)
<b>γ</b>	90	90
<b>V (Å<sup>3</sup>)</b>	4154.5 (26)	4168.2 (26)

The strong differences of the diffraction peaks with respect to Beta25c both in terms of intensity and position (Figure 4.7) and as variations in unit cell parameters (Table 4.6) give evidence of the effective incorporation of ATN inside the pores of the zeolite. As for porous materials, the adsorption involving the framework is generally more relevant than the surface physical adsorption; the difference in surface area should not be the origin of the observed difference in the adsorption efficiency of Beta25 and Beta360. Thermogravimetric (TG) analyses have been carried out on calcined BEAs after saturation with the selected drugs; curves concerning Beta25c are reported in Figure 4.8.

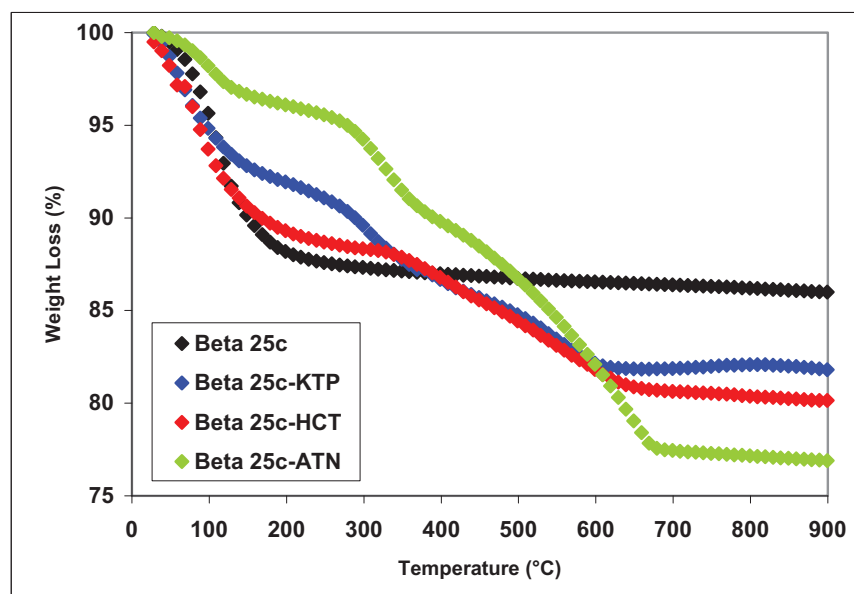


**Figure 4.8** Thermogravimetric curves of calcined Beta25c before and after drugs adsorption

The TG analyses of Beta25c and Beta360c after saturation with ATN, HCT and KTP indicate a strong affinity towards the considered drugs. In particular, the TG curves of Beta25c before and after drug adsorption (Figure 4.8.) show weight losses of about 23% (ATN-Beta25c), 19.8 % (HCT-Beta25c) and 18.2 % (KTP-Beta25c) at 900 °C compared to 8.3% of the calcined material at the same temperature. This finding further strengthens the hypothesis that drug adsorption happens into the beta zeolite framework. In conclusion, the chemical composition of zeolites plays an important role in the adsorption of pharmaceuticals on BEAs and this process takes place in the porous structure of the zeolites.

Adsorption isotherm of ERY on the calcined BEAs are reported in Figure 4.9 and the related data are reported in Table 4.7.

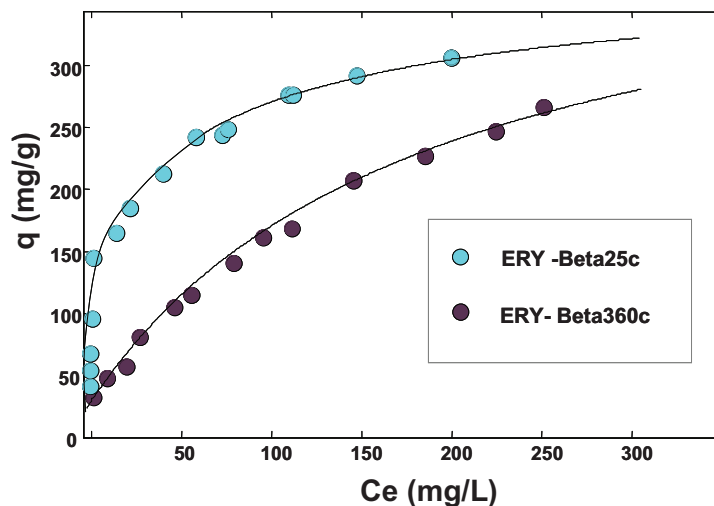


**Figure 4.9** Adsorption isotherms of ERY on calcined BEAs

**Table 4.7** Parameters estimated by non linear fitting, according to Langmuir model, of ERY adsorption on calcined BEAs. The confidence limits at 95% of probability of parameters are reported in brackets.

Drug-zeolite	b (L mg <sup>-1</sup> )	qs (mg g <sup>-1</sup> )	R <sup>2</sup>
ERY – Beta25c	0.077 (0.021, 0.13)	302 (262, 366)	0.9718
ERY – Beta360c	0.079 (0.024, 0.13)	287 (233, 330)	0.9563

The adsorption of ERY onto calcined BEAs shows saturation capacities ( $q_s$ ) considerably greater than what observed for the other three drugs. These values belong to the same magnitude order of ERY- SiO<sub>2</sub>-based mesoporous materials systems [Vallet-Regí et al., 2007] in acetonitrile: this work was focused on the possible employ of mesoporous materials, in some case surface-functionalized with alkylic chains, as controlled drug delivery systems. Also in our study, some adsorption tests with BEAs have been conducted in acetonitrile instead of water as solvent, but the results were not satisfactory hence no further investigation using organic solvents have been carried out.

Since in natural waters drugs are present at very low levels of concentration (ppb), the adsorption on BEAs in this concentrations range has been investigated by employing HPLC-MS, which is characterized by detection limits lower than HPLC-DAD.

In the low concentration range, the adsorption is usually linear, according to Henry's law (see paragraph 3.3), where the slope represents the Henry's constant ( $K_{ads}$ ):

$$q = K_{ads}C_e$$

As example, in Figure 4.10 the adsorption isotherms of KTP and HCT on Beta 25 are reported.

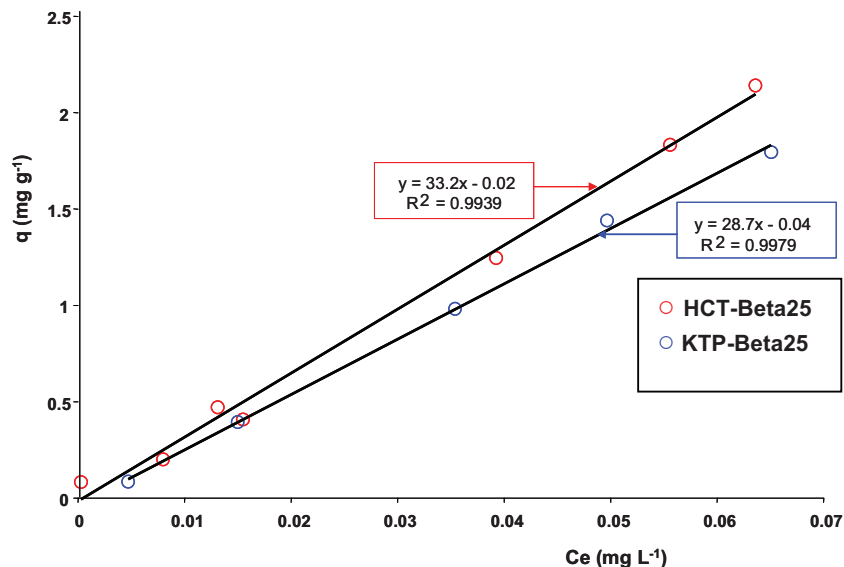


**Figure 4.10** Adsorption isotherms in a low concentration range of KTP and HCT on Beta25

It can be noted that a satisfying correlation coefficient has been obtained, confirming the linearity between the adsorbed amount ( $q$ ) and the concentration at equilibrium ( $C_e$ ). The adsorption constants obtained in the low concentrations range and the adsorption constants obtained from Langmuir isotherms ( $K_{ads} = q_s b$  from Tables 4.3 and 4.4) for higher concentrations almost agree.

#### 4.1.1.2.2 Effect of pH and ionic strength

Since the alumina content in zeolites is responsible for the hydrophilicity and ionic exchange properties of these materials, higher adsorption efficiency of Beta25 with respect to Beta360 could be related to electrostatic interactions between drug molecules and zeolite framework. The BEAs investigated are currently classified as hydrophobic, even though it has already been proved that ion exchange can contribute to adsorption on BEAs with Si/Al equal to 30 (i.e. SAR = 25) [Krohn et al., 2005].

To investigate the role of electrostatic interactions, adsorption measurements of drugs from solution at different pH were carried out. In fact, pH determines the extent of



protonation of surface silanols and thus the ion exchange properties of the material: in the exploited pH range (2–11), the zeolite surface is mainly negatively charged [Kuzniatsova et al., 2007]. Depending on the pH, the drugs can be neutral, positively or negatively charged (see their  $pK_a$ s in paragraph 1.3). Accordingly, the ionic contribution can be attractive (if the drug ion is positively charged) or repulsive (if an anion is formed) [Gantiva et al., 2010; Meloun et al., 2007; Radjenovic et al., 2008; Küster et al., 2010].

The influence of pH on the amount of adsorbed analyte per unit weight of zeolite on Beta25c and Beta360c is shown in Figure 4.11 a) and b), respectively.

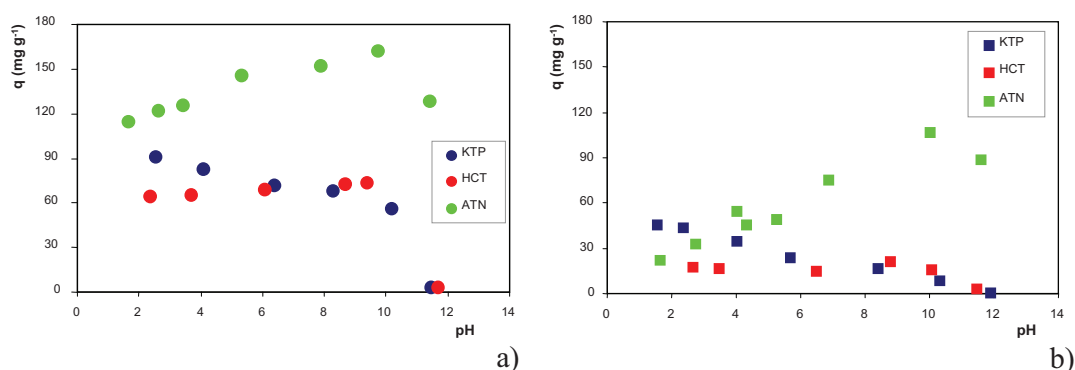


**Figure 4.11** Adsorbed amount ( $q$ ) versus pH of KTP, HCT and ATN on a) Beta25c and b) Beta 360c

The adsorption of KTP decreases with pH for both the materials and it is lower on Beta360c than on Beta25c for all the pHs. KTP's  $pK_a$  is 4.02, hence it is mainly in neutral form at  $pH < 4$  and negatively charged at  $pH > 4$ : consequently, the electrostatic interaction between KTP and beta surface is repulsive at pH over 4 and the repulsive contribution increases as the pH increases. This can explain the decrease of  $q$  with the basicity of the solution. As far as HCT was concerned, its adsorption amount ( $q$ ) on Beta25c displays relative insensitivity to pH up to 8, then it decreases to be practically unadsorbed at pH 11. Analogously to KTP, the decrease in the adsorbed quantity with pH can be related to electrostatic repulsions between the zeolite surface and the HCT anion. In fact, from the speciation distribution of HCT, the undissociated molecule prevails at  $pH < 8$ , whereas the negatively charged HCT is dominant in more basic solution. Therefore HCT, analogously to KPT, can interact with zeolite surface mainly in its neutral form by hydrophobic interactions. These results indicate that hydrophobic interactions play an important role in the adsorption of acid drugs on hydrophobic Beta.

To investigate the behaviour of a basic drug, ATN was selected as a probe. The adsorption amount of ATN on Beta25c is almost constant in the pH range 2–10, while at  $\text{pH} > 10$  the adsorbed quantity decreases. However, the relative decrease in the adsorption efficiency in basic solutions is lower than that observed for HCT and KTP. This can be explained from the fact that ATN was in protonated form at  $\text{pH} < 9$ , whereas in basic solution the neutral ATN molecule is the dominant specie. Therefore, for ATN, attractive electrostatic interactions can take place in the lower pH range, while for the neutral molecule the adsorption is driven solely by hydrophobic interactions.

The model proposed by Tsapatsis [Krohn et al., 2005; Krohn et al., 2006] described amino acid adsorption as occurring by two mechanisms: ion exchange of cationic amino acid and adsorption of zwitterions. This model could be extended to drug adsorption by considering the ion exchange between the cationic drug and zeolite protons.

On the more hydrophobic Beta360c the adsorbed amount of ATN increases with pH. This behaviour can be related to the increased concentration of neutral ATN molecules with the pH of the solution and such molecules are preferentially adsorbed onto the hydrophobic Beta360 framework than the cationic ATN form.

Furthermore, the adsorption isotherms of KTP on Beta25 obtained in MilliQ water ( $\text{pH} 4$ ) and in phosphate buffer at  $\text{pH} 6$  are reported in Figure 4.12.

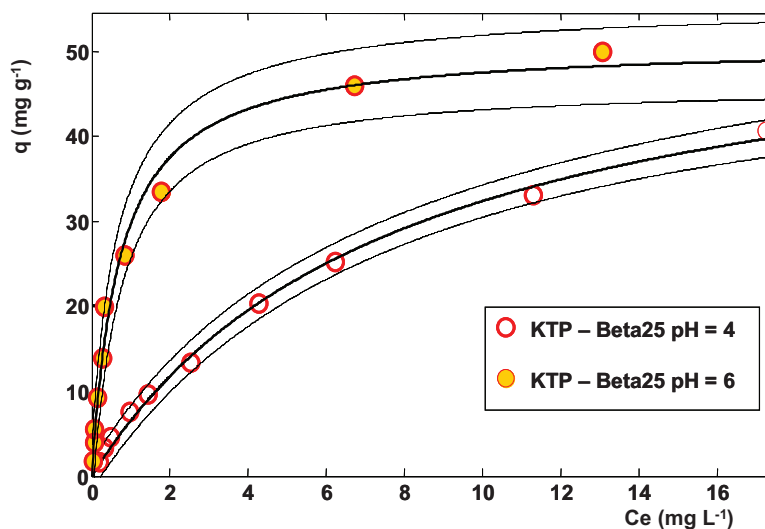


**Figure 4.12** Adsorption isotherms of KTP on as-synthesized Beta25 at two pH values

**Table 4.8** Parameters estimated by non linear fitting, according to Langmuir model, of KTP adsorption on as-synthesized Beta25. The confidence limits at 95% of probability of parameters are reported in brackets.

Drug-zeolite	b (L mg <sup>-1</sup> )	q <sub>s</sub> (mg g <sup>-1</sup> )	R <sup>2</sup>
KTP – Beta25 pH=4	0.53 (0.41; 0.65)	58 (53; 62)	0.9856
KTP – Beta25 pH=6	1.41 (1.11; 1.70)	59 (53; 64)	0.9883

From Table 4.8 it can be seen that the binding constant (b) decreases with pH, indicating lower interactions energies in acidic solution. According to the aforementioned hypothesis on repulsive interaction, the driving force for adsorption of KTP should mainly be the hydrophobic interaction of the neutral molecule.

Analogously to KTP, the adsorption isotherms of ATN on calcined Beta25c in MilliQ water (pH 9) and in phosphate buffer at pH 11 have been obtained and are reported in Figure 4.13.

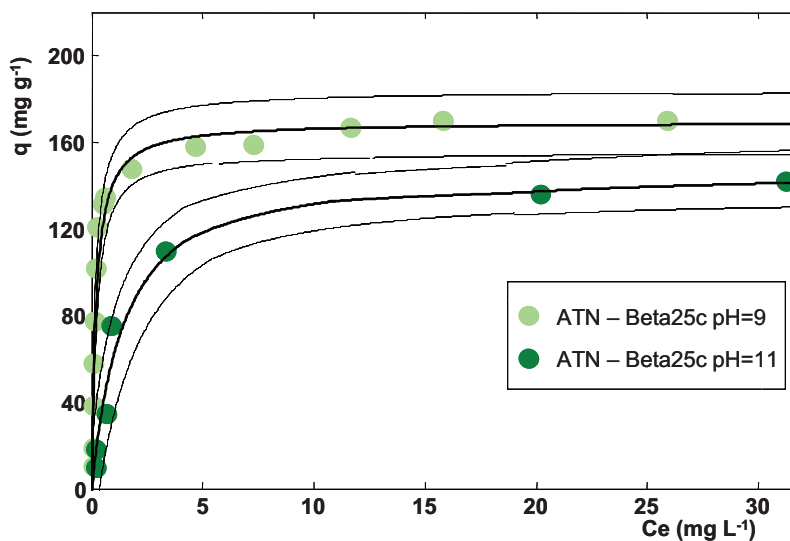


**Figure 4.13** Adsorption isotherms of ATN on calcined Beta25c at two pH values

**Table 4.9** Parameters estimated by non linear fitting, according to Langmuir model, of ATN adsorption on calcined Beta25c. The confidence limits at 95% of probability of parameters are reported in brackets.

Drug-zeolite	b (L mg <sup>-1</sup> )	q <sub>s</sub> (mg g <sup>-1</sup> )	R <sup>2</sup>
ATN – Beta25c pH=9	5.8 (3.0, 8.6)	160 (151, 170)	0.9832
ATN – Beta25c pH=11	2.05 (1.57, 2.55)	142 (131, 152)	0.9876

According to the model proposed by Tsapatsis [Krohn et al., 2005; Krohn et al., 2006], the binding constants (b) of ATN isotherms indicate that the contribution of ion exchange mechanism to the adsorption is relevant for ATN-Beta25c system.

For what concerns erythromycin, a systematic study which covers the entire pH range was not possible because of the instability of the molecule at acidic pHs [Kurath et al., 1971]. In fact, in acidic aqueous media, erythromycin is rapidly degraded via intramolecular dehydration to form erythromycin-6,9-hemiketal and then anhydroerythromycin, both of which possess little antimicrobial activity [Fiese et al., 1990; Brisaert et al., 1996].

The influence of ionic strength on the amount of adsorbed analyte per unit weight of zeolite (q) on Beta25c has been investigated, by varying the NaCl concentration in water solution (Figure 4.14). KTP and ATN have been chosen as acid and basic drug probes, respectively.

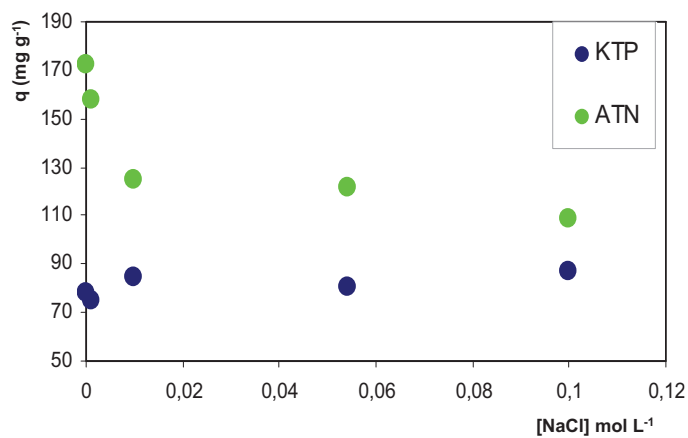


**Figure 4.14** Adsorbed amount (q) versus NaCl concentration of KTP and ATN on Beta25c

The addition of NaCl to the solution reduces the adsorption of ATN on Beta25c in comparison to the adsorption from pure water. This effect indicates that Na<sup>+</sup> cations compete with ATN molecules for the adsorption on Beta25c [Wijntje et al., 2007]. Consequently, this finding also confirms that electrostatic interactions can contribute to ATN adsorption at pH < 9.

On the contrary, the KTP adsorbed quantity was not significantly affected by the ionic strength of the solution, thus confirming that the interactions involved in the KPT–Beta25c system are mainly hydrophobic.

Another information that can be gathered by observing the behaviour for ATN is that salt addition may help the release of adsorbed drug: this finding can be of interest in the application of zeolite in analytical clean-up steps.

#### 4.1.1.2.3 Effect of solute's hydrophobicity

The influence of drug hydrophobicity on the adsorption on Beta25c and Beta360c was investigated by considering the adsorption isotherms of undissociated KTP, HCT and ATN molecules. The adsorption isotherms were measured at pH values of 3, 6 and 11 for KTP, HCT and ATN, respectively, as in these pHs the drugs are mainly in their undissociated forms. Therefore, under these conditions, the difference in adsorption amount should be only due to the different hydrophobic interactions between drugs and zeolites.

The Henry's constants ( $K_{ads}$ ) for adsorption were calculated by the isotherm parameters (see paragraph 3.3) as by:

$$K_{ads} = q_s b \quad (4.1)$$

and put in graph vs.  $K_{ow}$  as reported in Figure 4.15

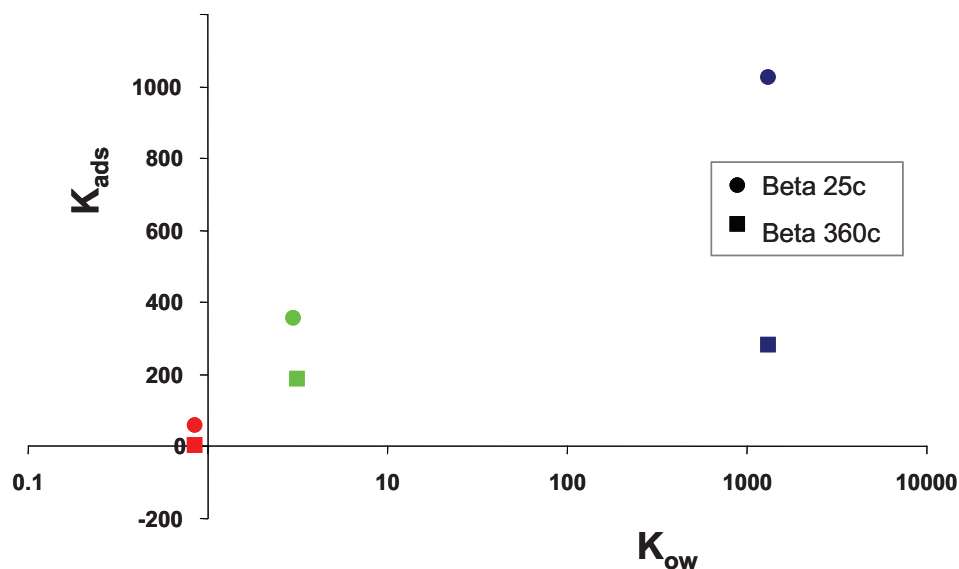


**Figure 4.15**  $K_{ads}$  vs.  $K_{ow}$  for KTP (blue), HCT (red) and ATN (green) on calcined BEAs

The figure shows that for the three drugs,  $K_{ads}$  increases with the octanol–water partition coefficient  $K_{ow}$  (in logarithmic scale). Although, solely three compounds were studied so that general conclusions cannot be formulated, the dependence of  $K_{ads}$  on  $K_{ow}$  is qualitatively similar to that reported for the adsorption on zeolites of oxygenated compounds [Mallon et al., 2011]. It should also be noticed that in [Mallon et al., 2011] compounds having similar structure and close  $K_{ow}$  values were studied, whereas the selected drugs belong to different classes of organic compounds. These results confirm that for neutral drugs the separation selectivities of zeolites can be related to  $K_{ow}$ . This last finding can be useful for prediction of the adsorption behaviour of drugs on BEAs.

#### **4.1.2 Drugs adsorption on Y**

The adsorption of pharmaceuticals molecules KTP, HCT and ATN has been studied also on a different zeolite, that is an organophilic Y with SAR 200, in order to investigate the role of topology, channels system and free window apertures of the adsorbent. Compared with BEA, Y zeolite is characterised by larger 12-ring windows and by the presence of supercages inside its structure, as described in paragraph 2.3.

Similarly to the study focused on BEAs (paragraph 4.1.1), the aim is the evaluation of the influence of some physico-chemical parameters (i. e. pH and ionic strength of the aqueous solution, hydrophobicity of the solute) on the adsorption. For the moment, this study is at a preliminary level and hence the systematic study involving all the above mentioned variables is still in progress.

## EXPERIMENTAL

Adsorption experiments of drugs onto Y zeolite were conducted through the batch method, as previously described for BEAs (see paragraph 4.1.1).

Release experiments were carried out following a procedure retrieved by Pharmacopoeia.

In Table 4.10, the main features of the selected Y zeolite are reported.

**Table 4.10** Zeolite characteristics

	Producer	SiO <sub>2</sub> /Al <sub>2</sub> O <sub>3</sub> ratio (SAR)	Nominal cation form	Surface area (m <sup>2</sup> /g)
<b>Y200</b>	<b>Tosoh Corporation (HSZ-390HUA)</b>	200	Hydrogen	630

### 4.1.2.1 ADSORPTION

Adsorption isotherms of KTP, HCT and ATN on Y200 are shown in Figure 4.16 and the related data, fitted with Langmuir model (see paragraph 3.3), are reported in Table 4.11.

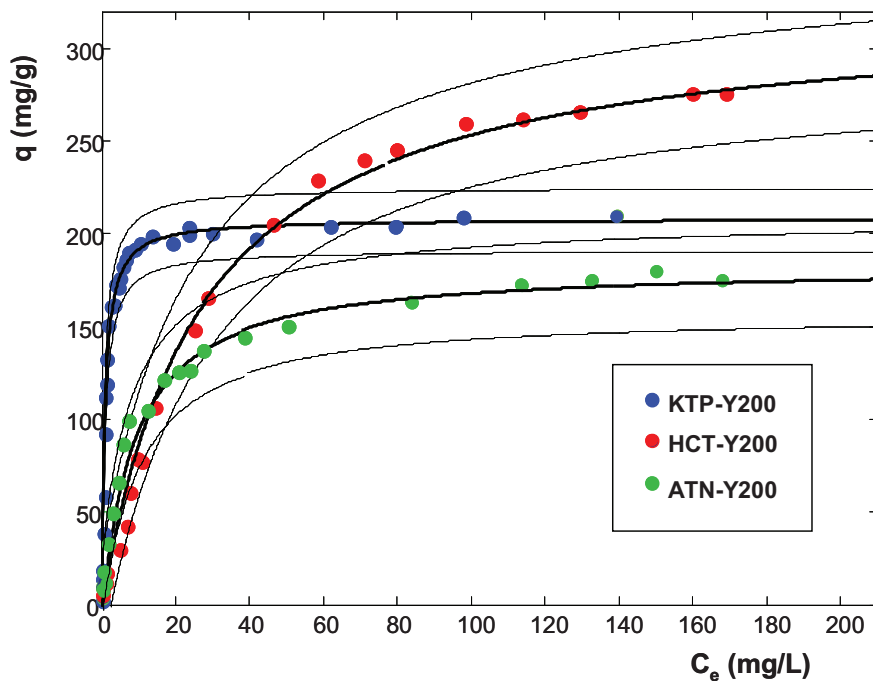


**Figure 4.16** Adsorption isotherms of KTP, HCT and ATN on Y200

**Table 4.11** Parameters estimated by non linear fitting, according to Langmuir model, of three drugs adsorption on Y200. The confidence limits at 95% of probability of parameters are reported in brackets.

Drug-zeolite	b (L mg <sup>-1</sup> )	q <sub>s</sub> (mg g <sup>-1</sup> )	R <sup>2</sup>
KTP – Y200	0.9038 (0.7581; 1.052)	208 (202; 214)	0.9887
HCT-Y200	0.03661 (0.02935; 0.04387)	322 (302; 342)	0.9856
ATN– Y200	0.1115 (0.0816; 0.1414)	183 (171; 195)	0.9737

By comparing the adsorption of three drugs on Y200, it can be noted that HCT reaches the highest saturation capacity (q<sub>s</sub>), but the isotherm slope (b), hence the adsorption constant, is the lowest. At low concentrations Y200 shows the greatest adsorption efficiency towards KTP, while at high concentrations HCT is the most adsorbed drug. In order to obtain other experimental evidences about adsorption, thermal and structural analysis have been carried out.

Thermogravimetric curves of Y200 before and after being saturated with drugs are shown in Figure 4.17.

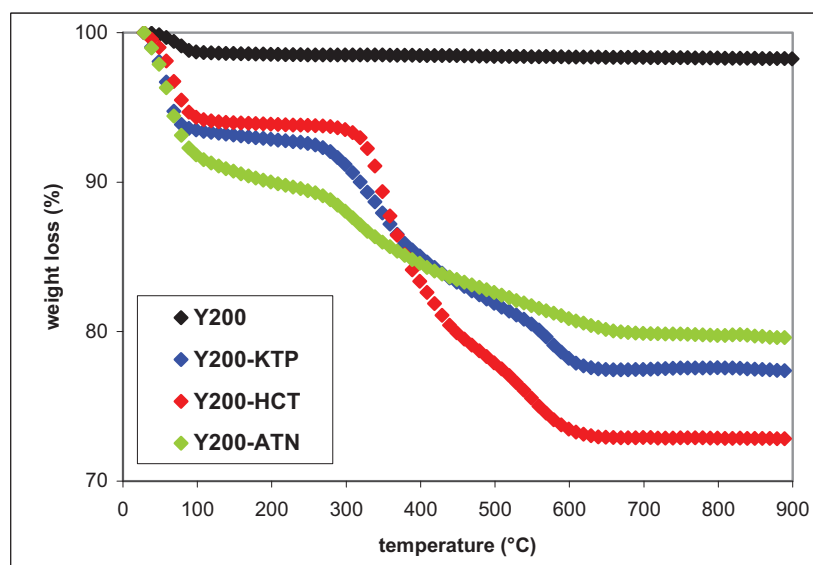


**Figure 4.17** Thermogravimetric curves of Y200 before and after drugs adsorption



TG curves of Y200 before and after drug adsorption (Figure 4.17) show weight losses of about 20.4 % (ATN-Y200), 27.2 % (HCT- Y200) and 22.6 % (KTP- Y200) at 900 °C compared to 1.7 % of the zeolite at the same temperature. This finding indicates that drug adsorption occurs into the zeolite framework.

Differential thermogravimetry (DTG) and differential thermal analysis (DTA), reported in Figure 4.18, give evidences that the recorded weight losses are actually due to decomposition of the adsorbed drug, because the corresponding temperatures agree with literature data [Tița et al., 2011; Silva Pires et al., 2011; Pereira et al., 2007].

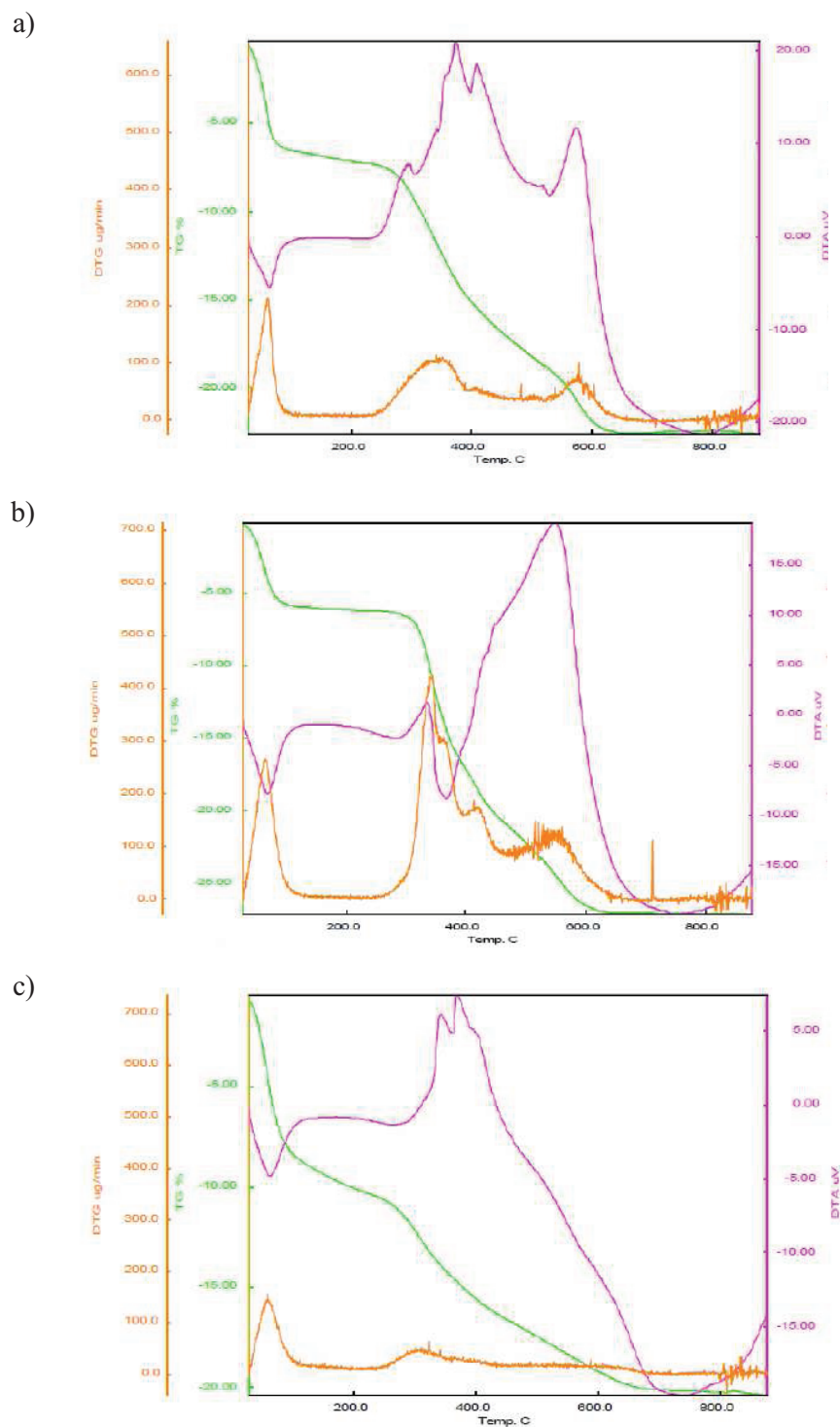


**Figure 4.18** TG (green), DTG (orange) and DTA (pink) curves of Y200 saturated with  
a) KTP, b) HCT and c) ATN

For what concerns structural analysis, XRD diffraction patterns of Y200 before and after KTP adsorption show changes in the entire  $2\theta$  range investigated. This effect is more evident in the low  $2\theta$  region: changes in the positions of peaks reveal cell

parameters modifications and changes in intensity of peaks reveal modifications in the extra-framework ions. These aspects confirm the adsorption of KTP inside structural microporosities of Y200 and not only on the external surface. In the intermediate 2 $\theta$  region, which gives information about the framework, peaks shift and intensity decrease suggest that structural modifications in the tetrahedral scaffold occurred after KTP adsorption.

In Table 4.12 cell parameters, cell volume, distances between the oxygen atoms of the 12-ring channel (Figure 4.19) and Crystallographic Free Area (CFA) are reported, for Y200 before and after KTP adsorption.

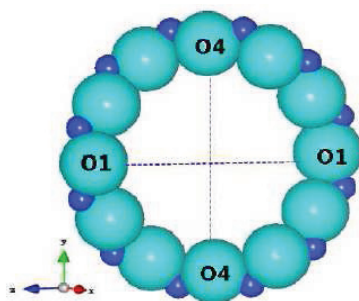


**Figure 4.19** Representation of 12-ring channel

**Table 4.12** Lattice parameters of Y200 before and after KTP adsorption

	<b>Y200</b>	<b>Y200-KTP</b>
<b>a=b=c (Å)</b>	24.259(1)	24.255(1)
<b>V (Å<sup>3</sup>)</b>	14277.1(1)	14269.1(1)
<b>O4-O4 (Å)</b>	9.81	10.30
<b>O1-O1 (Å)</b>	9.70	9.63
<b>CFA (Å<sup>2</sup>)</b>	39.07	41.43

Changes in distances O1-O1 and O4-O4 after KTP adsorption indicate that the 12-ring channel has been compressed, becoming more elliptical, due to drug adsorption. This phenomenon is not due to water adsorption because it does not cause deformation. On the contrary, the drug adsorption “forces” the channel to change in order to adapt to the morphology of the molecule, with a consequent increase in CFA. After KTP adsorption, the cell is slightly reduced while CFA greatly increased because of the significant increase in O4-O4 distance.

The difference Fourier maps allowed to identify an extra-framework site which, as binding distances confirmed, corresponds to the benzene ring of ketoprofen; it can

assume 4 possible orientations within the supercage, clearly visible in the [111] direction, as represented in Figure 4.20.

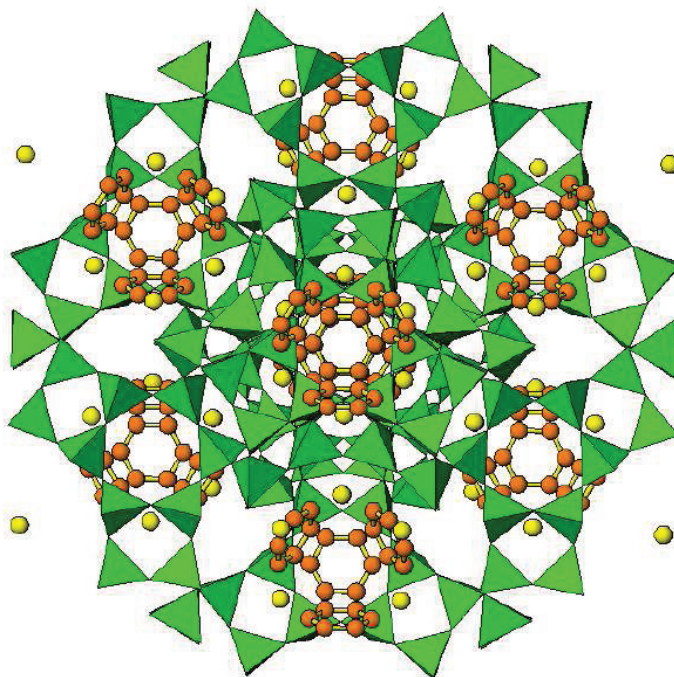


**Figure 4.20** Possible orientations of KTP molecule inside Y200 supercage [111]

XRD diffraction patterns of Y200 before and after ATN adsorption revealed that changes in extra-framework content occurred, demonstrated by a reduction of peaks intensity and a shift of peaks in low  $2\theta$  region peaks. Similarly to what observed for KTP, changes in intensity and position of peaks also in intermediate  $2\theta$  region indicated changes in the framework.

Table 4.13 highlights the variations occurred inside Y200 lattice after ATN adsorption.

**Table 4.13** Lattice parameters of Y200 before and after ATN adsorption

	<b>Y200</b>	<b>Y200-ATN</b>
<b>a=b=c (Å)</b>	24.259(1)	24.159(1)
<b>V (Å<sup>3</sup>)</b>	14277.1(1)	14101.5(1)
<b>O4-O4 (Å)</b>	9.81	9.90
<b>O1-O1 (Å)</b>	9.70	9.58
<b>CFA (Å<sup>2</sup>)</b>	39.07	38.9

The drug adsorption caused a lengthening of the 12-ring channel, making it more elliptical; consequently, both parameters and the volume of elementar cell decreased.

The difference Fourier maps show that ATN molecule has 4 possible orientations inside Y200 supercage (Figure 4.21).

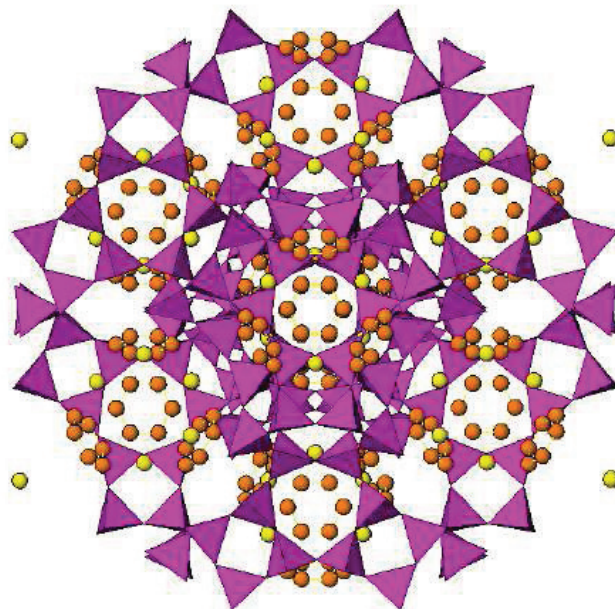


**Figure 4.21** Possible orientations of ATN molecule inside Y200 supercage [111]

#### 4.1.2.1.1 Effect of pH

Similarly to the study carried out on Beta zeolites, the effect of pH on adsorption has been evaluated by measuring the amount of adsorbed drug (q) vs. pH of solution.

In Figure 4.22 a) and b), the results for the adsorption on Y200 of KTP and HCT, respectively, are shown.

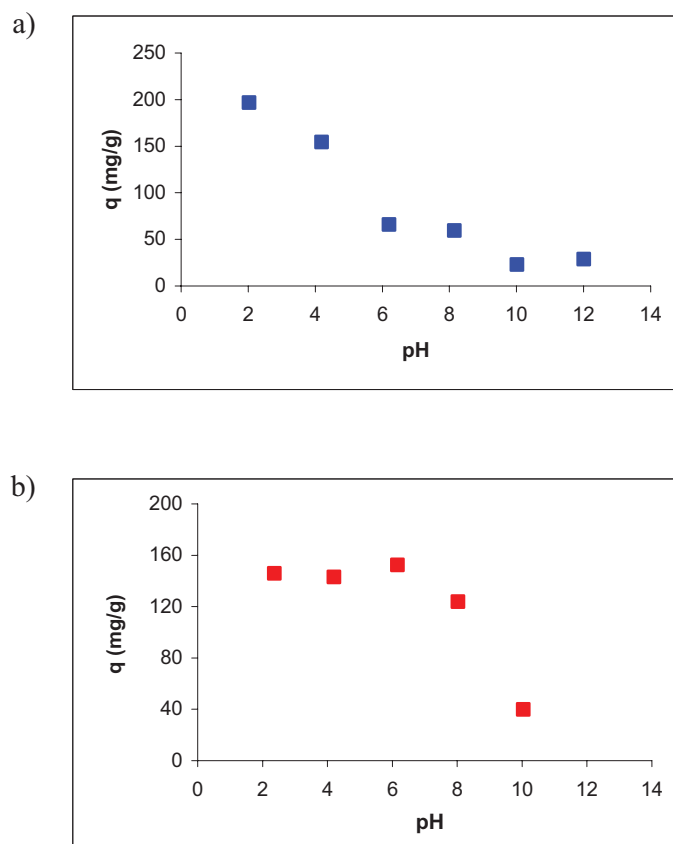


**Figure 4.22** Adsorbed amount (q) of a) KTP and b) HCT vs. pH on Y200

KTP adsorption decreases as pH increases: at  $\text{pH} > \text{pK}_a$  (KTP  $\text{pK}_a = 4.02$ ), repulsive interactions between the negatively charged KTP and the zeolite surface take place.

A similar behaviour has been observed for HCT: the adsorption remains almost constant at  $\text{pH} < \text{pK}_{a,1}$  (HCT  $\text{pK}_{a,1} = 7.9$ ) when hydrophobic interactions between zeolite and the neutral HCT occur. At  $\text{pH} > \text{pK}_{a,1}$ , negatively charged HCT is not adsorbed by zeolite because of repulsive forces.

Both for KTP and HCT, once negatively charged, two electrostatic mechanisms have to be considered: repulsive forces with zeolites and a major solubility in the aqueous solution contribute to reduce their adsorption.

ATN (not reported here) showed an opposite behaviour respect other two drugs. It should be minded that ATN is positively charged at  $\text{pH} < \text{pK}_a$  and neutral at  $\text{pH} > \text{pK}_a$  (ATN  $\text{pK}_a = 9.6$ ): unlike KTP and HCT, in this case no repulsive forces take place. Similarly to what observed for BEAs (see paragraph 4.1.1, Figure 4.11), the increase of adsorption with pH, and hence with the formation of the neutral form, could be due to

hydrophobic interactions between Y200 and ATN. Moreover, the cationic ATN is more soluble, and hence less adsorbed, than the neutral one.

#### 4.1.2.1.2 Effect of solute's hydrophobicity

The influence of drug hydrophobicity on the adsorption on Y200 was investigated by considering the Henry's constants ( $K_{ads}$ ), calculated by the isotherms parameters (Table 4.11) as previously done for BEAs (see equation 4.1), and put in graph vs.  $K_{ow}$  as reported in Figure 4.23.

Different to the case of BEAs, the adsorption constants have been calculated from the relative isotherms measured in water and not at specific pH values where the solutes are mainly in their undissociated forms; under these conditions, the adsorption is not only due to hydrophobic interactions because electrostatic ones are not excluded. The measures of adsorption at different pH are in progress.

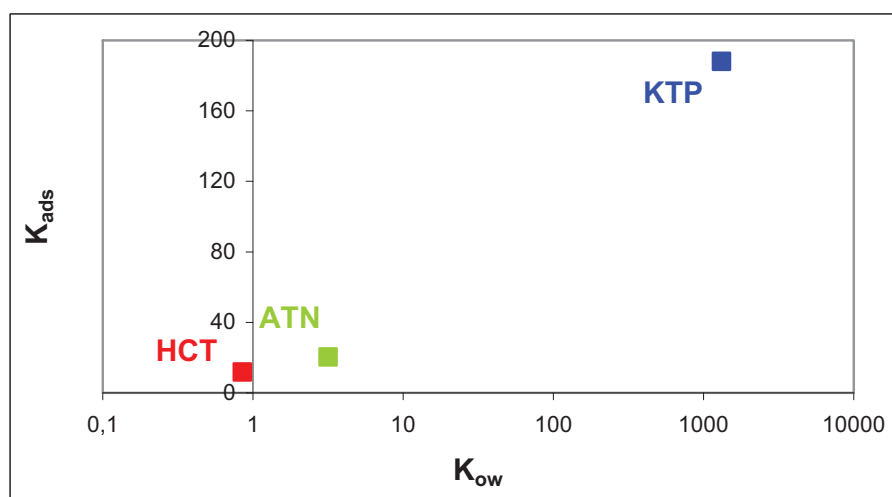


**Figure 4.23**  $K_{ads}$  vs.  $K_{ow}$  for KTP (blue), HCT (red) and ATN (green) on Y200

Similarly to what observed for BEAs zeolites and what retrieved in literature for oxygenate compounds adsorption on different zeolites [Mallon et al., 2011], an increase of the Henry's constant with the hydrophobicity ( $K_{ow}$  in logarithmic scale) of the solute has been observed.

Even if solely two zeolites and three solutes have been considered, the correlations between  $K_{ads}$  and  $K_{ow}$  for compounds characterised by different physical-chemical properties can be applied to different zeolite frameworks. Further investigations on other zeolites framework and molecules adsorbed are required to generalise this behaviour which can be a useful tool to predict adsorption selectivities.

#### 4.1.2.2 RELEASE TESTS

Some release experiments have been carried out in order to establish if the selected zeolite can be employed as adsorbent in pre-concentration methods. Water at different pH values, in presence or not of an organic solvent as methanol, have been tested as extracting phases and the percent releases for each extracting solvent were reported in Table 4.14.

**Table 4.14** Release of drugs from Y200 in different solvents

<b>Solute</b>	<b>Solvent</b>	<b>Release %</b>
<b>KTP</b>	H <sub>2</sub> O (pH 5.5)	0.10
	H <sub>2</sub> O (pH 10.5)	79
	MeOH : H <sub>2</sub> O = 70 : 30 (pH 3.3)	89
<b>HCT</b>	H <sub>2</sub> O (pH 5.5)	19
	H <sub>2</sub> O (pH 10.1)	75
	MeOH : H <sub>2</sub> O = 70 : 30 (pH 5.3)	95
<b>ATN</b>	H <sub>2</sub> O (pH 5.4)	12
	H <sub>2</sub> O (pH 3.2)	96
	MeOH : H <sub>2</sub> O = 70 : 30 (pH 10.1)	50

KTP is not at all released in water, but increasing the pH of water to pH 10 KTP release strongly increases, according to what observed in its q vs. pH graph (Figure 4.22a): KTP, negatively charged at pH 10, is quickly desorbed from zeolite, because electrostatic repulsions take place with zeolitic framework. By adding an organic solvent as MeOH, even though at pH 3 KTP adsorption on Y200 is relevant because the molecule is undissociated, the release increases reaching a value of 89%: this fact can suggest an increasing of the interactions between the neutral KTP and the solution enriched in organic modifier.

HCT release in water is low but not negligible, even though at pH 5.5 this molecule is in its neutral form; possibly this behaviour is due to the low adsorption constant of HCT on Y200 (see Table 4.11). Similarly to KTP, at pH 10 the release greatly increases because of electrostatic repulsions between the negatively charged drug and the zeolitic



framework. Furthermore, a release equal 95 % is observed in MeOH:H<sub>2</sub>O=70:30 at pH 5.5 due to an increase of the affinity of HCT with the solution.

A small ATN release in water is observed due to the high solubility of the positively charged form of this drug at  $\text{pH} < \text{pK}_a$  with respect to the neutral form: this fact confirms the q vs. pH trend. By lowering the pH to 3, the release strongly increases, reaching a satisfying value of 96 %.

Different from the other two drugs, the release in solution enriched with organic modifier does not exceed the 50 % at pH 10. It should be considered that at this pH value the ATN ( $\text{pK}_a = 9.5$ ) is not completely in its neutral form; probably a better release could be reach in more basic solutions.

## **4.2 PFOA adsorption on mesoporous materials**

Data which are next reported are part of my work of thesis and have been recently published: [Nassi M., Sarti E., Pasti L., Martucci A., Marchetti N., Cavazzini A., Di Renzo F., Galarneau A.; J Porous Mater 2014, DOI 10.1007/s10934-014-9788-5].

### **INTRODUCTION**

Perfluorinated compounds (PFCs) have increasingly attracted global concern in recent years because of their wide application, global contamination, environmental persistence and potential toxicity to animals [Giesy et al., 2002; Lindstrom et al., 2011]. PFOS and PFOA are the most typical PFCs used in different industries and detected in aqueous environments [Fujii et al., 2007; Ahrens et al., 2009]. Therefore, it is very critical to find effective techniques to remove PFOA from wastewaters before they reach natural and drinking waters. In fact, on the basis of risk assessment, it has been hypothesized that continued exposure to even relatively low PFOA concentrations in drinking water could substantially increase the risk of health effects [Post et al., 2012]. Different technologies have already been tested, such as advanced oxidation, which were not enough efficient for the degradation of these fluorinated chemicals [Panchangam et al., 2009]. Alternatively, adsorption was demonstrated to be an effective and economical method for the remove of PFOA from water [Ochoa-Herrera et al., 2008; Sun et al., 2011]. Some adsorbents such as activated carbon, resin, crosslinked chitosan and activated sludge have been used to adsorb PFOA in aqueous solution [Deng et al. 2012].

Recently, ordered mesoporous molecular sieves have received increasing interest from the scientific community because of their unique properties: high surface area, high pore volume, controlled pore size in the mesopore range. Their open-framework nature and the adjustable large mesopore size (2-20 nm) are the key features for increasing accessibility of the molecules to the binding sites of the adsorbent [Renard et al., 2005; Mureseanu at al., 2011; Qin et al., 2007].

The objective of this study is to investigate and to compare PFOA adsorption on three high surface area mesoporous silica adsorbents in order to demonstrate the promising application of these adsorbents for low concentration PFOA removal from aqueous solutions. The adsorption of PFOA was investigated in the concentration range usually encountered in wastewater and in drinking water. The effect of pH on the adsorption properties of the materials was also examined.

## EXPERIMENTAL

The nanostructured mesoporous silica materials evaluated in PFOA removal are MCM-41 and HMS. MCM-41, synthesized in alkaline conditions following a method proposed by Galarneau [A. Galarneau, J. Iapichella, K. Bonhomme et al., 2006], was calcined in air at 550°C for 8 h (MCM-41c) to remove the surfactant molecules occluded in the pore network.

HMS mesoporous silica was synthesized in neutral ambient conditions following a method proposed by Galarneau [A. Galarneau, J. Iapichella, D. Brunel et al., 2006]. The template removal was carried out either by calcination in air at 550 °C for 8 h (HMSc) or by solvent extraction (HMSe).

Perfluorooctanoic acid (PFOA) adsorption isotherms in aqueous medium on mesoporous silica materials were determined using the batch method. The concentrations were quantified by high performance liquid chromatography with an electrospray tandem mass spectrometer (HPLC-MS).

### **4.2.1 MATERIALS CHARACTERISATION**

Nitrogen sorption isotherms, reported in Figure 4.24, were performed at 77 K after the samples being outgassed at 523 K until a stable vacuum of  $3 \times 10^{-3}$  Torr.

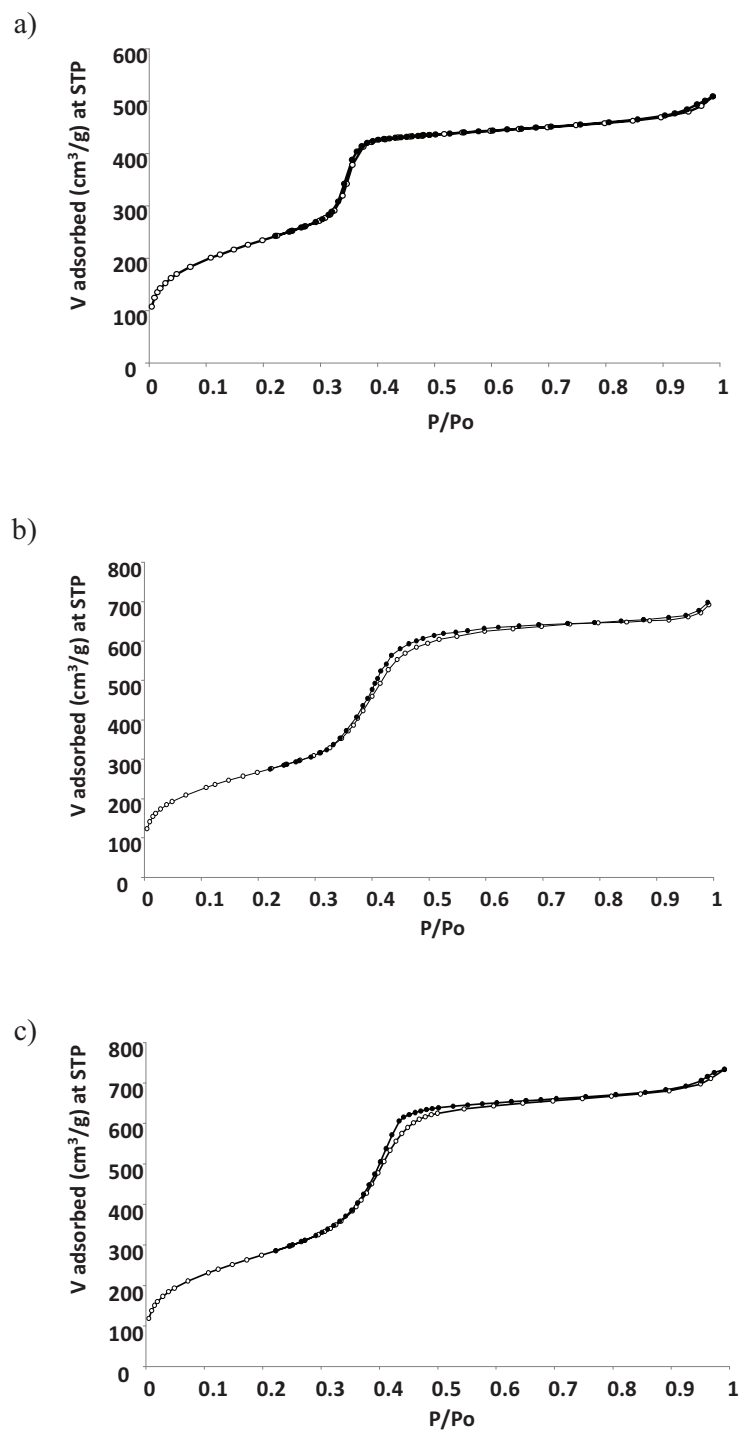


**Figure 4.24** Nitrogen adsorption/desorption isotherms at 77 K of mesoporous silica a) MCM-41c, b) HMSc and c) HMSe: adsorption (open circle) desorption (full circle)

From nitrogen adsorption isotherms, the BET surface area ( $S_{\text{BET}}$ ), the mesopore volume ( $V_{\text{L}}$ ) and the mesopore diameter ( $D_{\text{BdB}}$ ) of the mesoporous silica materials were determined and are reported in Table 4.15.

**Table 4.15** Textural characteristics calculated from nitrogen adsorption/desorption isotherms at 77 K of mesoporous silica materials

Materials	MCM-41c	HMSc	HMSe
$S_{\text{BET}}$ ( $\text{m}^2/\text{g}$ )	856	972	1019
$V_{\text{L}}$ ( $\text{mL}/\text{g}$ )	0.66	0.91	0.96
$D_{\text{BdB}}$ (nm)	3.7	3.9	4.2

The nitrogen sorption isotherms exhibited a type IV isotherm typical of mesoporous materials and a sharp step in the capillary condensation revealing a narrow pore size distribution around 4 nm for all materials. HMS adsorbents featured slightly higher surface areas ( $\sim 1000 \text{ m}^2/\text{g}$ ) and pore volumes ( $\sim 0.95 \text{ mL}/\text{g}$ ) in comparison to MCM-41c with surface area and pore volume of  $850 \text{ m}^2/\text{g}$  and  $0.70 \text{ mL}/\text{g}$ , respectively. The ethanol extraction of the template in HMS (HMSe) allowed to reach a slightly highest pore volume, pore size and surface area in comparison to the calcination process (HMSc), which often leads to a contraction of the network of as-synthesized mesoporous materials [A. Galarneau, M. Nader et al., 2007].

#### 4.2.2 ADSORPTION

As shown in Figure 4.25 a fast kinetics transfer process of PFOA from aqueous solution to mesoporous materials was observed for the three adsorbents.

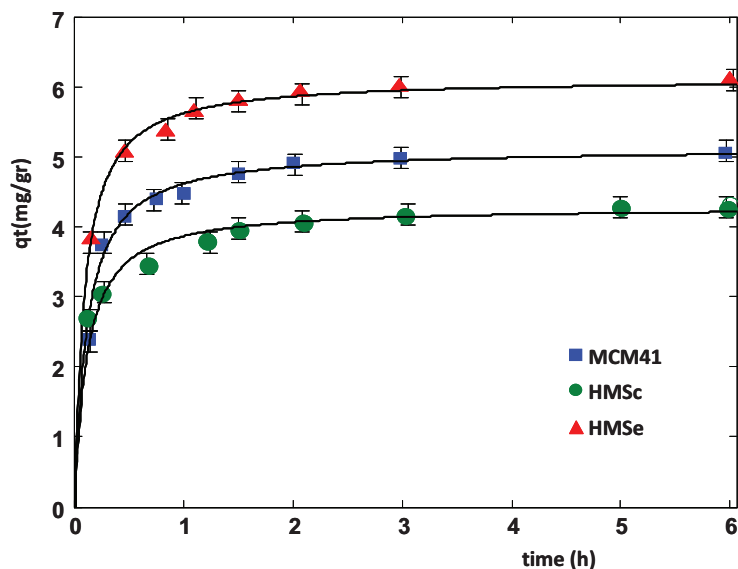


**Figure 4.25** Uptake of PFOA on mesoporous materials ( $q_t$  is the amount of solute sorbed per mass of sorbent at time  $t$ )

This first fast uptake was followed by a slower diffusional process towards the internal pore structure of the adsorbent. PFOA adsorption required about 2 h to reach the sorption equilibrium.

These results demonstrated that the kinetics of PFOA adsorption in mesoporous silica materials was very efficient in comparison to PFOA adsorption on other materials such as granular activated carbons (GAC) for which the sorption equilibrium was achieved after at least 10 h [Senevirathna et al., 2010] and alumina for which 48 h were needed [Wang et al., 2011]. The slow kinetics of GAC and alumina adsorption was interpreted on the basis of the long time required to the adsorbates to diffuse into the intraparticle pores of the materials [Yu, Zhang et al., 2009; Rattanaoudom et al., 2012]. Similarly, long equilibration times were also reported in studies of PFOA adsorption on a variety of minerals such as bohemite [Wang et al., 2012]. It has also been reported that shorter equilibration time could be obtained by reducing the particle sizes of activated carbon. Effectively, powder activated carbon (PAC) having particles size below 100  $\mu\text{m}$  showed a kinetic comparable [Hansen et al., 2010] to that obtained in our experiments on mesoporous silica materials with particles size ranging from 10 to 100  $\mu\text{m}$ . The smaller particles have larger external surface area and more functional groups are available for PFOS sorption, causing the faster adsorption on the PAC than that on the GAC [Yu et al., 2009]. Recently, fast kinetic of adsorption of PFOA (50 mg/L) was found using hydrotalcite (1 g/L) as adsorbents with 97% removal within 1 hour [Rattanaoudom et al., 2012]; however, hydrotalcite needed a pretreatment of 2h at 500  $^{\circ}\text{C}$  before to be used as adsorbents. Alternatively, silica based adsorbents do not need activation and can be regenerated by simple washing with acid solution to recover both the adsorbents and the adsorbed compounds or by calcination to recover the adsorbent, instead activated carbon are more difficult to regenerate. Moreover, reducing the size of the adsorbent materials did not always guarantee an increase of the adsorption kinetic, as an equilibration time of 10 h was reported for the adsorption of PFOA on multiwalled carbon nanotubes (MWNT) [Li et al., 2011].

The data of Figure 4.25 were fitted by the pseudo-second order model (see paragraph 3.4) and the results are reported in Table 4.16 where  $q_e$  is the amounts of solute sorbed per mass of sorbent at equilibrium,  $k_2$  is the second-order sorption rate constant,  $v_0$  is the initial rate,  $t_{1/2}$  is the half-time. The equilibrium uptake  $q_e$  and the adsorption rate constant  $k_2$ , were obtained from non linear fit of  $q_t$  versus  $t$ .

**Table 4.16** Adsorption kinetics parameters of PFOA on mesoporous silica materials

Adsorbents	$q_e$ (mg/g)	$k_2$ (g/mg/h)	$v_0$ (mg/h/g)	$t_{1/2}$ (h)	$R^2$
MCM-41c	4.29	1.76	32.3	0.13	0.9963
HMSc	5.13	1.12	29.6	0.17	0.9837
HMSe	6.12	1.83	68.7	0.089	0.9985

As shown, the pseudo-second-order model fits well all the sorption data as demonstrated by the resulting high coefficients of determination ( $R^2$ ). By comparing the kinetics parameters, HMSe reveals a much faster adsorption in comparison to HMSc and MCM-41c and furthermore allows a higher removal of the contaminant ( $q_e$ ) with 6.2 mg PFOA/g HMSe for an initial amount corresponding to 6.5 mg PFOA/g. HMSe led therefore to 95 % of PFOA removal whereas MCM-41c and HMSc eliminated 80 and 72 % of PFOA, respectively. The fitting of the kinetics data can be useful to compare adsorbents performances.

Experimental equilibrium isotherms of adsorption of PFOA with initial concentrations varying from 10  $\mu\text{g/L}$  to 10  $\text{mg/L}$  on mesoporous materials were measured and reported in Figure 4.26. The adsorption isotherms were fitted by the Langmuir model (Table 4.17), which is compatible with the size of the adsorbed molecule and with the pore size of the adsorbent materials (see paragraph 3.3). In fact, the effective diameter of PFOA was 0.91 nm, which was lower of the pore diameter of the mesoporous materials ( $\sim 4$  nm). Furthermore, the aqueous PFOA concentrations (0.010 – 15  $\text{mg/L}$ ) utilized in the current study were orders of magnitude lower than its critical micelle concentration (CMC of 25 mM or 10  $\text{g/L}$ ), and it has been demonstrated that in this concentration range, PFOA molecules preferred to form a monolayer.

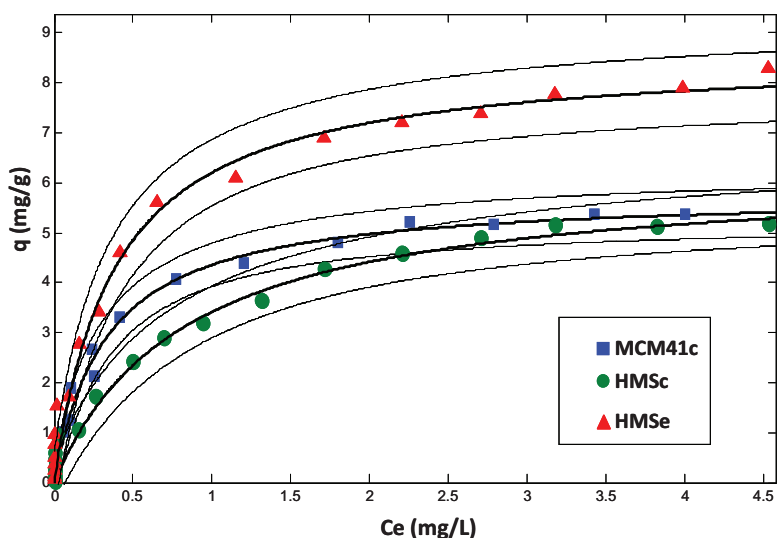


**Figure 4.26** Adsorption isotherm of PFOA on mesoporous materials.

**Table 4.17** Parameters estimated by non linear fitting, according to Langmuir model, of PFOA adsorption on mesoporous materials. The confidence limits at 95% of probability of parameters are reported in brackets.

Adsorbents	$q_s$ (mg/g)	$b$ (L/mg)	$R^2$
MCM-41c	5.21 (4.85, 5.57)	3.03 (2.57, 3.57)	0.9896
HMSc	4.27 (3.93, 4.61)	1.20 (0.94, 1.46)	0.9898
HMSe	9.29 (8.82, 9.76)	2.59 (2.15, 2.03)	0.9882

It can be noted that adsorption capacities of MCM-41c and HMSc for PFOA are lower than that of HMSe. Silica mesoporous materials revealed to be more efficient than alumina in PFOA removal; at the same time they showed adsorption capacity of the same order of magnitude respect powdered activated carbon [Hansen et al., 2010] especially when HMSe was considered.

Adsorption was investigated with thermogravimetric and diffractometric analysis too. Figure 4.27 shows thermogravimetric curves of mesoporous silica materials before and after saturation with PFOA.



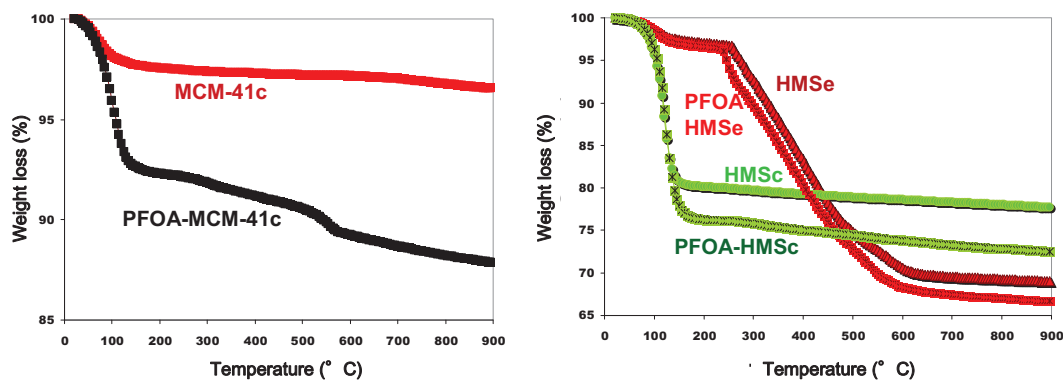


**Figure 4.27** Thermogravimetric curves of mesoporous materials before and after PFOA adsorption

From TGA performed on the three adsorbents, two weight losses due to water are expected: the first at low temperatures (25-150 °C) due to the desorption of water and the second from 200 to 900 °C due to the loss of water coming from the dehydroxylation of the silanols. For MCM-41c, the first water weight loss is very low (2.3 %), indicating the hydrophobic character of this material; the second water weight loss is low too (0.6 %), indicating a very low density of silanols (0.5 SiOH/nm<sup>2</sup>), which confirms its hydrophobicity. On the contrary, for HMSc the first water weight loss is high (23 %) revealing a more hydrophilic character; this is confirmed by the second weight loss (1.8 %), showing a higher calculated density of silanols (1.6 SiOH/nm<sup>2</sup>). This evidence suggests that silanols at the HMSc surface are randomly distributed with no hydrophobic patches on their surface as in MCM-41c. Concerning HMSe, TGA reveals a supplementary abrupt weight loss (27.6 %) from 250 to 800 °C, typical of organic degradation: this could be due to the incomplete removal of amines (70 %) by the ethanol extraction procedure. This result was different from literature data [A. Galarneau, M. Nader et al., 2007], where only a 6 % weight loss was obtained between 250 and 800 °C, relative to water loss due to silanol dehydroxylation and a complete template extraction. In our work, HMS synthesis was performed by a modified procedure [A. Galarneau, Iapichella, Bonhomme et al., 2006] in comparison to Tanev et al. [Tanev et al., 1996] with less ethanol and more water, which encountered for a higher ratio of protonated amines (as already observed for other composition of this synthesis) [A. Galarneau, Iapichella, Brunel et al., 2006], which are more difficult to extract with solvent in comparison to H-bonding amines at the surface of as-synthesized HMS. The extraction with ethanol of the protonated amines in strong electrostatic interaction with Si-O<sup>-</sup> was therefore difficult; to remove such strongly adsorbed

templates, acidic ethanol solutions are usually required. The remaining amount of hexadecylamine on our HMSe was corresponding to 0.077 mol of amines per mol of SiO<sub>2</sub> (or 0.76 amine/nm<sup>2</sup>). By taking into account the expected water loss for SiOH dehydroxylation (6 %) for a total extraction of the template as found by Tanev et al. [Tanev et al., 1996], one could hypothesize that the surface of our HMSe adsorbent was therefore composed of 0.8 protonated amine/nm<sup>2</sup> and around 0.8 SiOH/nm<sup>2</sup> giving a more hydrophobic character of HMSe in comparison to HMSc. This was confirmed by the first low weight loss of water below 150 °C (3.2 % for HMSe) in comparison to HMSc. During nitrogen adsorption isotherm measurement (Table 4.15) the remaining protonated amines were laying on the surface of the pores at 77 K and did not affect the nitrogen adsorption isotherm, which was similar as the nitrogen adsorption isotherm of calcined HSMc (with no organics at the surface).

This was an important point to highlight as HMSe featured in fact a hybrid organic/inorganic adsorbent, with protonated amines strongly adsorbed by electrostatic interaction at the surface of the pores conferring an hydrophobic character to HMSe adsorbent. It should also be mentioned that the incomplete removal of the template in HMS has been already observed in other works [Prado et al., 2002; Huang et al., 2011]; in particular, Huang et al. [Huang et al., 2011] found that only 78 % of the amine was removed by liquid extraction.

Three parts in TGA of MCM-41c-PFOA and HMSc-PFOA (Figure 4.27) were observed: 1) a sharp loss of adsorbed water between 25 and 200 °C, which is higher than what observed in absence of PFOA, showing a lower hydrophobicity of the materials after PFOA adsorption, 2) a smooth loss of PFOA between 200 and 350 °C [Ren et al., 2004], 3) a smooth loss of water due to dehydroxylation of silanols between 350 and 800 °C, which amount is higher than what observed in absence of PFOA, confirming the lower hydrophobicity of the silica mesoporous after adsorption. The amount of silanols, calculated from the water loss between 200 and 800 °C, corresponds to 0.5 and 1.6 SiOH/nm<sup>2</sup> for MCM-41c and HMSc respectively, and after PFOA adsorption these amount increased to 3.1 and 2.7 SiOH/nm<sup>2</sup> respectively. A long stay in water for MCM-41c and HMSc led to the opening of the siloxane groups into silanols rendering these materials fragile for further adsorptions. On the contrary, HMSe-PFOA shows exactly the same TGA profile as HMSe revealing no siloxane opening after a long stay in water so a very high stability in water. The only difference is a small very sharp loss of weight at 250 °C corresponding to a rapid loss of PFOA at this temperature. However the weight loss (2.27 %) is higher than the one expected from

Langmuir isotherm (0.97 %): the excess weight loss would correspond to the loss of hexadecylamine (HDA) at 250 °C together with PFOA, suggesting the formation of a complex  $\text{HDA}^+/\text{PFOA}^-$  during the adsorption process. This could be the explanation for the faster and the higher capture of anionic PFOA on HMSe in comparison to MCM-41c and HMSc, due to these preferential sites of adsorption closed to the protonated HDA head groups at the silica surface driven mainly by electrostatic interaction. Figure 4.28 shows XRD patterns of mesoporous silica materials before and after saturation with PFOA.

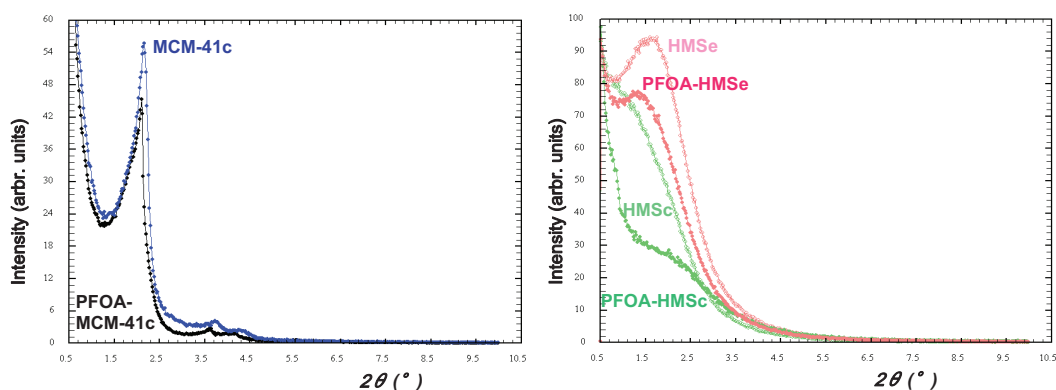


**Figure 4.28** XRD patterns of mesoporous materials before and after PFOA adsorption

XRD patterns of all materials after PFOA adsorption are similar to those before adsorption, suggesting a small modification of the initial mesoporous lattice during the subsequent adsorption of PFOA. Only a slight shift to higher  $2\theta$  values corresponding to an increase of unit cell parameter from  $a = 4.64$  to  $4.73$  nm for MCM-41c and an increase of pore distance from  $5.2$  to  $6.8$  nm for HMSe have been noticed.

#### 4.2.2.1 Effect of pH

It was recognized that the PFOA adsorption could be influenced by the pH of the aqueous solution. In particular, it has been reported in the sorption of PFOA on boehmite and on alumina, a decrease in the adsorbed quantity by increasing pH: this behaviour was explained as due to protonation of the alumina or boehmite surface, thereby reducing the number of positive sites on the sorbent, while considering PFOA in its anionic form [Wang et al., 2011; Wang et al., 2012].

In order to investigate the possible influence of pH on adsorption, the amount of adsorbed PFOA has been evaluated varying the pH of the solution (Figure 4.29).

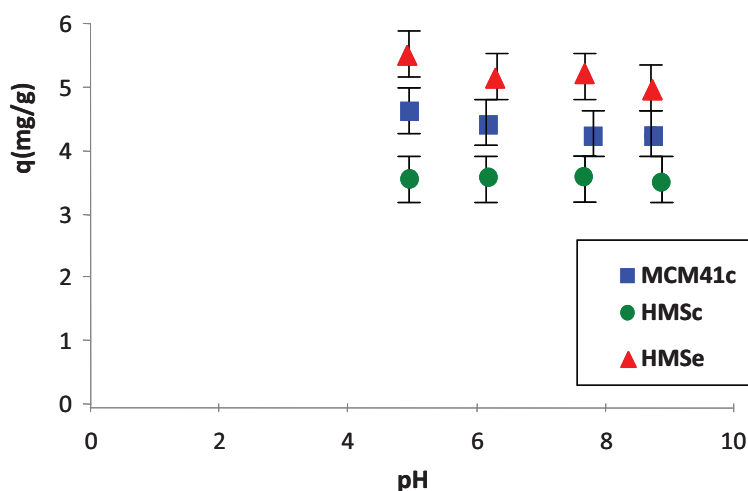


**Figure 4.29** Adsorbed amount ( $q$ ) versus pH of PFOA on mesoporous materials

Figure 4.29 evidences that the adsorption of PFOA on the three mesoporous materials is not significantly affected by the solution pH in the studied range. Consequently, the adsorption is not influenced by the charge modification of both adsorbent surface and dissolved molecules from pH 5 to 9. The driving force to the adsorption of PFOA on silica materials is due to hydrophobic interactions between the hydrophobic part of the molecule and hydrophobic -Si-O-Si moieties of the mesoporous silica surface [Ottaviani et al., 2001; Moscaletti et al., 2004], and possibly to some H-bonding with some COOH head groups of PFOA (in equilibrium with its anionic form) and silanols at the lowest studied pH [Pasti et al., 2013]. However, since the adsorption does not decrease with pH, the contribution due to H-bonding is supposed to be lower than that due to hydrophobic interaction. Similarly, the electrostatic interactions between PFOA and siliceous surface are negative at pH over 4 ( $pK_a < 4$ ) and they don't contribute to the adsorption driving forces. In conclusion, the interactions responsible for PFOA adsorption on silica mesoporous materials are mainly hydrophobic ones. Perfluorochemicals are a family of aliphatic hydrocarbons with hydrophobic properties and both MCM-41c and HMSc are sufficient hydrophobic materials, because of the low content in silanol groups. For HMSe, which demonstrated higher adsorption capacities than the other two mesoporous, two supplementary driving forces probably occur: 1) electrostatic interaction between  $\text{COO}^-$  head group of anionic PFOA form and protonated head group of hexadecylamines  $\text{HDA}^+$  of HMSe, 2) hydrophobic interaction between alkyl chains of both HDA and PFOA. For the PFOA-HMSe system the electrostatic forces seem to give a lower contribution than hydrophobic forces, since the pH of the solution does not significantly influence the adsorbed quantity.

### **4.3 MTBE adsorption on ferrierite**

Data which are next reported are part of my work of thesis and have been accepted for publication in Mineralogical Magazine on 23<sup>rd</sup> of January 2014.

#### **INTRODUCTION**

According to the United States Geological Survey, an emerging organic contaminant can be defined as “any synthetic or naturally occurring chemical or any microorganism that is not commonly monitored in the environment but has the potential to enter the environment and cause known or suspected adverse ecological and/or human health effects”.

Methyl-*tert*-butyl-ether (MTBE) is an octane enhancing fuel additive that is widely used and constitutes an important environmental pollutant. Sources of MTBE contamination include gasoline leaking from underground fuel-storage tanks, urban runoff and water craft [Rossner et al., 2008]. MTBE has received attention in surface, underground and drinking waters because it is a potential human carcinogen [Amberg et al., 2001; OEHHA, 1999] and it is difficult to remove because of its high water solubility and low volatility. In addition, MTBE is fairly resistant to biodegradation and chemical oxidation. In fact, traditional treatment technologies, such as air stripping, aerobic biodegradation, chemical oxidation reactions and activated carbon adsorption are expected to be less effective than zeolites in MTBE removal from contaminated waters [Chang et al., 2000; Knappe et al., 2005; Anderson 2000].

The objective of this study was to test the ability of a siliceous commercial ferrierite (*Zeolyst International* ferrierite, Si/Al ratio 35) in removing MTBE from water, in order to quantify aspects of its removal efficiency for potential use in wastewater and groundwater remediation.

#### **EXPERIMENTAL**

An X-ray powder diffraction study of siliceous silica H<sup>+</sup>-FER and of its precursor NH<sub>4</sub><sup>+</sup>-FER was undertaken in order to: 1) determine whether there is a structural basis for the sorption capacity of MTBE as observed in the hydrogen form of a silica-rich ferrierite; 2) investigate the flexibility of this zeolite; 3) determine the water amount in siliceous ferrierite. Thermal analyses (TG and DTA) of both materials and the saturated MTBE/H-FER have been carried out too.

An adsorption isotherm was determined using the batch method. MTBE concentration in water was determined using Gas Chromatography – Flame Ionization Detector (GC-

FID). Prior to this, MTBE was extracted from the water sample by Head Space - Solid Phase Micro Extraction (HS-SPME).

### 4.3.1 MATERIALS CHARACTERIZATION

The structure of ferrierite is shown in Figure 4.30.

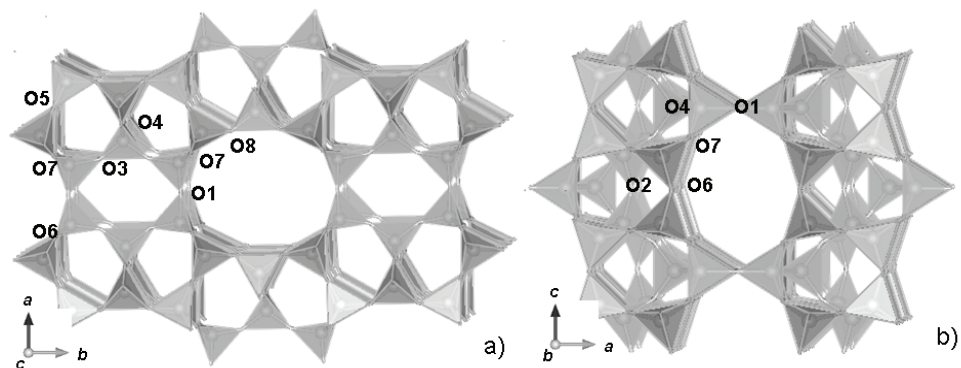


**Figure 4.30** Projection of FER framework along the crystallographic a) [001] and b) [010] direction

Powder patterns of  $\text{NH}_4\text{-FER}$ , H-FER and MTBE-FER were measured and are reported in Figure 4.31.

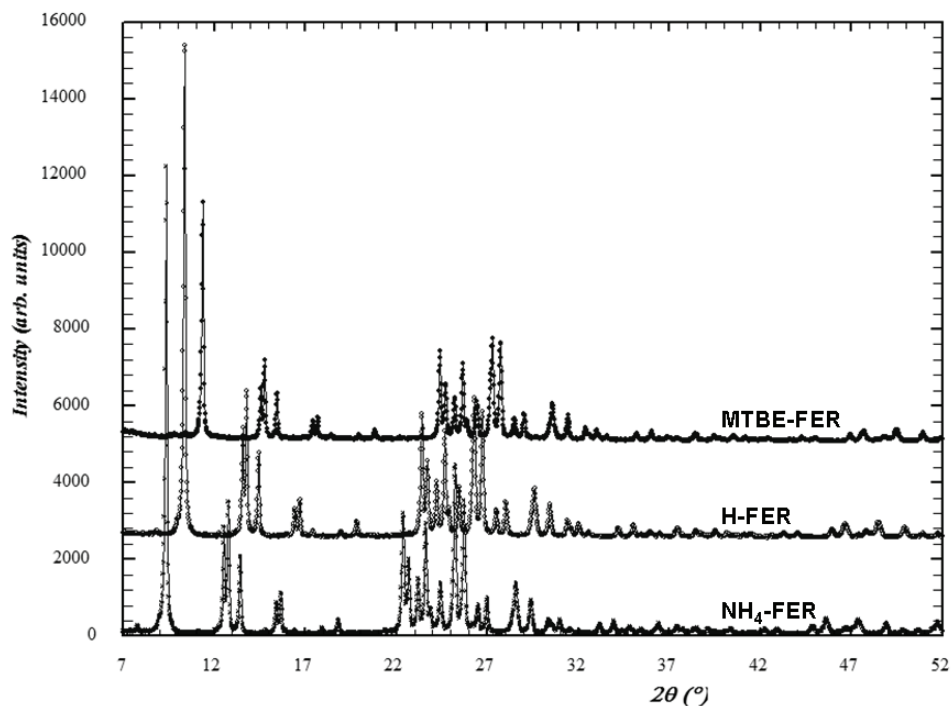


**Figure 4.31** Powder patterns of  $\text{NH}_4\text{-FER}$ , H-FER and MTBE-FER, respectively (the stacked plots have been shifted for easy comparison)

The unit cell parameters obtained by Rietveld refinement are given in Table 4.18.

**Table 4.18** Crystallographic data from the Rietveld refinements of NH<sub>4</sub>-FER, H-FER and MTBE-FER

	<b>NH<sub>4</sub>-FER</b>	<b>H-FER</b>
Space group	<i>Immm</i>	<i>Immm</i>
a (Å)	18.8477(8)	18.8367(7)
b (Å)	14.1049(5)	14.0733(4)
c (Å)	7.4425(2)	7.4420(2)
$\alpha=\beta=\gamma=90^\circ$	90	90
V (Å <sup>3</sup> )	1978.6(1)	1972.8(1)

NH<sub>4</sub>-FER crystal structure was determined by the Rietveld method in the *Immm* space group, using the structural model reported by [Cruciani et al., 1999] for a low-silica NH<sub>4</sub>-rich ferrierite.

The difference Fourier map revealed the presence of five partially occupied extraframework sites (W1, N, W2, W3, W4) localized inside the 10MR channel (W1 and W3), in the FER-cage (W2 and W4) and almost at the centre of the 8MR (N site), respectively (Figure 4.32).

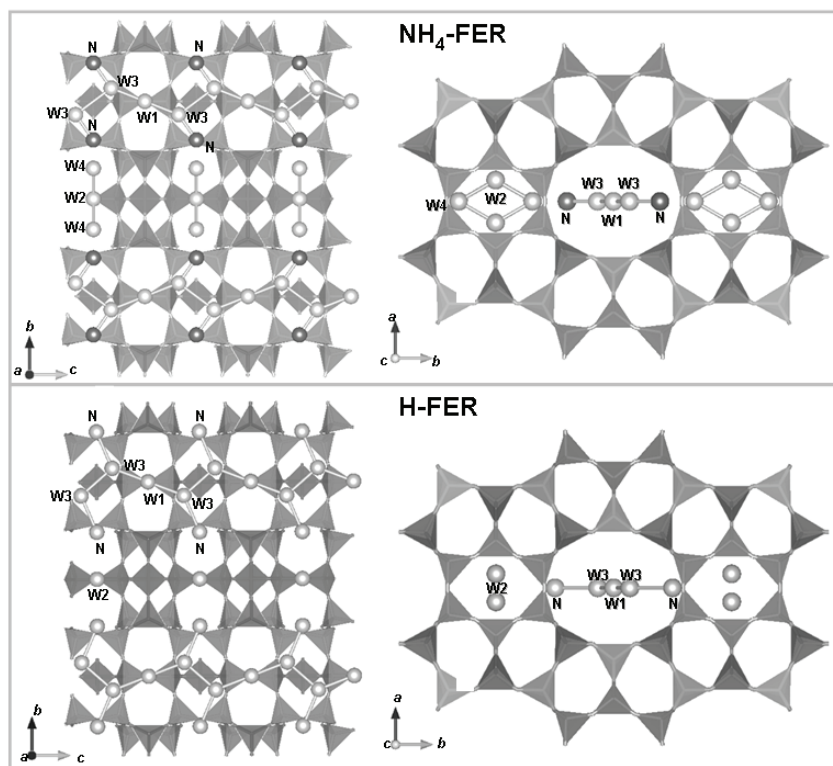


Figure 4.32 Projection of the extraframework sorbed molecules in  $\text{NH}_4\text{-FER}$  and  $\text{H-FER}$ , respectively.

On the basis of thermal analyses (Figure 4.33) it is reasonable to assume that these sites can host both water molecules and ammonium cations.

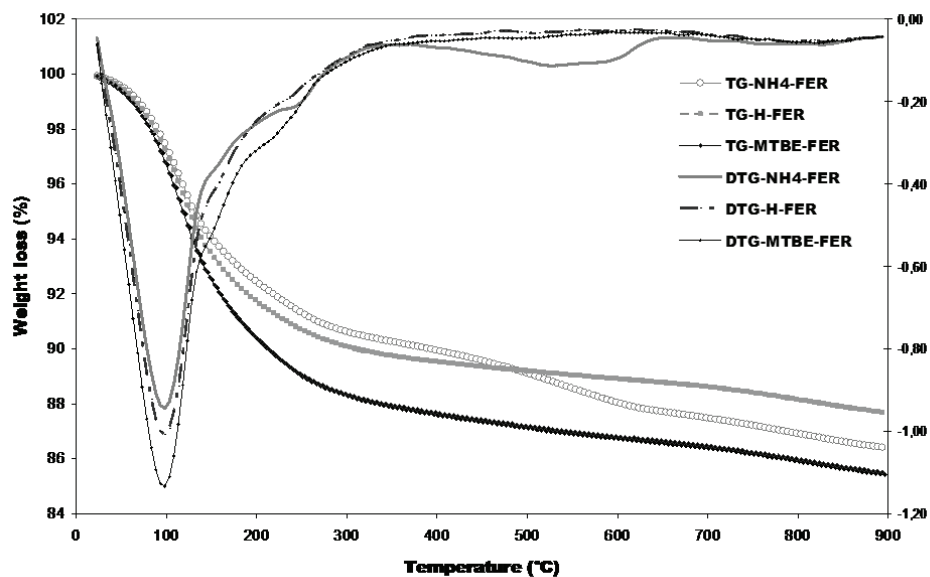


Figure 4.33 TG and DTG curves of  $\text{NH}_4\text{-FER}$ ,  $\text{H-FER}$  and  $\text{MTBE-FER}$ ,



Thermogravimetric curve (TG) of NH<sub>4</sub>-FER (Figure 4.33) reveals that total weight loss at 900 °C is about 13.6 %. In particular, the loss below 110 °C (~ 4.0 % in weight) could be associated with water molecules being weakly bonded to the surface, whereas residual weight loss (~ 9.7 % in weight) is due to decomposition of ammonium and water molecules. According to the TG and DTG curves, it is reasonable to assume that the weight loss below 400°C can be ascribed to water molecules, whereas the further weight loss at higher temperature is strictly related to the decomposition of ammonium. On the basis of the SAR, ammonium content corresponds to about 1 % in weight, suggesting that the weight loss at higher temperatures (110-900 °C) is mainly related to water molecules being trapped in the FER channel systems. Although distinguishing between NH<sub>4</sub><sup>+</sup> and H<sub>2</sub>O by X-ray diffraction is complicated owing to similar scattering factors, a reasonable level of discrimination was possible on the basis of the extraframework bond distances (Table 4.19).

**Table 4.19** Selected bond distances (Å) and angles (°) of the NH<sub>4</sub>-FER, H-FER and MTBE-FER extraframework sites

<b>NH<sub>4</sub>-FER</b>			
W1-W3	2.62(2)[x4]	W2-W2	2.54(6)
N-O6	2.87(1)[x2]	W2-W4	2.55(3)[x2]
N-O7	3.25(1)[x4]	W3-W3	1.92(4)
N-W3	2.23(4)[x2]	W3-W3	2.57(4)
N-W4	2.06(5)	W3-W3	3.21(4)
		W4-O6	3.33(2)[x2]
<b>H-FER</b>			
W1-W3	2.78(2)[x4]	W2-W2	1.82(6)
N-O6	2.93(1)[x2]	W3-W3	1.99(5)
N-O7	3.17(1)[x4]	W3-W3	2.26(4)
N-W3	2.87(4)[x2]	W3-W3	3.01(4)
<b>MTBE-FER</b>			
<i>MTBE 1</i>		<i>MTBE 2</i>	
C11-C12	1.506(2)[x2]	C21-C22	1.508(5)[x4]
C11-O1m	1.431(1)[x2]	C21-O2m	1.423(4)[x4]
O1m-C13	1.425(3)	O2m-C23	1.481(8)
C12-C11-C12	105.5(2)	C22-C21-C22	106.0(4)[x2]
C12-C11-O1m	109.4(1)	C22-C21-O2m	108.1(2)[x2]
O1m-C11-O1m	113.5(2)	O2m-C21-O2m	117.7(8)[x2]
C11-O1m-C13	124.5(3)[x4]	C21-O2m-C23	119.1(7)
C13-C13	1.202(7)	C22-C22	1.815(3)
C13-O8	2.78(1)[x2]	C22-O2m	1.722(1)[x2]
O1m-O8	2.518(8)[x2]	C22-O3	2.96(2)[x2]
		C22-O4	3.06(6)
		O2m-O6	3.36(5)
		C23-O6	3.11(3)[x2]
		C23-O7	3.36(5)[x4]

The refined distances of the oxygen atom in the water molecules from the nitrogen atoms (see Table 4.19) suggest that water molecules are connected to each other to form W3-W3-W1-W3 zig-zag water chains parallel to *c*-direction with lateral branch of NH<sub>4</sub> bonded to W3 (N-W3 2.23(4) Å) and W3-W3 (2.57(4) Å: see Table 4.19 and Figure 4.32). A water oligomer (W4-W2-W4) aligned along *b*-direction and weakly interacting with O6 framework oxygen atoms (W4-O6 3.33(2) Å) was also detected. On the whole, ~ 8.6 water molecules (which correspond about to 6.6 % in weight) and approximately 1 ammonium cation (which corresponds to approximately 1 % in weight) per formula unit are localised inside the ferrierite channels system. Therefore, the structure refinement gave an extraframework content of about 7.5 % in weight, with respect to 9.7 % given by TG analysis.

After calcinations, only slight variations in both the positions and intensities of the diffraction peaks have been observed in the diffraction pattern when compared to NH<sub>4</sub>-FER (Figure 4.31), indicating that no remarkable structural deformations induced by calcination. Moreover, no evidence of symmetry changes have been found: consequently, the same *Immm* space group as in NH<sub>4</sub>-FER was adopted for H-FER structure refinement.

Rietveld refinement indicates a small but significant decrease in unit-cell parameters respect to the NH<sub>4</sub>-form (Table 4.18). Four partially occupied extraframework sites were recognized in H-FER and attributed to readsorbed water molecules. These sites corresponded to W1, N, W2 and W3 sites found in the NH<sub>4</sub>-FER sample. The N site, attributed to nitrogen ions in NH<sub>4</sub>-FER and replaced by water molecules in H-FER, is at about 0.9 Å from the same site in NH<sub>4</sub>-FER. As in the case of NH<sub>4</sub>-FER, the W1 and W3 sites form W3-W3-W1-W3 chains parallel to *c*-direction (see Table 4.19 and Figure 4.32) which are lateral branched to N site (N-W3 2.77(4) Å), W3-W1 (2.80(2) Å) and hydrogen bonded to O6 and O7 framework oxygen atoms (N-O6 2.91(1) Å and N-O7 3.16(1) Å). At the same time, N and W3 water molecules are connected to each other to form N-W3-W3-N water molecular oligomer parallel to *b*-direction (N-W3 2.77(4) Å), W3-W3 2.92(4) Å). The presence of water clusters in calcined rehydrated low silica ferrierite was also detected by Alberti [Alberti et al., 2010] by neutron powder diffraction. On the whole, Rietveld refinement reveals about 7.3 water molecules per unit cell corresponding to approximately 5.7 % in weight. The TG curve (Figure 4.33) of H-FER sample shows a sudden change in its slope at about 100°C thus indicating the presence of water molecules which are weakly bonded to the surface (~ 3 %). At the same time, weight loss at higher temperatures indicated the simultaneous presence of

structural water molecules hosted in the FER channels (~ 9.3 %). This result suggests that other water molecules are strongly disordered and spread on extraframework partially occupied sites which were not identified by the Rietveld structure refinement. The calcination process causes an expansion in both 10MR channel and in 8MR of the FER-cage as indicated by their Crystallographic Free Area (C.F.A.) values reported in Table 4.20; O-O distances refer to Figure 4.30.

**Table 4.20** Ten-membered ring (10MR) and eight-membered ring (8MR) dimensions, Crystallographic Free Area (C.F.A.) and channel's ellipticity ( $\epsilon$ : ratio between the larger and the smaller O-O diameters)

	FER-NH <sub>4</sub>	H-FER	FER-MTBE
<b>10MR</b>			
O1-O1	8.19(3)	8.28(4)	7.93(6)
O8-O8	6.65(1)	6.68(1)	6.72(2)
O7-O7	8.16(1)	8.18(2)	7.98(3)
C.F.A.	19.37	19.74	18.42
$\epsilon$	1.23	1.24	1.18
<b>8MR</b>			
O1-O1	7.44 (1)	7.44 (1)	7.44 (1)
O6-O6	5.71(1)	5.77(2)	5.57(2)
O7-O7	6.35(1)	6.33(1)	6.32(2)
C.F.A.	11.34	11.42	11.01
$\epsilon$	1.30	1.29	1.33

#### 4.3.2 ADSORPTION

A comparison of the X-ray diffraction patterns for H-FER and MTBE-FER (Figure 4.31) highlights that the peak intensities in the two patterns are markedly different. This effect is mainly evident in the low 2-theta region, which is strongly related to extraframework content, suggesting that MTBE molecules enter the ferrierite channels. At the same time, the diffraction peak positions are quite similar and consequently unit-cell parameters are not remarkably modified (Table 4.18). Moreover, the absence of *I*-centering forbidden peaks indicates that the space group does not change after adsorption. Consequently, the *Immm* space group was also adopted in MTBE-FER structure refinement, which was performed starting from the framework atomic coordinates obtained for H-FER.

Difference Fourier maps allowed to determine the exact location of MTBE molecules inside the ferrierite microporosities. Two crystallographically independent MTBE sites were localized inside the ferrierite microporosities: the first one (MTBE1) in the 10MR channel and the second one (MTBE2) in the FER-cage (Figure 4.34 and 4.35, respectively). MTBE1 and MTBE2 sites are partially occupied and each show, on a statistical basis, four possible orientations.

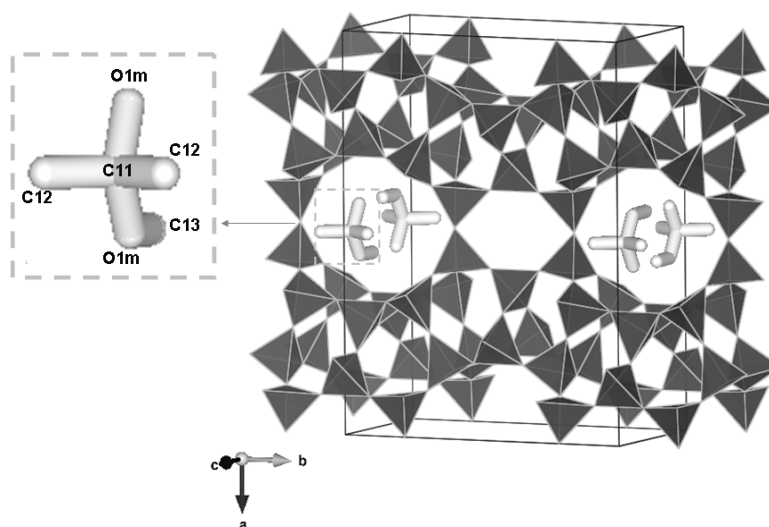


**Figure 4.34** Location of MTBE1 molecules in FER; the four possible orientations of MTBE1 molecule are drawn in two different 10MR channels for sake of clarity.

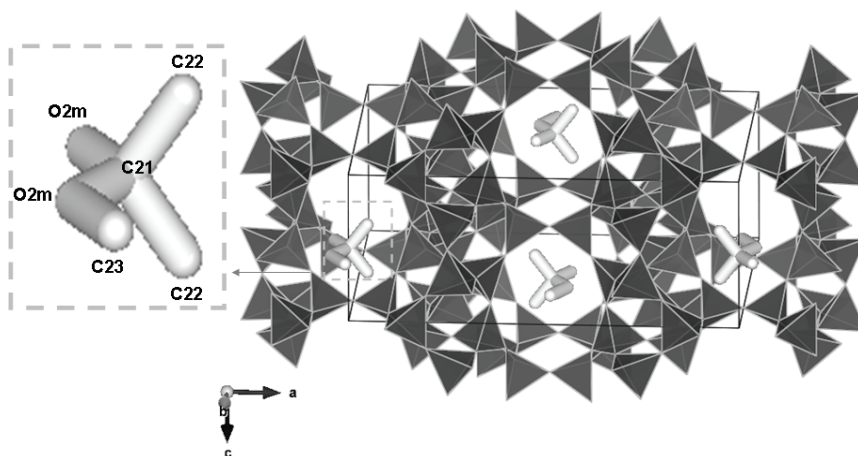


**Figure 4.35** Location of MTBE2 molecules in FER; the four possible orientations of MTBE2 molecule are drawn one in every FER cage for sake of clarity.

In particular, two and four orientations were identified for the *tert*-butyl and methoxy groups, respectively. The two possible *tert*-butyl group orientations are symmetrically related by the mirror plane perpendicular to *c*-axis in MTBE1 (Figure 4.34), and by the mirror plane perpendicular to *a*-axis in MTBE2 (Figure 4.35), respectively. Only one of these two positions can be occupied at any one time, due to the short methoxy C-methoxy C distance (C13-C13  $\sim$  1.2 Å) of neighbouring MTBE1 molecules, and to the short C22-C22 and C22-O2m distances of neighbouring MTBE2 molecules (Table 4.19). The MTBE1 methoxy group resides on the mirror plane perpendicular to *b*-axis and is aligned along *c*-axis, while the one belonging to MTBE2 is aligned along *b*-axis and lies on the mirror plane perpendicular to *c*-axis. Hence, the four possible methoxy group orientations are related by the mirror planes perpendicular to *a* and *c* axes, in MTBE1, and by mirror planes perpendicular to *a* and *b* axes, in MTBE2, respectively. On the whole, Rietveld refinement reveals the incorporation of about 1.8 MTBE molecules per unit cell (1.2 in MTBE1 and 0.6 in MTBE2 sites), corresponding to  $\sim$  6.6 % in weight. This result is in good agreement with the saturation capacity determined by the adsorption isotherm, reported in Figure 4.36.

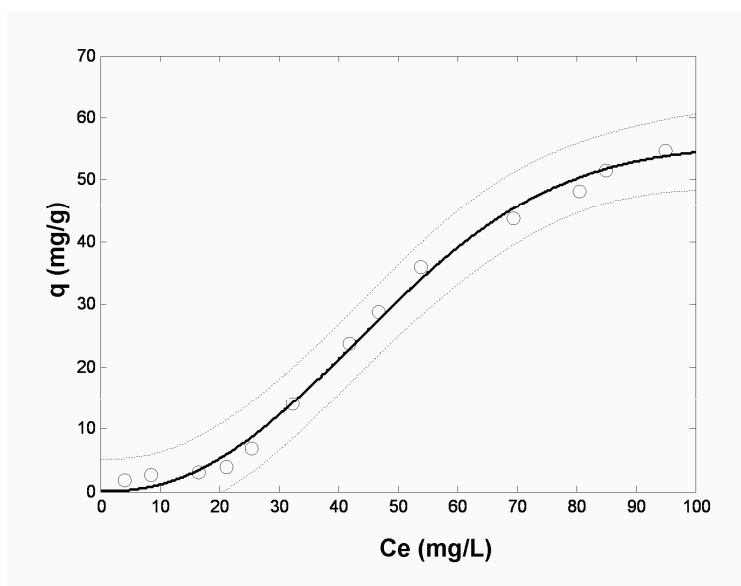


**Figure 4.36** Adsorption isotherm of MTBE on H-FER

In Figure 4.36 it can be seen that the adsorption data for MTBE on FER follows an S-class or type V isotherm (see paragraph 3.2).

The equilibrium isotherms of various organic-zeolite systems are usually Langmuirian in shape (concave downwards), suggesting the formation of a simple monolayer [Martucci, A., Pasti, L., Marchetti, N., Cavazzini, A., Dondi, F., Alberti, A., 2012].

However, S-shaped (concave upwards) isotherms have been already reported for the adsorption on Y zeolite of phenol and aniline derivatives from aqueous solutions [Koubaissy et al. 2011] as well of dichloroethane [Pasti et al. 2012].

S-shaped isotherms could describe systems where adsorption extends beyond the formation of a simple monolayer: in such cases, the BET isotherm model, which assumes an infinite number of adsorbed layers of the species, could be employed to fit the experimental data. Recently, Gritti et al. [Gritti et al., 2002] have shown that the BET isotherm is also suitable to describe multilayer isotherm of approximately 13 layers. However, if the ferrierite pore opening is considered, even for such a relatively small number of layers, there is insufficient space in the pores to hold this amount of analytes. S-shaped isotherms are also theoretically possible when lateral interaction between adsorbed molecules has an impact on sorption thermodynamics. Such models are, e.g., Ruthven and Fowler–Guggenheim isotherms [Fowler et al., 1965], which assume ideal adsorption on a set of localized sites with weak interactions between molecules adsorbed on neighbouring sites.

The experimental data were fitted through a quadratic model (see paragraph 3.3) giving a saturation capacity of 68.2 mg/g. The confidence limits at 95% of probability are 55.54 and 81.9, in good agreement with that obtained from Rietveld refinement.

The refined distances of the MTBE oxygen atoms from the framework oxygen atoms (O1m-O8 2.52(2) Å and O2m-O6 3.36(5) Å from Table 4.19) suggest that MTBE1 and MTBE2 molecules could interact with the framework causing remarkable deformations. In particular, after MTBE adsorption, the 10MR hosting the MTBE1 molecules narrows and becomes more circular, as indicated by the decrease in its C.F.A. and in its channel ellipticity  $\varepsilon$  values (Tables 4.20). At the same time, a narrowing (C.F.A. = 11.01 Å<sup>2</sup> in MTBE-FER and 11.42 Å<sup>2</sup> in H-FER) accompanied by an increase in ellipticity ( $\varepsilon$  = 1.33 in MTBE-FER and 1.29 in H-FER) is observed in the 8MR.

Thermogravimetric analysis (Figure 4.33) indicate that apart from the elimination of species which are weakly bonded to the surface (~ 4 % in weight below 100 °C), weight loss occurring at higher temperatures (~ 10 % in weight) is related to the expulsion of extraframework molecules (MTBE and H<sub>2</sub>O) trapped in the FER channels. According to the literature [Zhang et al. , 2008] the thermal decomposition pathway of MTBE (see DTG curve in Figure 4.33) includes formation of methanol and isobutene, CH<sub>4</sub> and H<sub>2</sub> elimination and C-H, C-C, C-O bond cleavage reactions.

Difference Fourier maps also showed the occurrence of several weak and diffuse maxima which can be attributed to co-adsorbed water molecules. This result suggests

that part of the weight loss above 100 °C in the TG curve (Figure 4.33), must be ascribed to a relatively small water amount in our FER-MTBE sample (~ 3.8 %). These molecules were spread over a number of weakly occupied sites, which were not localized by Rietveld structure refinement.



## **4.4 Toluene adsorption on ZSM-5**

### *INTRODUCTION*

Studies and applications on organic pollutants adsorption in microporous zeolitic materials from aqueous media have been relatively scarce. On the contrary, to date adsorption mechanisms in gas phase systems have been deeply investigated. Adsorption from gas phase systems can significantly differ from that obtained from the corresponding aqueous solutions due to the highly polar nature of water molecules. Therefore, research on hydrocarbon removal has mainly been focused on single components from air matrices, whereas the studies involving aqueous dilute solutions are few. However, in most environmental applications, these pollutants are present in the form of mixtures in very dilute aqueous solution.

The purpose of this work is to study the interaction and mobility of groundwater pollutants adsorbed in zeolite pores in order to improve the removal efficiency of water treatment plants. The efficiency of an organophilic ZSM-5 zeolite for the removal of an organic contaminant, i.e. toluene (TOL) was tested in order to get a better understanding of host–guest interactions occurring during adsorption processes.

This study aims to evaluate the effects on toluene adsorption in aqueous systems of:

- 1) the temperature. Variations of kinetic adsorption and diffusion coefficients may be induced by temperature variations: this aspect is important to evaluate the removal efficiency of ZSM-5 in surface waters as well as groundwaters, which are characterized by different temperatures.
- 2) the presence of ligni-derived phenolic monomers of molecular dimensions comparable to those of the pores of the adsorbent material. The literature shows that zeolites are generally less affected by the presence of organic material in the aqueous phase respect activated carbons. As phenolic monomers, caffeic acid (CA) and para-hydroxybenzaldehyde (HBA) have been chosen because their molecular dimensions and structures are quite similar to toluene ones, with the exception of polar functional groups. These two monomers are characterized by different acid-basic behaviour: in the pH range of natural waters, caffeic acid is partially dissociated because of its first dissociation constant ( $pK_{a,1}$  4.36) while para-hydroxybenzaldehyde is almost completely indissociated ( $pK_a$  7.72). Caffeic acid is employed in many pharmaceutical products thank to its antioxidant properties and para-hydroxybenzaldehyde is an ingredient or a reaction intermediate for fragrances production (see paragraph 1.4): it follows that these two phenolic monomers could be found in natural waters and so considered emerging pollutants, even if no adverse health or environmental effects have been yet observed.

In conclusion, during this study chromatographic, diffractometric and thermogravimetric techniques have been employed in order to achieve the following goals:

- to investigate the adsorptive properties of this hydrophobic synthetic zeolite towards toluene and the phenolic monomers
- to characterise its structure after the adsorption of the selected compounds
- to localise the solute inside the zeolite channels system
- to evaluate the possible competition on toluene adsorption from the selected phenolic monomers

### EXPERIMENTAL

Characteristics of the selected zeolite are reported in Table 4.21.

**Table 4.21** Structural and chemical characteristics of the zeolite under investigation

	<b>ZSM-5</b>
Supplier	Zeolyst
Supplier name	CBV 28014
Nominal cation form	NH <sub>4</sub> <sup>+</sup>
SiO <sub>2</sub> /Al <sub>2</sub> O <sub>3</sub>	280
Surface area (BET, m <sup>2</sup> /g)	400
Mean particles size (µm)	3

To obtain adsorption equilibrium isotherm data, aqueous phase adsorption experiments were performed in glass vials using a fixed sorbent/liquid ratio and varied concentrations of solute initial solutions. In all experiments, the vials were agitated on a fixed speed rotator for almost 24 hours, for adsorption equilibrium to be achieved. The solutes concentrations in the aqueous solutions were analyzed by HPLC/DAD.

#### **4.4.1 ADSORPTION OF TOLUENE**

The experimental kinetic data of toluene adsorption on ZSM-5 are shown in Figure 4.37 where the decrease in concentration  $C/C_0$  ( $C$ : concentration at time  $t$ ,  $C_0$ : initial concentration) is plotted vs. time, for three initial concentration levels.

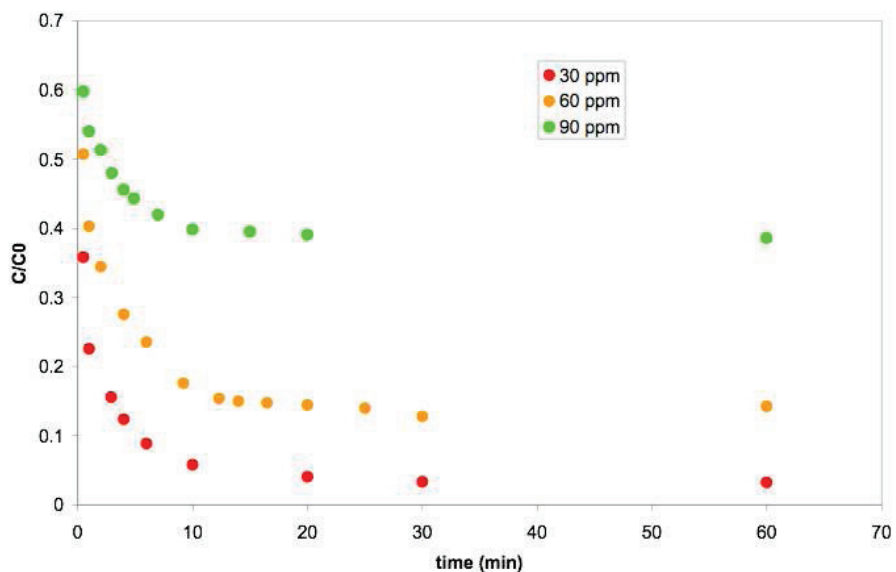


**Figure 4.37** Kinetic data for toluene adsorption on ZSM-5

Data have been fitted with the pseudo-second order model (see paragraph 3.4), which gave a satisfying correlation (coefficient of determination higher than 0.98). In Table 4.22, the pseudo-second order constant ( $k_2$ ) and the amount of solute sorbed per mass of adsorbent at equilibrium ( $q_e$ ) are reported.

**Table 4.22** Adsorption kinetics parameters of toluene adsorption on ZSM-5

Initial concentration $C_0$ (mg/L)	$k_2$	$q_e$ (mg/g)
30	0.0366	50.5
60	0.0502	65,8
90	0.0577	74.6

From Figure 4.37 it can be seen that the adsorption of toluene onto ZSM-5 is very fast. The adsorption isotherm was measured in order to define the adsorption capacity toward toluene of ZSM-5 and it is reported in Figure 4.38. Langmuir model (see paragraph 3.3) demonstrated to be suitable to fit experimental data (Table 4.23).

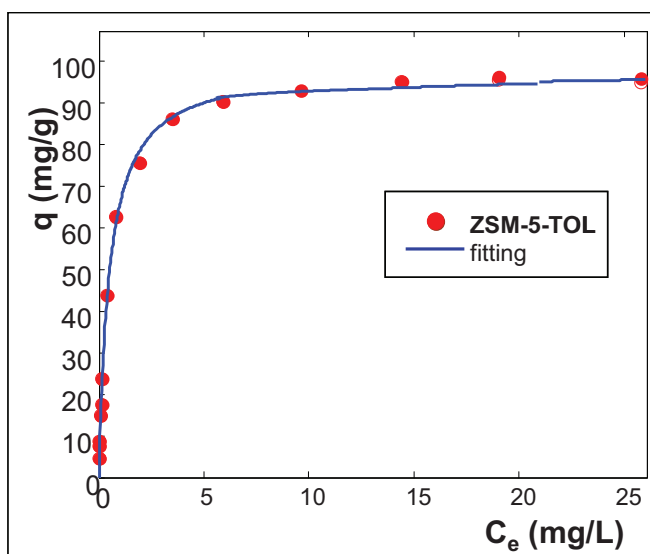


**Figure 4.38** Adsorption isotherms of TOL on ZSM-5

**Table 4.23** Parameters estimated by non linear fitting, according to Langmuir model, of TOL adsorption on ZSM-5. The confidence limits at 95% of probability of parameters are reported in brackets.

	<b>b</b> (L mg <sup>-1</sup> )	<b>q<sub>s</sub></b> (mg g <sup>-1</sup> )	<b>R<sup>2</sup></b>
<b>ZSM-5-TOL</b>	1.96 (1.65, 2.26)	91.5 (87.8, 95.2)	<b>0.9882</b>

This zeolite shows a very high SAR but notwithstanding its high hydrophobicity, the presence of adsorbed water molecules was detected by TG analyses (Figure 4.39).

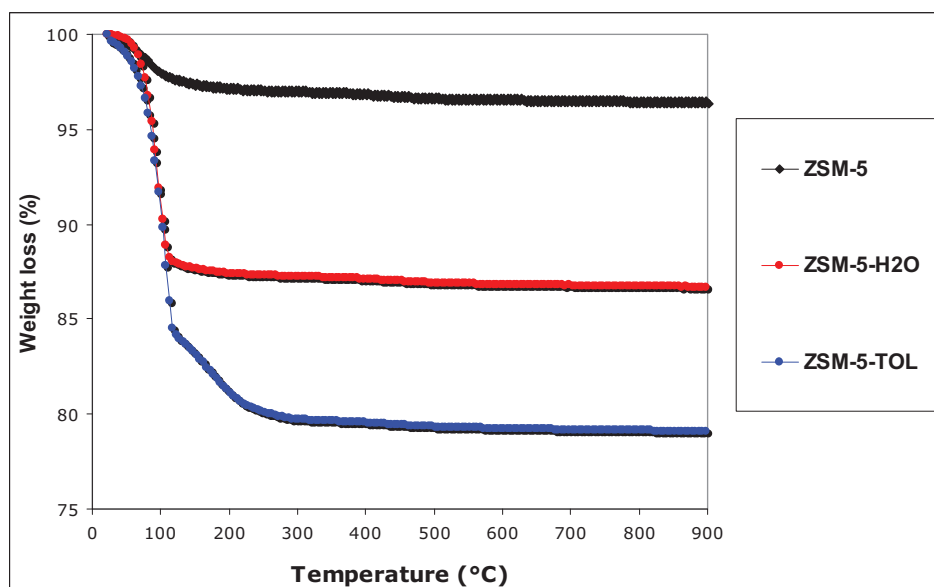


**Figure 4.39** Thermogravimetric analysis of ZSM-5 before and after adsorption of water and of toluene

TG analyses of ZSM-5 indicates the presence of H<sub>2</sub>O physisorbed to the surface (about 1 % in weight) which is lost at temperatures lower than 100 °C. At the same time, XRD analysis revealed the simultaneous incorporation of structural water molecules in all the investigated samples (about 1.8%) which are lost at higher temperature. Thermal analyses confirms toluene adsorption data: the TG curve of ZSM-5 after adsorption of TOL shows that, apart from the elimination of species bonded to the surface of the grains, a sudden change in its slope occurs at temperatures higher than 100 °C, which is probably due to the elimination of TOL and/or H<sub>2</sub>O molecules trapped within the zeolite pores. The estimated weight loss due to TOL is about 8%.

TOL adsorption onto ZSM-5 was confirmed also by X-ray powder diffraction: the results obtained by Rietveld structure refinements are shown in Figure 4.40.

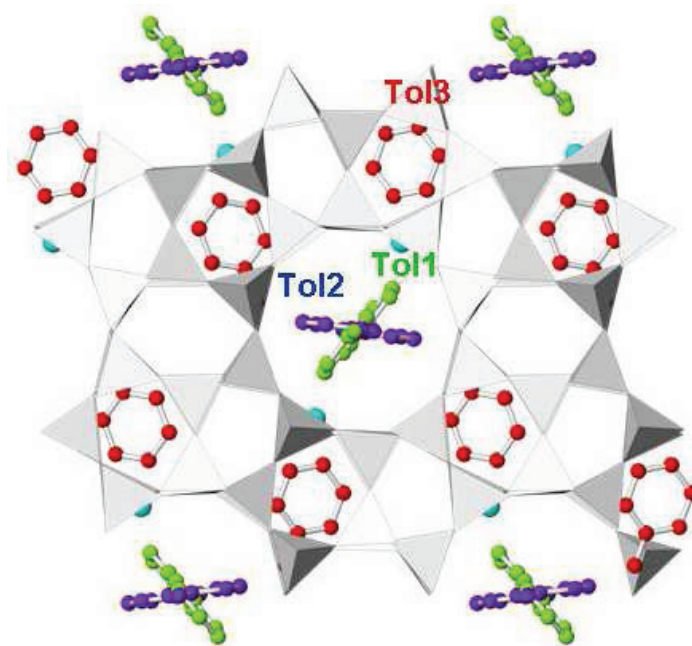


**Figure 4.40** Rietveld refinement of ZSM-5 saturated with toluene

The symmetry changes from monoclinic  $P2_1/n$  to orthorhombic  $P2_12_12_1$  and consequently remarkable variations of unit cell parameters are detected: toluene adsorption strongly modifies the geometry of the channel systems, which becomes more elliptical.

Rietveld refinement reveals the presence of 8 TOL molecules per unit cell, corresponding to about 9 % in weight, in good agreement with TG analysis (Figure 4.39) and with the adsorption capacity  $q_s$  (Table 4.23). Three disordered toluene sites were recognized (Figure 4.40): two of these sites (TOL1 and TOL2) are located at the intersection of the straight and sinusoidal channels and the third (TOL3) in the sinusoidal channel.

#### Effect of temperature

The adsorption of toluene on ZSM-5 was investigated at different temperatures, ranging from surface waters to groundwaters typical ones: the adsorption isotherms and the relative fitting parameters at four temperatures are reported in Figure 4.41 and Table 4.24.

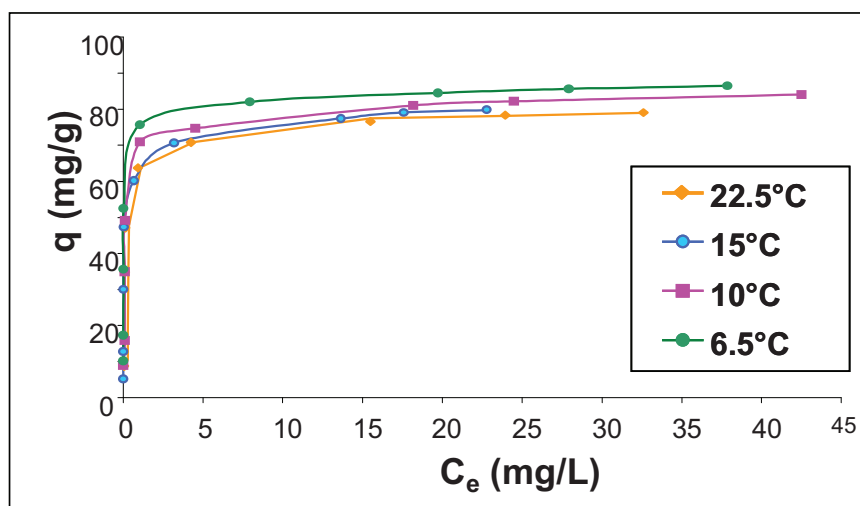


**Figure 4.41** Adsorption isotherms of TOL on ZSM-5 at four temperatures

**Table 4.24** Parameters estimated by non linear fitting, according to Langmuir model, of TOL adsorption on ZSM-5 at four temperatures. The confidence limits at 95% of probability of parameters are reported in brackets.

Temperature (°C)	b (L mg <sup>-1</sup> )	q <sub>s</sub> (mg g <sup>-1</sup> )	R <sup>2</sup>
22.5	2.31 (1.79, 2.83)	79 (73, 86)	0.9836
15	2.92 (2.12, 3.71)	80 (73, 87)	0.9778
10	4.6 (4.1, 5.2)	82 (77, 87)	0.9877
6.5	5.0 (4.6, 5.5)	82 (78, 86)	0.9912

It could be noted from Table 4.24 that the saturation capacities  $q_s$  are not statistically different in the considered temperature range, while the adsorption constant  $b$  increases as temperature decreases and, therefore, adsorption is exothermic for these systems.

Since the  $b$  parameter represents the equilibrium constant, it is possible to substitute it into the Van't Hoff equation (equation 4.2), in order to calculate the enthalpy.

$$\ln\left(\frac{K_{ads,2}}{K_{ads,1}}\right) = -\frac{\Delta H}{R}\left(\frac{1}{T_2} - \frac{1}{T_1}\right) \quad (4.2)$$

where  $K_{ads,2}$  and  $K_{ads,1}$  are the equilibrium constants at temperatures  $T_2$  and  $T_1$ , respectively,  $\Delta H$  is the enthalpy change for the process and  $R$  is the universal gas constant. The resulting Van't Hoff plot is shown in Figure 4.42.

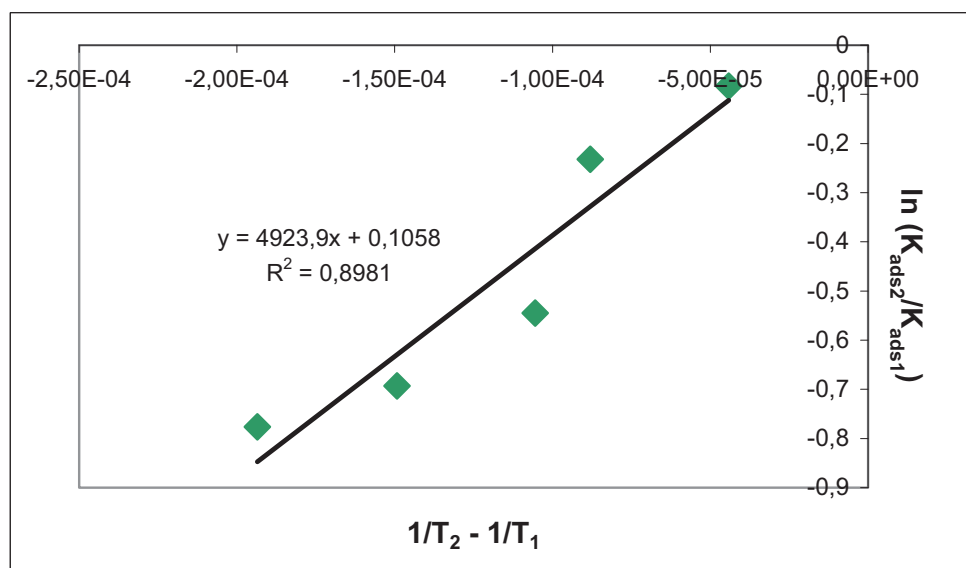


**Figure 4.42** Van't Hoff plot for toluene adsorption on ZSM-5

By multiplying the slope and the gas constant, a  $\Delta H$  value of  $-40.9 \text{ kJ mol}^{-1}$  has been obtained. This value accords with some literature data: Eder et al. [Eder et al., 1997] used TGA-DSC to find that the adsorption enthalpies on H-ZSM5 for butane ( $-58 \text{ kJ mol}^{-1}$ ) and pentane ( $-70 \text{ kJ mol}^{-1}$ ) are  $-6 \text{ kJ mol}^{-1}$  more exothermic than their branched counterparts, iso-butane ( $-52 \text{ kJ mol}^{-1}$ ) and iso-pentane ( $-64 \text{ kJ mol}^{-1}$ ). Mallon [Mallon, 2012] observed for adsorption of propylene glycol and 1,3-propanediol onto H-ZSM5 and H-Beta that the transfer from the bulk to the zeolite was slightly exothermic with enthalpies ranging from  $-4$  to  $-10 \text{ kJ mol}^{-1}$ .

Since the Henry's constant, enthalpy and temperature are known, the process entropy change ( $\Delta S$ ) can be calculated for each temperature using Equation 4.3:

$$\ln K_{ads} = \frac{\Delta H}{R} - \frac{\Delta S}{R} \quad (4.3)$$

The mean value obtained for  $\Delta S$  is  $-37.4 \text{ J mol}^{-1} \text{ K}^{-1}$ . Also entropy accords to what found by Mallon [Mallon, 2012], who observed that propylene glycol and 1,3-propanediol lose entropy upon transfer to H-ZSM-5 ( $-14$  and  $-18 \text{ J mol}^{-1} \text{ K}^{-1}$ , respectively).



#### 4.4.2 ADSORPTION OF CAFFEIC ACID

The adsorption isotherm measured at equilibrium (pH=4) is shown in Figure 4.43; analogously to toluene, the data fit well with Langmuir model (Table 4.25).

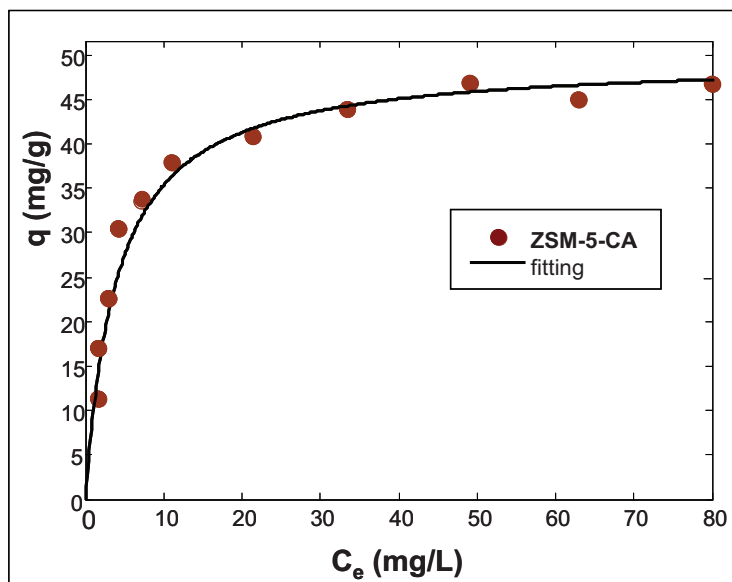


**Figure 4.43** Adsorption isotherms of CA on ZSM-5

**Table 4.25** Parameters estimated by non linear fitting, according to Langmuir model, of CA adsorption on ZSM-5. The confidence limits at 95% of probability of parameters are reported in brackets.

	<b>b</b> (L mg <sup>-1</sup> )	<b>qs</b> (mg g <sup>-1</sup> )	<b>R<sup>2</sup></b>
<b>ZSM-5-CA</b>	0.62 (0.54, 0.71)	47 (42, 52)	<b>0.9765</b>

Both adsorption constant  $b$  and saturation capacity  $q_s$  are lower for caffeic acid than the ones for toluene, indicating a higher affinity of ZSM-5 for toluene molecule. Caffeic acid adsorption on ZSM-5 has been studied also by thermal (Figure 4.44) and structural analysis (Figure 4.45).

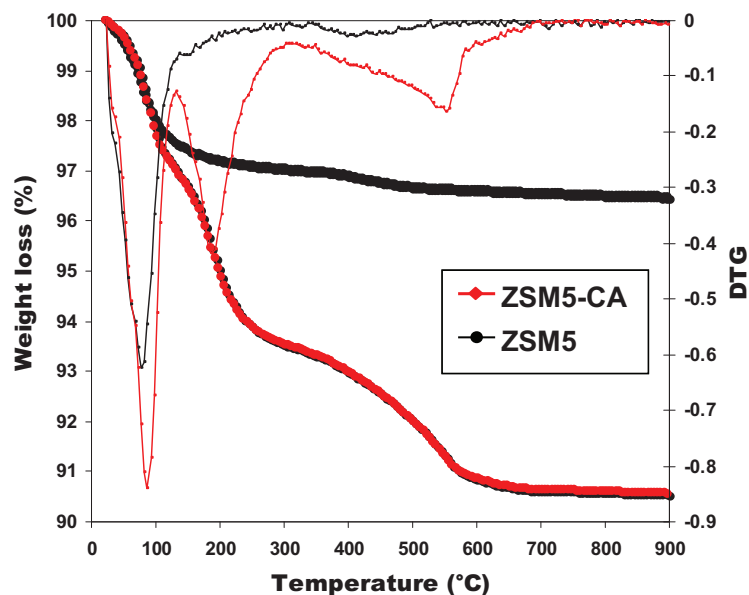


**Figure 4.44** Thermogravimetric analysis of ZSM-5 before and after adsorption of caffeic acid

In thermogravimetric curve of ZSM-5 saturated with CA it can be noted a 2.0 % weight loss at temperatures below 100°C, indicating species adsorbed solely on the external surface, and a total weight loss of 9.5%. Structural adsorption could be evaluated as 7.5 % in weight: this value doesn't strongly disagree with the saturation capacity ( $q_s$ ) value obtained from isotherm (Table 4.25).

CA adsorption onto ZSM-5 was confirmed also by X-ray powder diffraction: the results obtained by Rietveld structure refinements are shown in Figure 4.45.

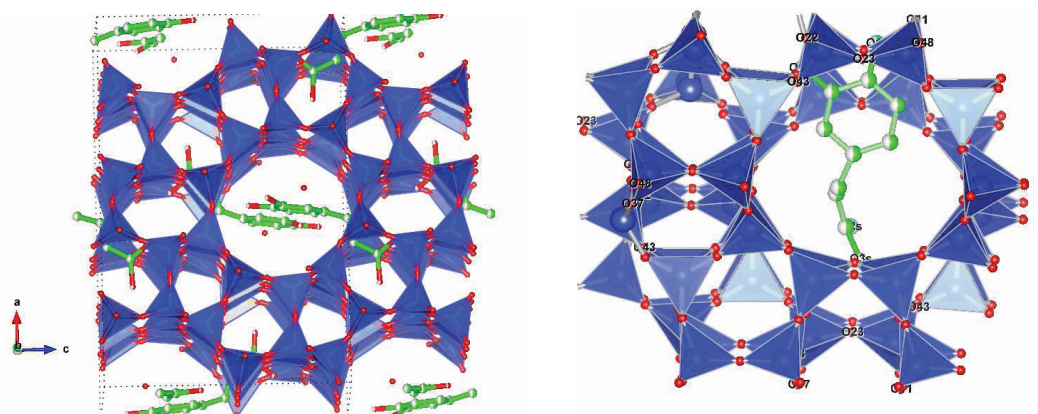


**Figure 4.45** Rietveld refinement of ZSM-5 saturated with caffeic acid

CA adsorption is confirmed by strong variations in elementary cell dimensions as well as clear changes in shape and dimensions of channels system. In fact, after CA adsorption, both straight and sinusoidal cavities of ZSM-5 tend to expand and to become less elliptical. Only one CA molecule, with two possible orientations, is located in the 10-ring. Both phenolic and carboxylic hydroxyl groups interacts with the framework.

#### Effect of pH

The adsorption of CA at a fixed concentration (40 ppm) from aqueous solutions at different pH has been studied and the results are shown in Figure 4.46.

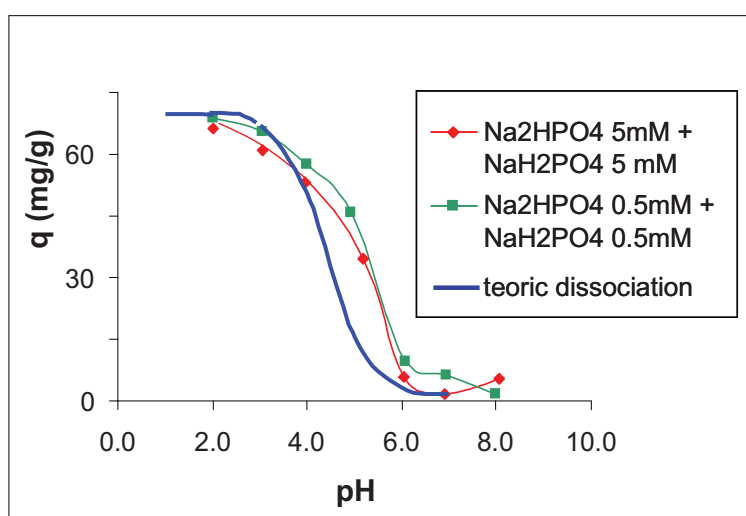


**Figure 4.46** Adsorbed amount ( $q$ ) of CA versus pH in phosphate buffer at two concentrations

CA adsorption decreases with increasing pH, due to the increase of the dissociated fraction negatively charged. At pH values when caffeic acid is almost totally dissociated, its adsorption on ZSM-5 approaches to zero.

For a given value of pH, the caffeic acid adsorption on ZSM-5 does not seem significantly affected by the presence of buffer solutions at different concentrations.

It can also be noted that there is a small shift between the two experimental curves and the theoretic dissociation one. This could be due to an acidic constant of the adsorbed CA which is slightly different from the one of the CA in bulk solution.

Sorption isotherms of CA on ZSM-5 at different pH values are shown in Figure 4.47.

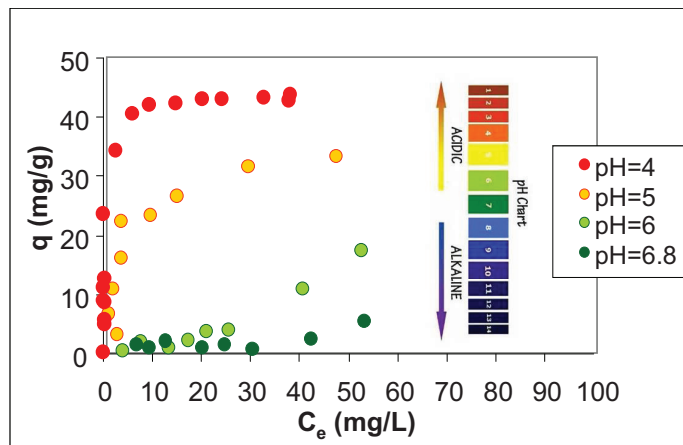


**Figure 4.47** Adsorption isotherm of CA in phosphate buffer at different pH values

Sorption is greater at pH 4 due to the greater abundance of the molecular form and the lower negative charge of the surface compared to pH 7.

Effect of ionic strength

The adsorption of CA from aqueous solutions with different ionic strength has been studied, varying NaCl content (Figure 4.48): this conditions well mimic natural sea waters.

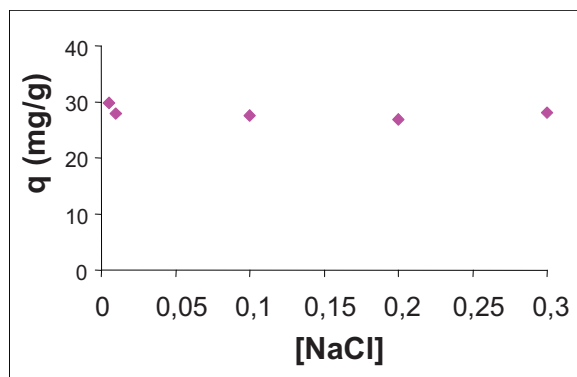


**Figure 4.48** Adsorbed amount (q) of caffeic acid at pH 5 versus NaCl concentration

As expected from Figure 4.46, ionic strength does not significantly influence the adsorption.

In freshwater, the most abundant cation is  $Ca^{2+}$ , so the adsorption of CA from solutions with different concentrations of  $CaCl_2$  has been investigated (Figure 4.49).

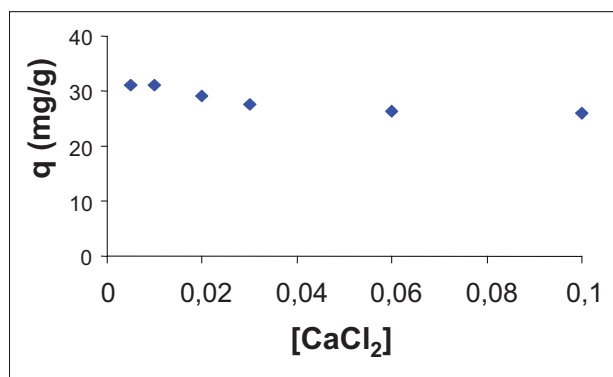


**Figure 4.49** Adsorbed amount ( $q$ ) of caffeic acid at pH 5 versus  $\text{CaCl}_2$  concentration

Also in this case, variations are not significant, indicating the absence of specific interactions with this cation.

Structural analysis confirm that salts presence does not influence CA adsorption, because it is located in the same crystallographic sites, with similar occupancies and maintaining interactions with zeolitic framework almost unchanged. For completeness, also adsorption measurements of toluene from solutions at different ionic strength using both  $\text{CaCl}_2$  and  $\text{NaCl}$  have been carried out: also in this case, no significant variations have been observed.

#### 4.4.3 ADSORPTION OF PARA-HYDROXYBENZALDHEYDE

The experimental kinetic data of HBA adsorption on ZSM-5 are shown in Figure 4.50 where the decrease in concentration  $C/C_0$  ( $C$ : concentration at time  $t$ ,  $C_0$ : initial concentration) is plotted vs. time, for five initial concentration levels.

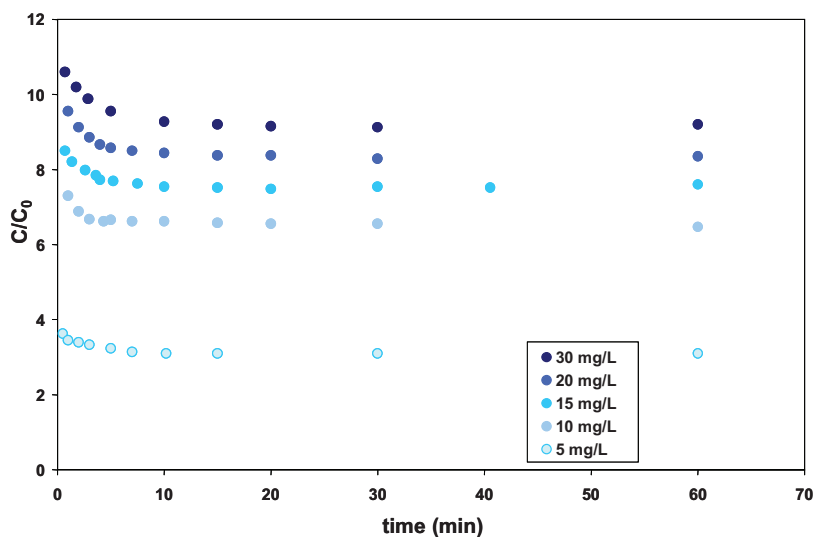


**Figure 4.50** Kinetic data for HBA adsorption on ZSM-5

Data have been fitted with the pseudo-second order model (see paragraph 3.4), which gave a satisfying correlation. In Table 4.26, the pseudo-second order constant ( $k_2$ ) and the amount of solute sorbed per mass of adsorbent at equilibrium ( $q_e$ ) are reported.

**Table 4.26** Adsorption kinetics parameters of HBA adsorption on ZSM-5

Initial concentration $C_0$ (mg/L)	$k_2$	$q_e$ (mg/g)
5	0.029	3.33
10	0.023	7.79
15	0.063	15.97
20	0.084	24.51
30	0.092	39.37

The pseudo-second order constant ( $k_2$ ) depends on the initial concentration  $C_0$  as indicated in equation 4.4:

$$k_2' = k_2 C_0^n \quad (4.4)$$

A value of 0.012 for  $k_2'$  was estimated, indicating a fast adsorption process.

The adsorption isotherm measured at equilibrium is shown in Figure 4.51 and the related data fitted with the quadratic model (see paragraph 3.3) are reported in Table 4.27.

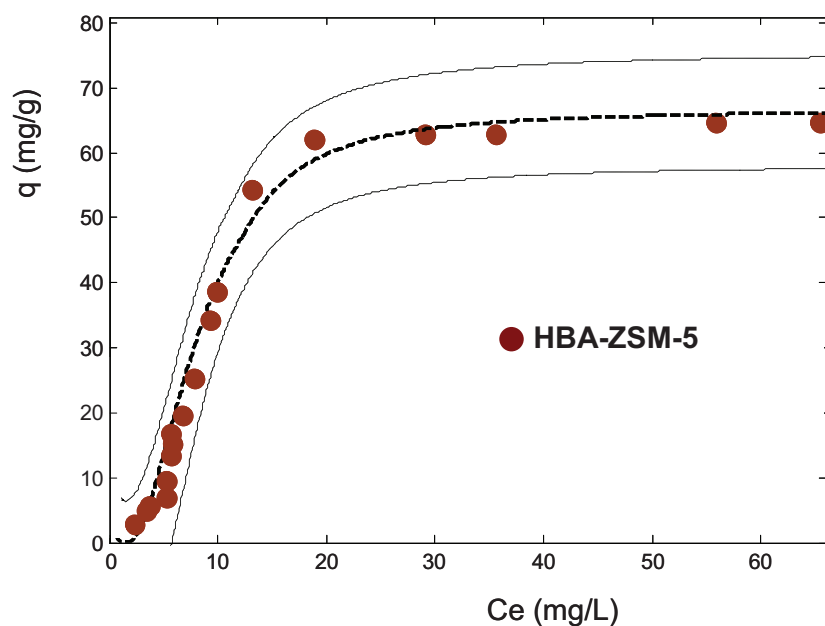


**Figure 4.51** Adsorption isotherm of HBA on ZSM-5

**Table 4.27** Parameters estimated by non linear fitting, according to the quadratic model, of HBA adsorption ZSM-5. The confidence limits at 95% of probability of parameters are reported in brackets.

	<b>b</b> (L mg <sup>-1</sup> )	<b>c</b> (mg g <sup>-1</sup> )	<b>q<sub>s</sub></b> (mg g <sup>-1</sup> )	<b>R<sup>2</sup></b>
<b>ZSM-5-HBA</b>	0.0326 (0.0166, 0.0486)	3.66 (2.83, 4.49)	66.7 (61.9, 71.5)	0.9821

In Figure 4.51, it can be seen that for the HBA-ZSM-5 system the adsorption isotherm does not follow a langmuirian trend, different from what observed for the TOL-ZSM-5 and CA-ZSM-5 systems (see Figures. 4.38 and 4.43, respectively). This behaviour seems to be due to a cooperative mechanism. To examine this aspect, IR and XRD analysis are required. This investigation is not reported herein.

#### Effect of pH

The adsorption of HBA at a fixed concentration (50 mg/L) from aqueous solutions at different pH has been studied and is shown in Figure 4.52.

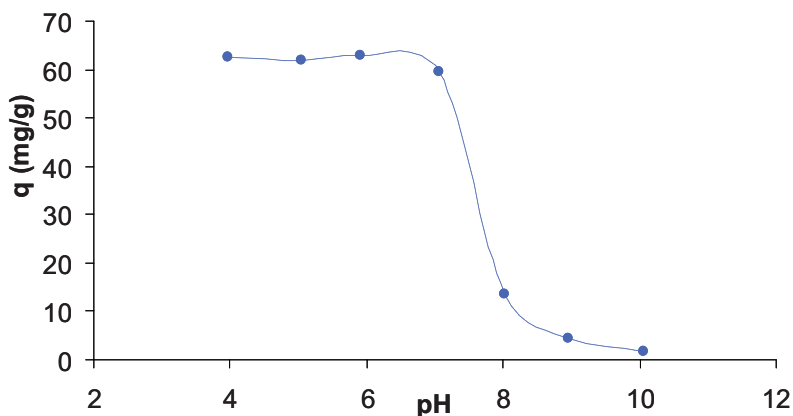


**Figure 4.52** Adsorbed amount (q) of HBA versus pH in water

Similarly to what observed for CA, at pH values when HBA is almost totally dissociated (pK<sub>a</sub> 7.72) hence negatively charged, its adsorption on ZSM-5 approaches to zero, revealing that ionic interactions assume an important role for adsorption.

#### **4.4.4 COMPETITION TOLUENE/CAFFEIC ACID**

The evaluation of the possible competition carried out by two phenolic monomers towards toluene adsorption has been studied.

The adsorption isotherms of toluene in absence and in presence of caffeic acid are shown in Figure 4.53.

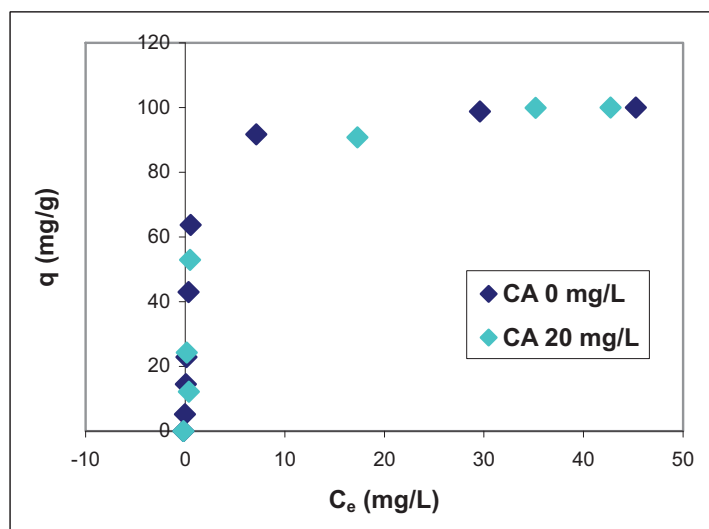


**Figure 4.53** Adsorption isotherm of toluene in absence (CA 0 mg/L) and in presence (CA 20 mg/L) of caffeic acid

The adsorption isotherm of toluene in presence of caffeic acid in solution doesn't significantly differ from the isotherm of toluene alone, suggesting that the presence of the phenolic monomer doesn't affect the adsorption of toluene. The competition between the two components has been investigated by keeping constant the initial concentration of TOL (30 mg/L) and by varying caffeic acid in a wide range of concentration, from 0 to 100 mg/L (Figure 4.54)

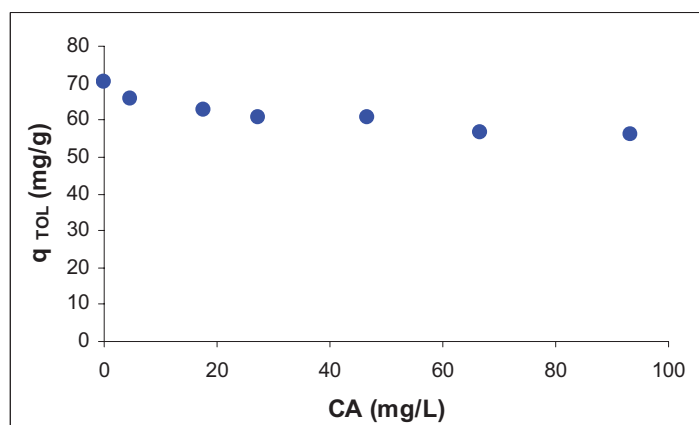


**Figure 4.54** Adsorbed amount of toluene ( $q_{TOL}$ ) at a fixed concentration vs. caffeic acid content in solution



A slight but not significant decrease of the amount of adsorbed toluene with increasing of caffeic acid concentration has been observed, suggesting that ZSM-5 adsorb preferentially toluene.

This observation has been confirmed by keeping constant the initial concentration of CA (20 mg/L) and by varying toluene in a wide range of concentration, from 0 to 100 mg/L (Figure 4.55)

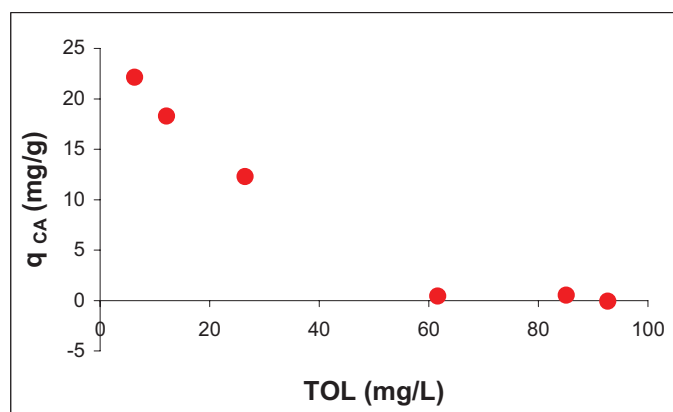


**Figure 4.55** Adsorbed amount of caffeic acid ( $q_{CA}$ ) at a fixed concentration vs. toluene content in solution

Caffeic acid adsorption on ZSM-5 quickly decreases, approaching to zero for concentration of toluene above 50 mg/L. Experimental data suggest that toluene and caffeic acid compete for the same sites inside ZSM-5 and that between the two components, the first is preferentially and exclusively adsorbed. In order to obtain some evidences about this, structural (Figure 4.56) and spectroscopic (Figure 4.57) analysis have been carried out.

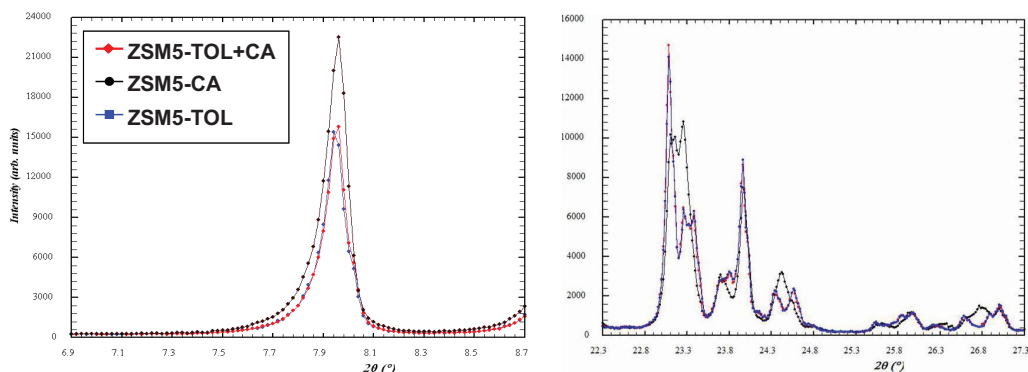


**Figure 4.56** Diffraction patterns of ZSM-5 saturated with toluene, caffeic acid and a mixture of them

From Figure 4.56, it can be seen that the XRD diffraction pattern of ZSM-5 saturated with the binary mixture TOL/CA results very similar with the zeolite saturated with toluene. The zeolite shows a strongly selective behaviour: while being able to adsorb caffeic acid, it "chooses" preferably toluene from the mixture, up to adsorb a content similar that with solely toluene in solution. Toluene always occupies the three crystallographic sites TOL1, TOL2, TOL3. The refinement confirms that the sites occupied by caffeic acid are now empty, indicating that the presence of this organic acid absolutely does not compromise the effectiveness of ZSM-5 toward toluene.

In Figure 4.57, the IR spectra of ZSM-5 before and after TOL and/or CA adsorption are shown.

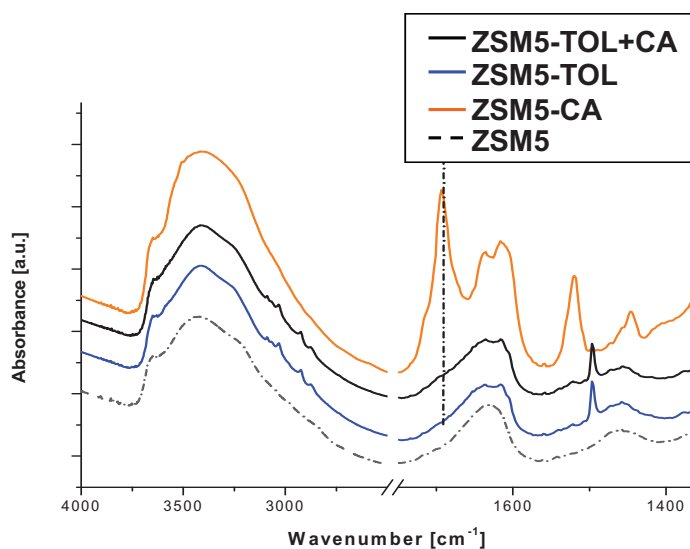


**Figure 4.57** IR spectra of ZSM-5 saturated with toluene, caffeic acid and a mixture of them

Infra-red spectra of Figure 4.57 can be so interpreted:

- $3400\text{ cm}^{-1}$  band in every lines is due to O-H stretch both of zeolite framework and of caffeic acid
- $3000\text{ cm}^{-1}$  small peaks in blue and black lines are due to C-H stretches (aromatic at frequencies  $>3000\text{ cm}^{-1}$ , aliphatic at frequencies  $<3000\text{ cm}^{-1}$ )
- $1680\text{ cm}^{-1}$  band in yellow line is due to C=O stretch of caffeic acid
- $\approx 1500\text{ cm}^{-1}$  peaks in blue, black and yellow lines are due to C-C stretches in the aromatic ring

Similarly to what observed from XRD diffraction patterns, there are many similarities between spectra of ZSM-5 saturated with the binary mixture and the zeolite saturated with solely toluene.

#### 4.4.5 COMPETITION TOLUENE/PARA-HYDROXYBENZALDHEYDE

In addition to caffeic acid, the possible competition on toluene adsorption by para-hydroxybenzaldehyde has been studied.

The adsorption isotherms of HBA in absence and in presence of TOL are shown in Figure 4.58 and the relative fitted data are reported in Table 4.28.

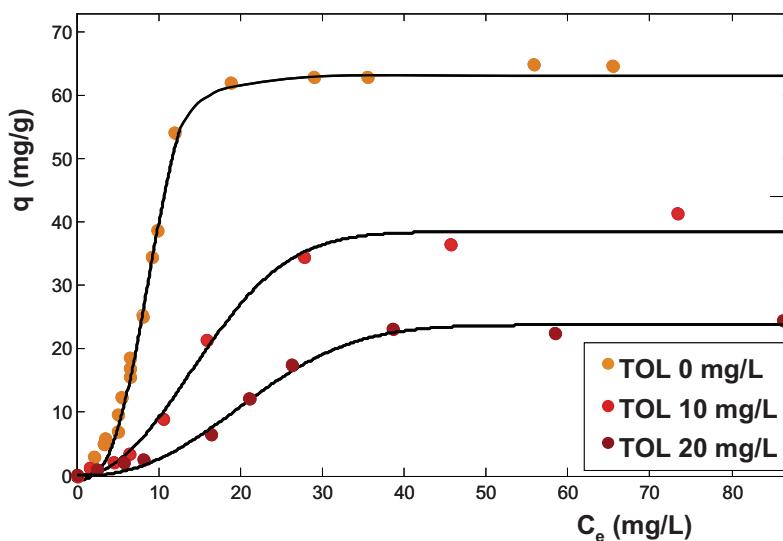


**Figure 4.58** Adsorption isotherm of HBA in absence (TOL 0 mg/L) and in presence (TOL 10 and 20 mg/L) of toluene

**Table 4.28** Parameters estimated by non linear fitting, according to quadratic model, of HBA adsorption ZSM-5 in absence and in presence of TOL. The confidence limits at 95% of probability of parameters are reported in brackets.

ZSM-5-HBA	<b>b</b> (L mg <sup>-1</sup> )	<b>c</b> (mg g <sup>-1</sup> )	<b>q<sub>s</sub></b> (mg g <sup>-1</sup> )	<b>R<sup>2</sup></b>
TOL 0 mg/L	0.0326 (0.0166, 0.0486)	3.66 (2.83, 4.49)	66.7 (61.9, 71.5)	0.9821
TOL 10 mg/L	0.00514 (0.00213, 0.00816)	2.35 (1.63, 3.06)	42.5 (38.7, 46.4)	0.9867
TOL 20 mg/L	0.0026 (0.00083, 0.0042)	2.47 (1.74, 3.21)	26.6 (22.5, 30.6)	0.9851

Figure 4.58 and Table 4.28 indicate that the presence of toluene in solution highly affects HBA adsorption: both the saturation capacity  $q_s$  and the adsorption constant  $b$ , decrease with increasing the toluene concentration. Also the parameter  $c$ , which accounts for the cooperation of the adsorbed solute, decreases when toluene is present in the solution.

In order to further investigate the possible competition between these two compounds, the adsorbed amount of HBA was measured by keeping the concentration of HBA constant at two initial concentration levels and by varying TOL content in solution in a wide range of concentration, from 0 to 100 mg/L (Figure 4.59).

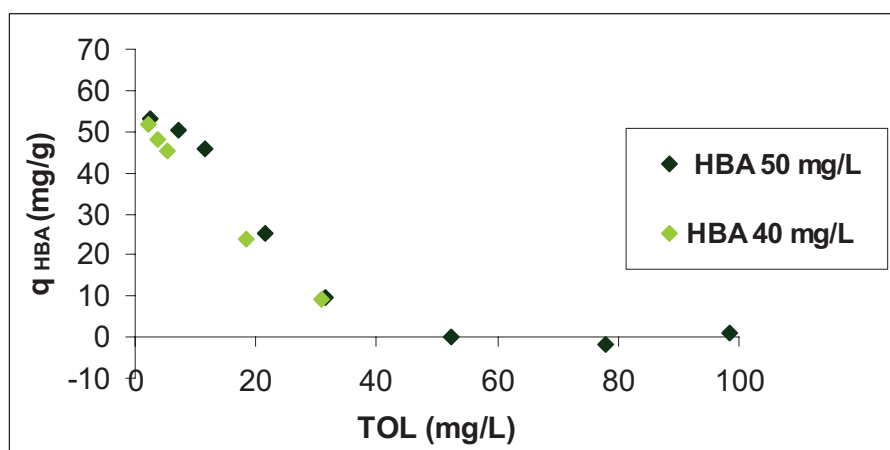


**Figure 4.59** Adsorbed amount of HBA ( $q_{\text{HBA}}$ ) at two concentration levels vs. TOL content in solution

Similarly, the concentration of TOL has been kept constant at two concentration levels and the HBA content in solution has been varied from 0 to 100 mg/L (Figure 4.60).

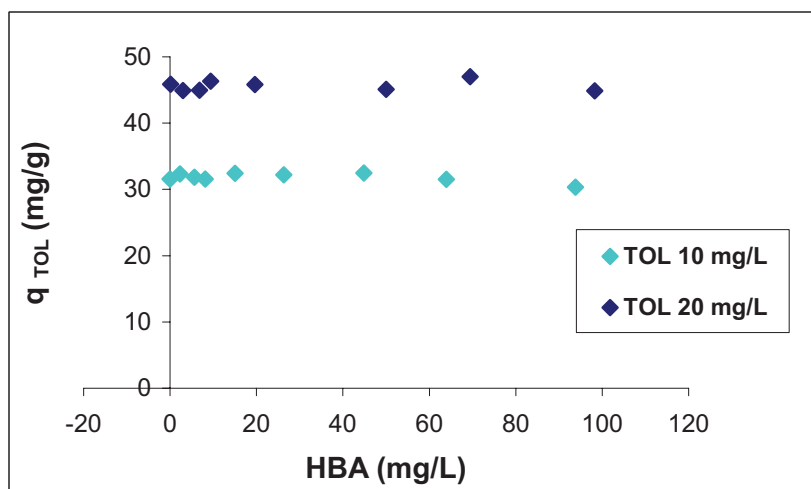


**Figure 4.60** Adsorbed amount of toluene ( $q_{TOL}$ ) at two concentration levels vs. para-hydroxybenzaldehyde content in solution

Figures 4.59 and 4.60 suggest that between the two components, toluene is preferentially adsorbed. In fact  $q_{TOL}$  remains almost unchanged with increasing of HBA concentration; on the contrary,  $q_{HBA}$  rapidly decreases with increasing of TOL concentration.

#### 4.4.6 EFFECT OF SOLUTE'S HYDROPHOBICITY

In the low concentration range, the adsorption was proved to be linear. The Henry's constants ( $K_{ads}$ ) for adsorption were calculated by the isotherm parameters (see equation 4.1) and put in graph vs.  $K_{ow}$ , as shown in Figure 4.61.

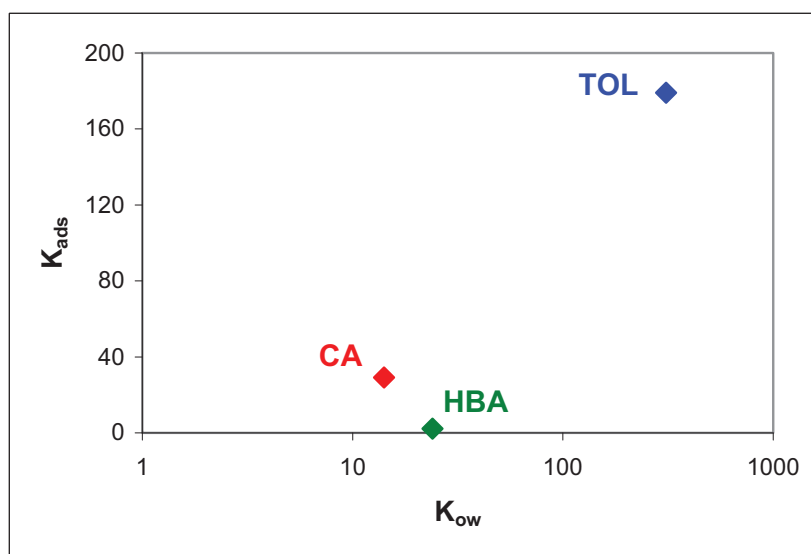


**Figure 4.61**  $K_{ads}$  vs.  $K_{ow}$  for TOL (blue), CA (red) and HBA (green) on ZSM-5

Although, solely three compounds were studied so that general conclusions cannot be formulated, the dependence of  $K_{ads}$  on  $K_{ow}$  shows that the adsorption constant increases with the hydrophobicity of the solute (in logarithmic scale), analogously to what observed for drugs adsorption on BEAs and Y zeolites (see paragraph 4.1).

However, for ZSM-5 it can be noticed that the relationships between  $K_{ads}$  and  $K_{ow}$  is not linear for CA and HBA: similar results were also reported by Mallon et al., 2011 which dealt with the adsorption of oxygenated compounds on several zeolites. This behaviour can derive from specific molecular interaction between the solutes and the zeolite framework.

Nevertheless, the increase of the adsorption constant with the hydrophobicity of the solute for different molecules adsorption (KTP, HCT, ATN in paragraph 4.1 and TOL, CA, HBA in this paragraph) onto different zeolitic framework (zeolites Beta and Y in paragraph 4.1, ZSM-5 in this paragraph) is observed and it can be useful for prediction of the adsorption behaviour on zeolites.

## CONCLUSIONS

The study of the thermodynamics and the kinetics of the adsorption process of organic contaminants in aqueous solution onto siliceous microporous and mesoporous materials provided the following results:

- ✓ The adsorption process is very fast in all the studied zeolites towards several classes of pollutants. Also the adsorption kinetic of PFOA on mesoporous silica materials is satisfying if compared with literature data dealing with other types of adsorbents.
- ✓ The adsorption capacities of zeolites depend on their structure and surface area. High adsorption capacities have been observed for zeolite Y and BEA, (about 20 % w/w) with respect of different organic compounds. ZSM-5 has generally lower adsorption capacity (about 6-8% w/w). However, ZSM-5 can be applied in water remediation since it is more efficient than Y in the removal of contaminants from very dilute solutions, as determined from the whole adsorption isotherm. Therefore, it can be used as adsorbent in finishing adsorption unit, where the regulation limits of concentration of contaminants in the effluent are low.
- ✓ The amount of the organic pollutant embedded inside the framework is influenced by the lattice structure, the hydrophobicity and the thermal treatments of the adsorbent. For mesoporous silica materials, an important role is also played by the procedure of template removal (thermal treatment or solvent extraction).
- ✓ Both hydrophobic and electrostatic interactions contribute to the adsorption process: in fact, hydrophobicity and dissociation constant of the solute strongly affect the adsorption. An increase of the adsorption constant with the solute's octanol-water partition coefficient has been observed for systems involving different framework type zeolites and molecules having different physico-chemical properties.
- ✓ From the dependence of adsorption on the solution compositions it was found that both Y and BEA zeolites represent efficient adsorbent materials for pre-concentration systems or for simultaneous concentration and analysis of several pharmaceutical compounds.

- ✓ It has been proved that solute molecules are generally adsorbed inside the framework of the adsorbents, often causing modifications in the lattice structure, in terms of both dimensions and shape of the channel system of the zeolites.
  
- ✓ Zeolites are selective adsorbents for organic pollutants in presence of natural organic matter (lignin-derived phenolic monomers). In fact, toluene is preferentially adsorbed from mixtures of toluene and humic acid monomers in aqueous solutions.

In conclusion, favourable adsorption kinetics along with the effective and selective adsorption of contaminants into zeolites and mesoporous siliceous materials make these cheap and environmentally-friendly materials a tool with interesting applications for the removal or enrichment of organic contaminants from wastewaters.



## REFERENCES

- Achten C., Kolb A., Puttman W. (2002), *Environmental Science & Technology*, 36, 3663–3670.
- Ahrens L., Plassmann M., Xie Z.Y., Ebinghaus R., *Environ. Sci. Eng. China* 3 (2009) 152–170.
- Ahrens L., Xie Z.Y., Ebinghaus R., 2010, *Chemosphere* 78, 1011–1016.
- Aktas E. S., Imre S., Ersoy L., *Wat. Res.* Vol. 35, No. 9, pp. 2336–2340, 2001
- Alberti A., Martucci A. (2010), *The Journal of Physical Chemistry C*, 114, 7767–7773.
- Amberg A., Rosner E., Dekant W. (2001), *Toxicological Sciences*, 61, 62–67.
- Amor L., Eiroa M., Kennes C., Veiga M.C., 2005, *Water Res.* 39, 2915–2920.
- Andersen A., *Int J. Toxicol*, (25 Suppl 1), 11-27, (2006)
- Anderson M. A. (2000), *Environmental Science & Technology*, 34, 725–727.
- Arroyo 2013; Water Resources Research Center, College of Agriculture and Life Sciences, The University of Arizona
- Azizian S.; *J. Colloid Interface Sci.* 2004, 276, 47–52.
- Azizian S.; *J. Colloid Interface Sci.* 2006, 302, 76–81.
- Baerlocher Ch., Meier W.M., Olson D.H. (2001) *Atlas of Zeolite Framework Types*, 5th ed., Elsevier, Amsterdam.
- Bailly F., Cotelle P. 2005, *Curr. Med. Chem.* 12: 1811-1818.
- Banat F.A., Simandl J., *Chem. Eng. Science* 51 (8), 1257-1265, 1996

Bansode R.R., Losso J.N., Marshall W.E., Rao R.M., Portier R.J., *Bioresource Technology* 90, 175-184, 2003

Barceló D., Special issue, *Trends in Analytical Chemistry*, 2003, 22 (10).

Bendz D., Paxéus N. A., Ginn T. R., Loge F. J.; *Journal of Hazardous Materials* 122 (2005) 195–204

Bertanza G., Pedrazzani R., Zambarda V. (2009), *Ingegneria Ambientale*, 48, II supplemento alla rivista.

Bhatarai B., Gramatica P., *Environ. Sci. Technol.* 2012 Jan 3;46(1):566.

Blanchard G., Maunaye M., Martin G.; *Water Res.* 1984, 18, 1501–1507.

Bolong N., Ismail A.F., Salim M.R., Matsuura T. (2009), *Desalination*, 239: 229-246.

Boulanger B., Vargo J.D., Schnoor J.L., Hornbuckle K.C., 2005, *Environ. Sci. Technol.* 39, 5524–5530.

Breck D. W., U.S. Patent 3,130,007 (1964).

Brisaert M., Heylen M., Plaizier-Vercammen J., *Pharm World Sci.* 1996 Oct;18(5):182-186.

Carballa M., Omil F., Lema J. M., Llompart M., Garcia C., Rodriguez I.; *Water Sci Technol* 2005; 52(8) 29–35.

Castiglioni S., Bagnati R., Fanelli R., Pomati F., Calamari D., Zuccato E., *Environ. Sci. Technol.* 2006, 40, 357-363

Čejka J., van Bekkum H., Corma A., Schüth F.; *Introduction to Zeolite Science and Practice*, 3<sup>RD</sup> revised edition; Elsevier, Vol.168, 2007

- Chang P., Young, T. (2000), *Water Research*, 34, 2233-2240.
- Cleuvers M. (2008). Kümmerer, K. (Ed.), *Pharmaceuticals in the Environment. Sources Fate Effects and Risks*, third ed. Springer, Berlin Heidelberg, 277–284.
- COM(2006) 397, Commission of the European Communities (CEC), Proposal of Directive of the European Parliament and of the Council.
- Cruciani G., Alberti A., Martucci A., Knudsen K.D., Ciambelli P., Rapacciuolo M. (1999). *Proceedings 12th International Zeolite Conference*, Materials Research Society. Treacy, M.M.J., Marcus, B.K., Bisher, M.E., Higgins, J.B. 2361-2369.
- Csicsery S.M., *Zeolites chemistry and Catalysis*. ACS Monographs 171, Am. Chem. Soc., Washington DC, 1976.
- Daifullah A.H., Mohamed M.M., *Journ. Of Chem. Technol. And Biotechnol.* 79, 468-474, 2004
- Daughton C.G., ACS Symposium Series 791, American Chemical Society, Washington, DC, 2001.
- Daughton C.G., Ternes T.A. (1999). *Environmental Health Perspectives*, 107: 907–942.
- Dejaegher B., Vander Heyden Y.; *Acta Chromatographica* 21 (2009) 161
- Deng S., Zheng Y.Q., Xu F.J., Wang B., Huang J., Yu G.; *Chemical Engineering Journal* 193-194 (2012) 154–160
- Deppeler H. P.; *Analytical Profiles of Drug Substances*, Volume 10, 1981, Pages 405-441
- Ebadi A., Soltan Mohammadzadeh J.S., Khudiev A., *Adsorption* 15 (2009) 65-73.
- Eder F., Stockenhuber M., Lercher J. A. *Journal of Physical Chemistry B* 101(27), 5414–5419 (1997)

Erdem-Senatalar A., Bergendahl J. A., Giaya A., Thompson R. W., *Environ. Eng. Sci.* 21 (2004) 722-729.

Fayolle F., Vandecasteele J.-P., Monot F.; *Appl Microbiol Biotechnol* (2001) 56:339–349

Fiese E. F., Steffen S. H., , *J. Antimicrob. Chemother.* (1990) 25 (suppl A): 39-47.

Fowler R. H., Guggenheim E. A. (1965) *Statistical Thermodynamics, Theory of the Properties of Matter in Equilibrium* Cambridge University, Press, New York.

Fujii S., Polprasert C., Tanaka S., Lien N.P.H., Qiu Y., 2007, *J. Water Supply Res. Technol.* 56, 313–326

Galarneau A., Iapichella J., Bonhomme K., Di Renzo F., Kooyman P., Terasaki O., Fajula F., *Adv. Funct. Mater.* 16, 1657 (2006)

Galarneau A., Iapichella J., Brunel D., Fajula F., Bayram-Hahn Z., Unger K. K., Puy G., Demesmay C., Rocca J. L., *J. Sep. Sci.* 29, 844 (2006)

Galarneau A., Nader M., Guenneau F., Di Renzo F., Gedeon A., *J. Phys. Chem. C.* 111, 8268 (2007)

Gantiva M., Martínez F., *Fluid Phase Equilib.* 2010, 293, 242–250.

Giaya, A., Thompson, R. W., Denkwicz Jr., R., *Micropor. Mesopor. Mat.* 40 (2000) 205-218.

Giesy J.P., Kannan K., *Environ. Sci. Technol.* 35 (2001) 1339.

Giesy, J.P., Kannan, K., 2002. *Environ. Sci. Technol.* 36 (7), 146A–152A.

Giovannini L., Migliori M., Filippi C., Origlia N., Panichi V., Falchi M., Bertelli A. A., Bertelli A. 2002. *Int. J. Tissue React.* 24: 53-56.

Giraldo L. F., López B. L., Pérez L., Urrego S., Sierra L., Mesa M., *Macromol. Symp.* 2007, 258, 129–141

Graham D. J., *Phys. Chem.*, 57, 1953, 665

Gritti F., Piatkowski W., Guiochon G. (2002). *Journal of Chromatography A*, 978(1-2), 81-107.

Gros M., Petrović M., Ginebreda A., Barceló D., *Environment International* 36 (2010) 15–26

Guiochon G., Felinger A., Shirazi D.G., Katti A.M., *Fundamentals of Preparative and Nonlinear Chromatography*, Second Edition, Elsevier, 2006.

Guiochon G.; Shirazi S.G.; Katt A.M., *Fundamentals of Preparative and Nonlinear Chromatography*, 1994. Academic Press Inc., London, UK. pp 61-83

Haerifar M., Azizian S., *J. Phys. Chem. C* 2013, 117, 8310–8317

Hansen M. C., Børresen M. H., Schlabach M., Cornelissen G., *J. Soil Sediments*. 10, 179 (2010)

Hartig C., Storm T., Jekel M. (1999). *Journal of Chromatography A*, 854: 163-173.

Heberer T. (2002). *Toxicology Letters*, 131: 5–17.

Hitz S., Prins R., *Journal of Catalysis* 168, 194–206 (1997)

Huang Z., Xu L., Li J.-H., Kawi S., Goh A.H., *Sep. Purif. Technol.* 77, 112 (2011)

Huber M.H., Canonica S., Park G.-Y., von Gunten U., *Environ. Sci. Technol.* 37 (2003) 016.

Hung H.-W., Lin T.-F., *J. Hazard. Mater.* 135 (2006) 210.

IZA, International Zeolite Association, Delaware, [www.iza-online.org](http://www.iza-online.org).

Jensen A.A., Poulsen P.B., Bossi R., No. 99, Danish Environmental Protection Agency, Copenhagen, 2008.

Kasprzyk-Hordern B., Dinsdale R.M., Guwy A.J. (2007). *Journal of Chromatography A*, 1161: 132–145.

Kawai T., Yanagihara T., Tsutsumi K., *Colloid Polym. Sci.* 272 (1994) 1620-1626.

Kennedy G.L., Butenhoff J.L., Olsen G.W., O'Connor J.C., Seacat A.M., Perkins R.G., Biegel L.B., Murphy S.R., Farrar D.G., 2004. *Crit. Rev. Toxicol.* 34 (4), 351–384.

Knappe D. R. U., Campos A. A. R. (2005) *Water Science and Technology. Water Supply*, 5, 83–91.

Kokotailo G. T., Lawton S. L., Olson D. H., Meier W. M., *Nature* 272 (1978) 437-438.

Kolpin D.W., Furlong E.T., Meyer M.T., Thurman E.M., Zaugg S.D., Barber L.B., Buxton H.T. (2002). *Environmental Science and Technology*, 36: 1202–1211.

Koubaissy B., Joly G., Batonneau-Gener I., Magnoux P. (2011). *Industrial & Engineering Chemistry Research*, 50, 5705–5713.

Krohn J. E., Tsapatsis M., *Langmuir* 2005, 21, 8743–8750

Krohn J. E., Tsapatsis M., *Langmuir* 2006, 22, 9350–9356.

Kunkeler P. J., Zuurdeeg B. J., van der Waal J. C., van Bokhoven J. A., Koningsberger D. C., van Bekkum H., *J. Catal.* 1998, 180, 234–244.

Kurath P., Jones P. H., Egan R. S., Perun T. J., *Cellular and Molecular Life Sciences*, 27(4), 362, 1971

Küster A., Alder A. C., Escher B. I., K. Duis K., Fenner K., Garric J., Hutchinson T. H., Lapen D. R., Péry A., Römbke J., Snape J., Ternes T., Topp E., Wehrhan A., Knacker T.; Integrated Environmental Assessment and Management — Volume 6, Supplement 1—pp. 514–523 2009 SETAC

Küster A., Alder A. C., Escher B. I., K. Duis K., Fenner K., Garric J., Hutchinson T. H., Lapen D. R., Péry A., Römbke J., Snape J., Ternes T., Topp E., Wehrhan A., Knacker T.; Integr. Environ. Assess. Manage. 2010, 6, 514–523.

Kuzniatsova T., Kim Y., Shqau K., Dutta P. K., Verweij H., Microporous Mesoporous Mater. 2007, 103, 102–107.

Lafont F., Aramendia M. A., García I., Borau V., Jiménez C., Marinas J. M., Urbano F. J., Rapid Commun. Mass Spectrom. 13, 562–567 (1999)

Lagergren S., Kungliga Svenska Vetenskapsakademiens, Handlingar 1898, 24, 1–39.

Langmuir I., J. Amer. Chem. Soc., 38,1916, 2221

Lau C., Anitole K., Hodes C., Lai D., Pfahles-Hutchens A., Seed, J., 2007. Toxicol. Sci. 99, 366–394.

Leardi R., Analytica Chimica Acta 652 (2009) 161

Li X., Chen S., Quan X., Zhang Y., Environ. Sci. Technol. 45, 8498 (2011)

Li S., Tuan V. A., Noble R. D., Falconer J. L., Environ. Sci. Technol. 37 (2003) 4007-4010.

Li C. , Zhang B., Ertunc T., Schaeffer A., Ji R.; Environ. Sci. Technol., 2012, 46 (16), pp 8843–8850

Lindsey M.E., Meyer M., Thurman E.M. (2001) Analytical Chemistry, 73, 4640-4646.

Lindstrom A. B., Strynar M.J., Libelo E.L., Environ. Sci. Technol. 45 (2011) 7954–7961.

Liu Y., Sakagami H., Hashimoto K., Kikuchi H., Amano O., Ishihara M., Kanda Y., Kunni S., Kochi M., Zhang W., Yu G., Anticancer Research, (28), 229-236 (2008)

Lo H. H., Chung J. G., 1999. Anticancer Res. 19: 133- 139.

Loganathan B.G., Sajwan K.S., Sinclair E., Kumar K.S., Kannan K., 2007. Water Research 41, 4611–4620.

Lohse U., Altrichter B., Fricke R., Pilz W., Schreier E., Garkisch Ch., Jancke K., J. Chem. Soc., Faraday Trans. 1997, 93, 505–512.

Mackay D., Shiu W.Y., Ma K.C., Lee S.C. (2006) Illustrated handbook of physical–chemical properties and environmental fate for organic chemicals—volatile organic chemicals, Vol. III. Taylor & Francis Group, LLC., 1-925.

Mallon E. E., Aqueous Solution and Vapor Phase Adsorption of Oxygenates onto Zeolites, thesis, 2012

Mallon E. E., Babineau I. J., Kranz J. I., Guefrachi Y., Siepmann J. I., Bhan A., Tsapatsis M.; J. Phys. Chem. B 2011, 115, 11431–11438.

Martin J.W., Mabury S.A., Solomon K.R., Muir D.C.G., Environ. Toxicol. Chem. 22 (2003) 196.

Martucci A., Pasti L., Marchetti N., Cavazzini A., Dondi F., Alberti A.; Microporous and Mesoporous Materials 148 (2012) 174–183

McCusker L. B., Baerlocher C., "Zeolite structures" in Introduction to zeolite science and practice, Elsevier Sciences, 2001.

McCusker L. B., Liebau F., Engelhardt G., Pure Appl. Chem. 73 (2001) 381



Meier W.M., Zeit. Krist. 115(1961) 439-450.

Meloun M., Bordovská S., Galla L., J. Pharm. Biomed. Anal. 2007, 45, 552–564

Mishra H. N., Rajesh Kumar S., Vijay N., Satish C., Alok Kumar S., Vikas Kuamr S., Onkar P., Leena S.; J. Recent Sci., 2(1),150-157(2013)

Mitra S., (2003) Sample preparation techniques in analytical chemistry. Wiley, New York

Moscaletti A., Galarneau A., Di Renzo F., Ottaviani F., J. Phys. Chem B. 108, 18580 (2004)

Moulijn J.A., Makkee M., Van Dipen A. (2001) Chemical Process Technology. 1st Edn., John Wiley and Sons Ltd., Chichester, 1-453.

Mureseanu M., Galarneau A., Cioatera N., Trandafir I., Georgescu I., Fajula F., Microporous Mesoporous Mater. 146, 141 (2011)

Qin Q. D., Ma J., Liu K., J. Colloid Interface Sci. 315, 80 (2007)

Nakayama S.F., Strynar M.J., Reiner L.R., Delinsky A.D., Lindstrom A.B., Environ. Sci. Technol. 44 (2010) 4103.

Nassi M., Sarti E., Pasti L., Martucci A., Marchetti N., Cavazzini A., Di Renzo F., Galarneau A.; J Porous Mater 2014, DOI 10.1007/s10934-014-9788-5

Newsman J. M., Treacy M. M. J., Koestier W. T., De Gruyter C. B., Proc. R. Soc. London, A. 420, 375-405, 1988

Noble R. D., Terry P. A.; Principles of chemical separations with environmental applications; Cambridge

Ochoa-Herrera V., Sierra-Alvarez R., Chemosphere 72 (2008) 1588–1593.

OECD. Co-operation on existing chemicals: Hazard assessment of perfluorooctane sulfonate (PFOS) and its salts: OECD, 2002

OEHHA (Office of Environmental Health Hazard Assessment) (1999) Public Health Goal for Methyl Tertiary Butyl Ether (MTBE) in Drinking Water, Pesticide and Environmental Toxicology Section, California EPA, USA, available at [http://oehha.ca.gov/water/phg/pdf/mtbe\\_f.pdf](http://oehha.ca.gov/water/phg/pdf/mtbe_f.pdf).

Ottaviani M. F., Galarneau A., Desplantier-Giscard D., Di Renzo F., Fajula F., *Microporous Mesoporous Mater.* 1-8, 44 (2001)

Panchangam S. C., Lin A. Y., Shaik K. L., Lin C. F., *Chemosphere.* 77, 242 (2009)

Pasti L., Martucci A., Nassi M., Cavazzini A., Alberti A., Bagatin R., (2012), *Microporous and Mesoporous Materials*, 160, 182-193.

Pasti L., Sarti E., Cavazzini A., Marchetti N., Dondi F., Martucci A., *J. Sep. Sci.* 2013, 36, 1604–1611

Paul A.G., Jones K.C., Sweetman A.J., 2009. *Environ. Sci. Technol.* 43 (2), 386–392.

Pereira R. N., Valente B. R., Cruz A. P., Foppa T., Murakami F. S., Silva M. A. S.; *Lat. Am. J. Pharm.* 26 (3): 382-6 (2007)

Perez-Alvarez V., Bobadilla R. A., Muriel P., 2001. *J. Appl. Toxicol.* 21: 527-531.

Persson B-A. *Acta Pharm Suecica.* 1968; 5:335-342.

Petrovic M, Barceló D. (2006). *Journal of Mass Spectrometry*, 41, 1259–1267.

Petrovic M., Hernando M. D., Díaz-Cruz M. S., Barceló D.; *J Chromatogr* 2005;1067(1–2):1-14.

Poiger T., Buser H. R., Balmer M. E., Bergqvist P. A., Muller M. D.; *Chemosphere* 55 (2004) 951

- Post G. B., Cohn P-D., Cooper K. R., Environ. Res. 116, 93 (2012)
- Prado A. G. S., Airoidi C., J. Mater. Chem. 12, 3823 (2002)
- Prevedouros K., Cousins I.T., Buck R.C., Korzieniowski S.H., 2006. Environ. Sci. Technol. 40 (1), 32–44.
- Radjenovic J., Petrovic M., Barcelo D.; Anal Bioanal Chem 2007;387(4):1365–77.
- Radjenovic J., Petrovic M., Barcelo D.; Water Res 2009;43(3):831–41.
- Radjenovic J., Petrovic M., Ventura F., Barcelo D.; Water research 42 (2008) 3601 – 3610
- Raneva V., Shimasaki H., Ishida Y., Ueta U., Niki E. 2001. Lipids 36: 1111-1116.
- Rattanaoudom R., Visvanathan C., Kitpati Boontanon S., Journal of Water Sustainability, 2(4), 245 (2012)
- Regueiro J., Llompart M., Garcia-Jares C., Cela R.; J. Chromatogr. A 1216 (2009) 2816
- Ren B., Tong Z., Liu X., Wang C., Zeng F., Langmuir 20, 10737 (2004)
- Renard G., Mureseanu M., Galarneau A., Lerner D. A., Brunel D., New J. Chem. 29, 912 (2005)
- Richardson S.D.; Anal. Chem. 78 (2006), 4045
- Richardson S.D., Ternes T.A. (2011). Analytical Chemistry, 83, 4614–4648.
- Rosal R., Rodríguez A., Perdigón-Melón J. A., Petre A., García-Calvo E., Gómez M. J., Agüera A., Fernández-Alba A. R.; Water research 44 (2010) 578–588
- Rossner A., Knappe D. R.U., Water Research, 42, 2008, Pages 2287–2299

Rouquerol F., Rouquerol J., Sing K.; Adsorption by powders & porous solid. Principles, methodology and applications. Academic Press

Rudzinski W., Plazinski W.; J. Phys. Chem. B 2006, 110, 16514-16525

Safa Özcan A., Erdem B., Özcan A., Journal of Colloid and Interface Science 280 (2004) 44-54.

Scheytt T., Mersmann P., Lindstädt R., Heberer T., Water, Air, Soil Pollut. 165 (2005) 3.

Senevirathna S.T.M.L.D., Tanaka S., Fujii S., Kunacheva C., Harada H., Shivakoti B. R., Okamoto R.; Chemosphere. 80, 647 (2010)

Silva C. D., Gómez J., Houbron E., Cuervo-López F.M., Texier A.-C., Chemosphere 75 (2009) 1387–1391

Silva Pires M. A., Souza dos Santos R. A., Sinisterra R. D.; Molecules 2011, 16, 4482-4499

Sinclair E., Kannan K., 2006. Environ. Sci. Technol. 40 (5), 1408–1414.

Squillace P., Pankow J., Kortés N., Zogorski J. (2009). Environmental Toxicology and Chemistry, 16, 1836-1844.

Squillace P., Zogorski J., Wilber W. G., Price C. V.; Environ. Sci. Technol. 1996, 30, 1721-1730

Stanley B.J., Guicchiom G.; Langmuir, 1995, 11 1735-1743

Stockholm Convention, 2010. <<http://chm.pops.int/Convention/ThePOPs/tabid/673/language/en-US/Default.aspx>>.

Sugawara M., Takekuma Y., Yamada H., Kobayashi M., Iseki K., Miyazaki K., J. Pharm. Sci. 87 (1998) 960.

Sun H.W., Li F.S., Zhang T., Zhang X.Z., He N., Song Q., Zhao L.J., Sun L.N., Sun T.H., Water Res. 45 (2011) 4483–4490.

Szostak R., Molecular sieves: principles of synthesis and identification, Blackie Academic & Professional, an Imprint of Thomson Science, London, 1998.

Tanev P. T., Pinnavaia T. J., Science. 267, 865 (1995)

Tanev P. T., Pinnavaia T. J., Chem. Mater. 8, 2068 (1996)

Ternes T.A., Meisenheimer M., McDowell D., Sacher F., Brauch H.J., Haist- Gulde B., Preuss G., Wilme U., Zulei-Seibert N., Environ. Sci. Technol. 36 (2002) 3855.

Ternes T.A., Stüber J., Herrmann N., McDowell D., Ried A., Kampmann M., Teiser B., Water Res. 37 (2003) 1976.

Texier A.-C., Gomez J., 2002. Tolerance of nitrifying sludge to p-cresol. Biotechnol. Lett. 24, 321–324.

Thompson J., Eaglesham G., Reungoat J., Poussade Y., Bartkow M., Lawrence M., Mueller J. F., Chemosphere 82 (2011) 9–17

Tița D., Fuliș A., Tița B.; J Therm Anal Calorim (2011) 105:501–508

Toth J., Acta Chim. Acad Sci. Hung., 1971 69, 311

Trenholm R. A., Vanderford B. J., Holady J.C., Rexing D. J., Snyder S. A.; Chemosphere 65 (2006) 1990

Tsou M. F., Hung C. F., Lu H. F., Wu L. T., Chang S. H., Chang H. L., Chen G. W., Chung J. G. 2000. Microbios 101: 37-46.

US EPA (1997) Drinking water advisory: Consumer acceptability advice and health effects analysis on methyl tertiary-butyl ether (MTBE). Washington, DC, US Environmental Protection Agency, pp. 11–13 (EPA-822-F-97-009; available at <http://www.epa.gov/ost/drinking/mtbe.pdf>).

U.S. Environmental Protection Agency, Perfluorooctanoic Acid (PFOA) and Fluorinated Telomers: <http://www.epa.gov/oppt/pfoa/pubs/pfoainfo.html>

U.S. Environmental Protection Agency, Pharmaceuticals and Personal Care Products as Pollutants: <http://www.epa.gov/esd/chemistry/ppcp/>.

U.S. Environmental Protection Agency, Toluene:  
<http://www.epa.gov/ttnatw01/hlthef/toluene.html>

Valcárcel Y., González Alonso S., Rodríguez-Gil J.L., Romo Maroto R., Gil A., Catalá M., Chemosphere 82 (2011) 1062–1071

Vallet-Regí M., Balas F., Arcos D.; Angew. Chem. Int. Ed. 2007, 46, 7548 – 7558

van Bekkum H., Flanigen E.M., Jacobs P.A., Jansen J.C., Studies in Surface Science and Catalysis 137 (2001) 11-35 (Chapter 2).

Vignola R., Sisto R., Grillo G., Cova U., Cesti P., US2009/0014390 A1 Patent, (2009).

Vignola R., Cova U., Della Penna G., Sisto R., WO 2005/06361 A2 Patent (2005).

Wandlinger R. L., Kerr G. T., Rosinski E. J., U.S. Pat. 3 308069, 1967

Wang L.-H., Hsu K.-Y., Hsu F.-L., Lin S.-J.; Journal of food and drug analysis, 2008, 16, 1, 34-40

Wang F., Liu C., Shih K., Chemosphere. 89, 1009 (2012)

Wang F., Shih K., Water Res. 45, 2925 (2011)

Wang T., Wang Y., Liao C., Cai Y., Jiang G., 2009. *Environ. Sci. Technol.* 43 (14), 5171–5175.

Wijntje R., Bosch H., de Haan A. B., Bussmann P. J. T., *J. Chromatogr. A* 2007, 1142, 39–47.

Xiangli L., Li Shichun L., Chongyu L., Tiangang L.; *Chinese J. Of Anal Chem* 34 (2006) 325

Xu J. W., Ikeda K., Kobayakawa A., Ikami T., Kayano Y., Mitani T., Yamori Y. 2005. *Life Sci.* 76: 2861-2872.

Yoon C. H., Zhu T., Row K. H.; *Korean Journal of Chemical Engineering*, 2012, Volume 29, Issue 2, pp 135-138

Yu J., Hu J.Y., Tanaka S., Fujii S., 2009. *Water Res.* 43, 2399– 2408.

Yu Q., Zhang R., Deng S., Huang J., Yu G., *Water Res.* 43, 1150 (2009)

Zhang T., Zhang L., Wang J., Yuan T., Hong X., Qi F. (2008), *The Journal of Physical Chemistry A.* 112, 10495-10501.

Zhao X.S., Ma Q., Lu G.Q., *Energy Fuels* 12 (1998) 1051.

Zuccato E., Castiglioni S., Bagnati R., Fanelli R.; *Quaderni acp* 2007; 14(5): 203-206

## ACKNOWLEDGEMENTS

I would like to thank Dr. Luisa Pasti for the time, the energy and all the support she gave me during my years of PhD.

I would like to thank Prof. Francesco Dondi and the entire group of Analytical Chemistry.

I would like to give thanks ENI for their financial support on this project and the group of Earth Science of Ferrara University (in particular Prof. Alberto Alberti and Dr. Annalisa Martucci) for their collaboration.

Lots of thanks also to my family and friends.